

ACTIVE NONLINEAR FILTER DESIGN UTILIZING  
PARAMETER PLANE ANALYSIS TECHNIQUES

by

William August Tate



INTERNALLY DISTRIBUTED

REPORT

United States  
Naval Postgraduate School



THE SIS

ACTIVE NONLINEAR FILTER DESIGN UTILIZING  
PARAMETER PLANE ANALYSIS TECHNIQUES

by

William August Tate

December 1970

*This document has been approved for public re-  
lease and sale; its distribution is unlimited.*

137818



INTERNALLY DISTRIBUTED  
REPORT

Active Nonlinear Filter Design Utilizing  
Parameter Plane Analysis Techniques

by

William August Tate  
Lieutenant, United States Navy  
B.S., Leland Stanford Junior University, 1963

Submitted in partial fulfillment of the  
requirement for the degrees of


ELECTRICAL ENGINEER

and

MASTER OF SCIENCE IN ELECTRICAL ENGINEERING

from the

NAVAL POSTGRADUATE SCHOOL  
December 1970





## ABSTRACT

A technique for designing nonlinear active networks having a specified frequency response is presented. The technique, which can be applied to monolithic/hybrid integrated-circuit devices, utilizes the parameter plane method to obtain a graphical solution for the frequency response specification in terms of a frequency-dependent resistance.

A limitation to this design technique is that the nonlinear parameter must be a slowly-varying quantity - the quasi-frozen assumption. This limitation manifests itself in the inability of the nonlinear networks to filter a complex signal according to the frequency response specification. Within the constraints of this limitation, excellent correlation is attained between the specification and measurements of the frequency response of physical networks.

Nonlinear devices, with emphasis on voltage-controlled nonlinear FET resistances and nonlinear device frequency controllers, are realized physically and investigated. Three active linear filters, modified with the nonlinear parameter are constructed, and comparisons made to the required frequency specification.





## TABLE OF CONTENTS

I.	INTRODUCTION -----	12
II.	OVERVIEW -----	15
	A. PARAMETER PLANE TECHNIQUES -----	15
	1. Basic Defining Equations -----	15
	2. Basic Assumptions -----	19
	B. FILTER DESIGN CONSIDERATIONS -----	19
	C. BASIC MONOLITHIC/HYBRID INTEGRATED-CIRCUIT TECHNOLOGY CONSIDERATIONS -----	29
	D. DESIGN OF HYBRID INTEGRATED-CIRCUIT NONLINEAR ACTIVE FILTERS UTILIZING FREQUENCY RESPONSE SPECIFICATIONS -----	33
III.	NONLINEAR DEVICE CONSIDERATIONS -----	35
	A. INTRODUCTION -----	35
	B. JUNCTION AND INSULATED GATE FIELD-EFFECT TRANSISTOR -----	36
	C. VOLTAGE CONTROLLED ATTENUATORS -----	53
	1. Introduction -----	53
	2. Triode Region FET Voltage-Controlled Attenuator -----	53
	3. Feedback-Connected FET Voltage-Controlled Attenuators -----	59
	4. MOSFET Voltage-Controlled Attenuators -----	61
	5. JFET Voltage-Controlled Attenuators -----	73
	D. FREQUENCY DEPENDENT ATTENUATORS -----	73
IV.	NONLINEAR DEVICE CONTROLLER -----	86
	A. INTRODUCTION -----	86



B.	PHASE SHIFT DISCRIMINATOR -----	88
C.	RETRIGGERABLE MONOSTABLE MULTIVIBRATOR/ INTEGRATOR -----	95
D.	ACTIVE FILTER DISCRIMINATOR -----	100
V.	ANALYTIC AND EXPERIMENTAL DESIGN OF HYBRID NONLINEAR ACTIVE FILTERS -----	107
A.	LOW-PASS FILTER -----	107
B.	THE HIGH-PASS FILTER -----	129
VI.	CONCLUSION -----	150
	BIBLIOGRAPHY -----	152
	INITIAL DISTRIBUTION LIST -----	158
	FORM DD 1473 -----	159



## LIST OF TABLES

- I Butterworth Filter Transient Response Characteristics.
- II Bessel Filter Transient Response Characteristics.
- III Characteristics of Hybrid Integrated Active Filters.
- IV Typical Performance of Integrated Circuit Components.
- V Operational Amplifier DC Characteristics.
- VI Attenuation Factors and Resistance ( $R_{DS}$ ) Values for 3N138 (Feedback-Connected) Voltage-Controlled Attenuator.
- VII Attenuation Factors and Resistance ( $R_{DS}$ ) Values for 3N138 (Conventionally-Connected) Voltage-Controlled Attenuator.
- VIII Low-Pass Nonlinear Filter  $\alpha$ -Characteristic Tabular Data.
- IX Low-Pass Nonlinear Filter Frequency Response Data.
- X Test One for Superposition of Two Sinusoids in Non-linear Active Low Pass Filter Case (Input Frequencies are 800 Hz(Odb) and 1000 Hz(Odb)).
- XI Test Two for Superposition of Two Sinusoids in Nonlinear Active Low-Pass Filter Case.
- XII High-Pass Nonlinear Filter  $\alpha$ -Characteristic Tabular Data.
- XIII High-Pass Nonlinear Filter Frequency Response Data (Example 1)
- XIV Harmonic Distortion of High-Pass Filters (Linear and Nonlinear).
- XV High-Pass Nonlinear Filter  $\alpha$ -Characteristic Tabular Data (Example 2).
- XVI High-Pass Nonlinear Filter Frequency Response Data (Example 2).



## LIST OF FIGURES

1. Ideal Low-Pass Filter.
2. Butterworth Approximation.
3. Cascading Networks to Obtain Bandpass Filter.
4. Concatenating Networks to Obtain Band-Stop Filter.
5. Nonideal Operational Amplifier With Equivalent Circuit Diagram.
6. Junction Field-Effect Transistor.
7. Enhancement IGFET.
8. Depletion IGFET.
9. Transfer Characteristics of FET's.
10. 2N3819 Low Level Drain Characteristic.
11. 2N3819 Low Level Drain Characteristic Photographs.
12. 2N3820 Low Level Drain Characteristic Photographs.
13. 3N138 Low Level Drain Characteristic.
14. 3N138 Low Level Drain Characteristic Photographs.
15. 3N172 Low Level Drain Characteristic.
16. Conventionally-Connected 3N138 Test Circuit Schematic.
17. Feedback-Connected 3N138 Test Circuit Schematic.
18. Feedback-Connected 2N3819 Low Level Characteristic.
19. Feedback-Connected 3N138 Low Level Characteristic.
20. Feedback-Connected 3N138 Low Level Characteristic.
21. Feedback-Connected 3N138 Low Level Characteristic.
22. Feedback-Connected 3N138 Low Level Characteristic.
23. Voltage-Controlled FET Attenuator Circuit Schematic.





24. Attenuator Characteristics for Different Values of Zero-Bias Attenuation.
25. Distortion Effects in Voltage-Controlled FET Attenuators.
26. 3N138, Feedback-Connected, Voltage-Controlled Attenuator Characteristics, Input Voltage is a parameter.
27. 3N138, Feedback-Connected, Voltage-Controlled Attenuator Circuit Schematic.
28. 3N138, Feedback-Connected, Voltage-Controlled Attenuator Characteristics, Input Frequency is a parameter.
29. 3N138, Feedback-Connected Voltage-Controlled Attenuator Characteristics, Series Resistance is a parameter.
30. 3N138, Conventionally-Connected, Voltage-Controlled Attenuator Circuit Schematic.
31. 3N138, Conventionally-Connected, Voltage-Controlled Attenuator Characteristic, Input Voltage is a parameter.
32. 3N138, Conventionally-Connected, Voltage-Controlled Attenuator Characteristic, Input Frequency is a parameter.
33. 3N138, Conventionally-Connected, Voltage-Controlled Attenuator Characteristics Series Resistance is a parameter.
34. 3N138 Drain-Source Resistance Characteristic, Log Plot.
35. 3N138 Drain-Source Resistance Characteristic, Linear Plot.
36. 2N3819, Conventionally-Connected, Voltage-Controlled Attenuator Characteristic; Input voltage is a parameter.
37. Frequency-Dependent FET Attenuator Circuit Schematic.
38. Slide Rule Analytic Solution For Parameter Plane, Frequency - Dependent Attenuator.
39. Parameter Plane Computer Solution for Frequency-Dependent Attenuator.
40. 2N3819 Low-Pass Frequency-Dependent Attenuator Characteristic.
41. 3N141 Low-Pass Frequency-Dependent Attenuator Characteristic.
42. 3N141 Low-Pass Frequency-Dependent Attenuator Characteristic.



43. 3N141 High-Pass Frequency-Dependent Attenuator Characteristic.
44. Block Diagram of Basic Nonlinear Device Controller.
45. Block Diagram of Phase Sensitive Discriminator.
46. Phase Sensitive Discriminator Circuit-Schematic.
47. Phase Response Characteristic of Phase-Sensitive Amplifier.
48. Phase Sensitive Discriminator Characteristic.
49. Phase Sensitive Discriminator Characteristics, Voltage Input is a parameter.
50. Phase Sensitive Discriminator Characteristics, Component Values - the parameter.
51. Retriggerable Monostable Multivibrator/Integrator Controller Block Diagram.
52. Integrated-Circuit TTL Fairchild Part Number 9601 Block Diagram.
53. 9601 Frequency Discriminator Wiring Diagram.
54. 9601 Frequency Discriminator Characteristic.
55. Filter Discriminator Block Diagram.
56. Filter Discriminator Characteristic Examples.
57. Filter Discriminator Characteristic,  $R_{LOAD}$  is a parameter.
58. Filter Discriminator Characteristic, Bias Voltage is a parameter.
59. Low-Pass Filter, R-C Ladder.
60. Low-Pass Filter, L-R-C Series Circuit.
61. Second Order Rauch Low-Pass Active Filter.
- 62a. Low-Pass Active Filter Frequency Response Characteristic,  $V_{in} = 435$  mv rms.
- 62b. Low-Pass Active Filter Frequency Response Characteristic,  $V_{in} = 2.78$ v rms.
63. Photographs of the Transient Response of the Low-Pass Linear Active Filter.



64. Physical Configuration of Frequency-Dependent Nonlinear Resistor.
65.  $\alpha$ -Characteristic Test Circuit with Pertinent Formulae.
66. Frequency-Dependent Attenuation Factor Characteristics. FET Type 2N3819. Low-Pass Filter  $\alpha$ .
67. Parameter Plane Curves, Low-Pass Filter, with Super-Imposed  $\alpha$ -Characteristic.
68. Nonlinear Active Low-Pass Filter Frequency Response Characteristics. (Experimental and Parameter-Plane Predictions).
69. Harmonic Distortion Photographs for Nonlinear Low-Pass Filter.
70. Test of Superposition (Test One). Photographs of Input and Output Waveforms of Filters.
71. Transient Response Photographs of the Nonlinear Active Filter.
72. Test Circuit for Harmonic Measurements.
73. High-Pass Filter, R-C Ladder.
74. High-Pass Filter, R-L-C Circuit.
75. High-Pass Active Filter.
76. Linear Active High-Pass Filter Frequency Response (example 1).
77. High-Pass Active Filter Parameter Plane Curves (Example 1).
78. Frequency-Dependent  $\alpha$ -Characteristic. FET Type 2N3820. High-Pass Filter (Example 1).
79.  $\alpha$ -Characteristic Test Circuit (Example 1).
80. High-Pass Nonlinear Active Filter Frequency Response Characteristic (Experimental and Parameter-Plane Predictions), (Example 1).
81. High-Pass Linear Filter (Example 2).
82. Linear Active High-Pass Filter Frequency Response (example 2).



83. Frequency-Dependent  $\alpha$ -Characteristic Test Circuit with Appropriate Formulae (Example 2).
84.  $\alpha$ -Characteristic Frequency Response. FET Type 2N3819 (Fdbk). High-Pass Filter (Example 2).
85. High-Pass Nonlinear Active Filter Frequency Response Characteristic (Experimental and Parameter Plane Prediction), (Example 2).





### ACKNOWLEDGEMENT

The author is indebted to a good number of people who made the completion of the research possible. The thesis advisor, Professor George Thaler is thanked for providing motivation and inspiration, for stimulating intellectual curiosity, and for challenging fundamental concepts. The thesis reader, Professor Don Kirk, is especially noteworthy for his enthusiastic response at a late date to a very challenging task of smoothing the style and language of the thesis. The typists, my wife Judith and Jeanne Belcher, are thanked for an expert job of translating my illegible notes into a finished manuscript. Joe Davis's art work freed the author from that tedious chore. And finally to my three children who patiently gave up a lot of frisbee time so that the job could be done - may the Good Fairy shine on them.



## I. INTRODUCTION

The goal of this thesis is to investigate the applicability of the parameter-plane techniques of Thaler and Thompson [Ref. 1], Siljak [Ref. 2], Hollister [Ref. 3], Glavis [Ref. 4], Nichols [Ref. 5], and others to the design and construction of nonlinear active networks having a specified frequency response. If the implementation of this technique yields networks capable of filtering a complex signal in a prescribed manner the applicability of the parameter plane technique to nonlinear active filter design has been established.

Nakajawa applied parameter-plane techniques to active filter systems. Nichols [Ref. 5] applied the parameter-plane frequency response techniques to the design of electrical filters containing nonlinear elements. Nichols produced a digital computer program (PARTF1 and PARTF2) which would permit graphical solution of a superimposed nonlinear parameter characteristic onto a family of linear frequency-response plots. His experimental verification of the validity of this technique was based on computer simulation of the network model. A major limitation to the Nichols design technique is that the nonlinear element must vary slowly, the so-called quasi-frozen approximation.

This research will investigate the design and construction of nonlinear active networks of specified frequency response.



The block diagram of the general nonlinear network is shown in Figure 44. The technique will begin with a specified frequency response for the nonlinear network and a given type of linear active filter whose frequency response is similar to the prescribed frequency response. The linear active filter will be modified by the substitution of a frequency-dependent nonlinear resistance for one of the resistors in the circuit. This nonlinear-resistance is the parameter in the parameter-plane computer program.

The frequency-dependent nonlinear parameter characteristic is obtained from the superimposition of the specified frequency response onto the set of linear frequency response plots of the linear filter obtained from PARTFl. The values of the FET resistance, which is to be the  $\alpha$ -parameter, are determined by the gate-source voltage characteristic established by the nonlinear device controller.

An overview of pertinent concepts from the following fields of interest is included: (1) parameter plane techniques, (2) filter design characteristics from approximating polynomials, (3) basic monolithic/hybrid integrated-circuit design principles, and (4) design of nonlinear active filters utilizing the parameter-plane technique.

Investigation of the FET drain-source resistance as a voltage-controlled nonlinearity is included. Different configurations of the interconnection of the leads of the FET are examined for improving the performance of the FET as a voltage-controlled resistor.



Frequency-dependent device controllers are investigated and physical models constructed. The controller will provide the gate-source voltage of the FET so that  $R_{DS}$  may vary as required to produce the requisite frequency response of the nonlinear network.

After the techniques of utilizing the FET resistance as a frequency-dependent nonlinear element have been established, filter or network design examples are demonstrated. The physical models of the networks are tested in the quasi-frozen mode by measuring the frequency response of the network to a slowly-varying frequency sinusoidal signal input of constant amplitude. Harmonic distortion is measured for square-wave inputs to the network. Multiple sinusoidal signals of selected amplitude and frequency are used to test the principles of superposition and homogeneity, ascertaining the amount of deviation from linear behavior.

Because of the scope of the concepts that are being combined in this work, the research is confined to operational-amplifier (UA741C Fairchild) R-C filters with a frequency-dependent nonlinear resistance used as a parameter. The nonlinear resistance will be a field-effect transistor, either a 3N138/3N141 (RCA MOSFET) or a 2N3819/2N3820 (TI JFET). It is felt that applicability of the parameter plane synthesis techniques to this set of nonlinear filters will permit inference of its applicability to the larger set of nonlinear monolithic/hybrid filters.





## II. OVERVIEW

### A. PARAMETER PLANE TECHNIQUES

The basic equations for understanding the parameter plane techniques are cited below. This brief development of parameter plane techniques with attendant equations is meant to serve as a basis for the use of the parameter plane computer programs of Nichols. The transformation in going from the complex-frequency domain to the parameter plane is indicated. The basic algorithm for solving for the magnitude and phase of the transfer function in the parameter plane is also briefly discussed. For a complete development of the frequency response techniques in the parameter plane, see [Refs. 1, 2, 3, 4, and 5].

#### 1. Basic Defining Equations

- a. Transformation Techniques Involving Chebyshev Polynomials [Ref. 4]

$$\text{Let } F(S) = \sum_{k=0}^n a_k S^k = 0$$

$$\text{where } S \triangleq \sigma + j\omega$$

$$a_k \triangleq a_k(\alpha, \beta)$$

$$\text{Let } -\zeta = \cos(\theta) = \sigma/\omega_n$$

$$\theta \triangleq \angle \text{ between } S \text{ and positive real axis.}$$



then  $\sigma = \omega_n \cos \theta$

$$\omega = \omega_n \sin \theta = \omega_n \sqrt{1 - \cos^2 \theta} = \omega_n \sqrt{1 - \zeta^2} \quad ;$$

therefore  $S = \omega_n (\cos \theta + j \sin \theta) = \omega_n e^{j\theta} \rightarrow s^k = \omega_n^k (e^{jk\theta})$

$$S^k = \omega_n^k (\cos k\theta + j \sin k\theta) \quad .$$

Introducing Chebyshev functions and setting

$$T_k(-\zeta) = \cos k\theta = \cos (k \cos^{-1}(-\zeta))$$

$$U_k(-\zeta) = \frac{\sin k\theta}{\sin \theta} = \frac{\sin (k \cos^{-1}(-\zeta))}{\sin (\cos^{-1}(-\zeta))}$$

$$T_k(-\zeta) = -1^k T_k(\zeta) \quad \text{and} \quad U_k(-\zeta) = -1^{k+1} U_k(\zeta)$$

$$S_k = \omega_n^k [T_k(-\zeta) + j \sqrt{1-\zeta^2} U_k(-\zeta)] = \omega_n^k [-1^k T_k(\zeta) + j \sqrt{1-\zeta^2} (-1)^{k+1} U_k(\zeta)] \quad .$$

$$\text{Then } F(S) = \sum_{k=0}^n a_n \omega_n^k (-1)^k T_k(\zeta) + j \sum_{k=0}^n a_k \omega_n^k U_k(\zeta) = 0$$

Requiring the quadrature components of  $F(\zeta)$  to go to zero independently yields (circled numbers are equation numbers):

$$\sum_{k=0}^n a_k \omega_n^k (-1)^k T_k(\zeta) = 0 \quad \textcircled{1}$$

$$\sum_{k=0}^n a_k \omega_n^k (-1)^{k+1} U_k(\zeta) = 0 \quad \textcircled{2}$$

The recurrence relations for Chebyshev functions are:

$$T_{k+1}(\zeta) - 2\zeta T_k(\zeta) + T_{k-1}(\zeta) = 0$$

$$U_{k+1}(\zeta) - 2U_k(\zeta) + U_{k-1}(\zeta) = 0 \quad .$$



Recalling that

$$T_k(\zeta) = \zeta U_k(\zeta) - U_{k-1}(\zeta) \quad \text{and}$$

substituting in (1) yields

$$\sum_{k=0}^n a_k \omega_n^k (-1)^k T_k(\zeta) = \sum_{k=0}^n a_n \omega_n^k (-1)^k [\zeta U_k(\zeta) - U_{k-1}(\zeta)];$$

therefore

$$\sum_{k=0}^n a_k \omega_n^k (-1)^k \zeta U_k(\zeta) - \sum_{k=0}^n a_k \omega_n^k (-1)^k U_{k-1}(\zeta) = 0 .$$

The first term is zero from (2) ;

$$\text{therefore } \sum_{k=0}^n a_k \omega_n^k (-1)^k U_{k-1}(\zeta) = 0 \quad (3) ,$$

and

$$\sum_{k=0}^n a_k \omega_n^k (-1)^k U_k(\zeta) = 0 \quad (2) .$$

b. Transformation Techniques [Ref. 2].

$$F(S) = \sum_{k=0}^n a_k S^k \rightarrow \begin{array}{ll} R(\sigma, \omega, \alpha, \beta) = 0 & \text{Reals} \\ I(\sigma, \omega, \alpha, \beta) = 0 & \text{Imaginarities} \end{array}$$

provided  $J = \begin{vmatrix} \partial R / \partial \alpha & \partial R / \partial \beta \\ \partial I / \partial \alpha & \partial I / \partial \beta \end{vmatrix}$  exists and is not equal to zero.

Then the basic equations are:



$$\begin{aligned}
 R &= \sum_{k=0}^n a_k X_k = 0 & \text{where } X_k &= X_k(\sigma, \omega) \\
 I &= \sum_{k=0}^n a_k Y_k = 0 & Y_k &= Y_k(\sigma, \omega) \\
 & & S^k &= X_k + j Y_k \\
 & & \alpha &= \alpha(\sigma, \omega) \\
 & & \beta &= \beta(\sigma, \omega) \\
 & & A_k &= A_k(\alpha, \beta)
 \end{aligned}$$

and recurrence relations become:

$$X_{k+1} - 2\sigma X_k + (\sigma^2 + \omega^2) X_{k-1} = 0$$

$$Y_{k+1} - 2\sigma Y_k + (\sigma^2 + \omega^2) Y_{k-1} = 0$$

c. Frequency Response Techniques [Ref. 1].

Let  $T(S) = \frac{N(S)}{D(S)}$  be the system transfer function

define

$$M^2 = |T(j\omega)|^2 = T T^* = T(j\omega) \cdot T(-j\omega)$$

$$T(S) T(-S) = \frac{N_e(S) + N_0(S)}{D_e(S) + D_0(S)} \cdot \frac{N_e(S) - N_0(S)}{D_e(S) - D_0(S)} = \frac{N_e^2(S) - N_0^2(S)}{D_e^2(S) - D_0^2(S)}$$

Since  $T(S)T(-S)$  is an even function, then  $T(j\omega) \cdot T(-j\omega)$  is an even function and consequently  $M^2$  is even!

Let:

$$M^2 = \frac{a_0 + a_1 \omega^2 + a_2 \omega^4 + \dots + a_n \omega^{2n}}{b_0 + b_1 \omega^2 + b_2 \omega^4 + \dots + b_n \omega^{2n}} \quad (4)$$





$$\theta = \tan^{-1} \frac{N_0(S) D_e(S) - N_e(S) D_0(S)}{N_e(S) D_e(S) - N_0(S) D_0(S)}$$

## 2. Basic Assumptions

In the use of the parameter plane technique for non-linear analysis and synthesis, some basic assumptions are made. The nonlinear element is allowed to vary only slowly.

Truxal, p. 560 [Ref. 6] declares:

In the case of a system with slow nonlinearity, the transfer function concept is valid and system behavior can be described in terms of poles and zeroes which wander slowly around the complex plane. In the case of a system with a fast nonlinearity, such as saturation, the conventional pole-zero, or transfer function, approach loses its significance. The describing function analysis ... is essentially to approximate a fast nonlinearity by a slow nonlinearity and, in this way; extend the transfer-function concepts to systems with fast nonlinearities.

The powerful tools of superposition and homogeneity do not obtain. Davis [Ref. 7] and Nichols utilized single-valued nonlinearities for sinusoids of fixed amplitude. These are all serious restrictions to be overcome if the parameter plane technique is to be useful as a synthesis tool for nonlinear active filters of specified frequency response.

### B. FILTER DESIGN CONSIDERATIONS (Weinberg [Ref. 8])

The Ideal low-pass filter is the basic building block of filter synthesis techniques. Characterized by the transfer function magnitude squared:



$$|z_{21}(j\omega)|^2 = \frac{1}{1 + A_n(\omega^2)} \quad \text{where } A_n(\omega^2) \ll 1 \text{ for } 0 \leq \omega \leq 1$$

$$\text{and } A_n(\omega^2) \gg 1 \text{ for } \omega > 1,$$

its characteristic is the ideal to which the Butterworth, Bessel, Chebyshev, and Butterworth-Thompson realizations are compared. Figure 1 depicts the ideal filter case.

The Butterworth approximation, known as the maximally flat case, is characterized by a transfer function magnitude squared:

$$|z_{21}(j\omega)|^2 = \frac{1}{1 + \omega^{2n}}.$$

Noticing the monotonicity of the Butterworth approximation, it can be concluded that as the degree of the polynomial (the number of reactive elements) is increased more of the passband has small attenuation and the rate of roll-off is increased. The plot of  $|z_{21}(j\omega)|^2$ , as a function of radian frequency with the parameter 'n' indicated, is demonstrated in Figure 2. In the s-domain, the normalized values of roots for the Butterworth polynomial, regardless of degree, fall on the unit circle.

The Chebyshev approximation, having the equal-ripple property in the pass-band and stop-band, is characterized by a transfer function magnitude squared:

$$|z_{21}(j\omega)|^2 = \frac{1}{1 + \epsilon^2 R_n^2(\omega)}$$

where  $\epsilon$  is the ripple factor and  $R_n(\omega)$  is the Chebyshev rational function. The plot of the locus of the roots in the s-domain for a Chebyshev filter is an ellipse whose semi-major



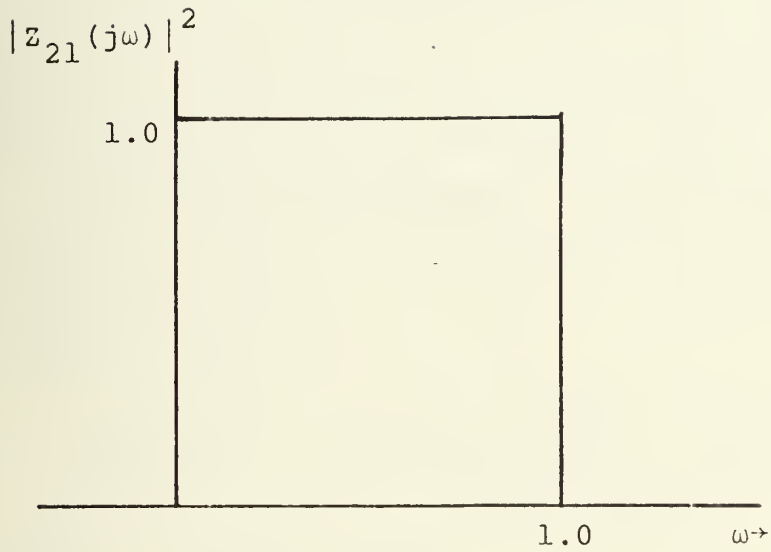


Figure 1. Ideal Low-Pass Filter.

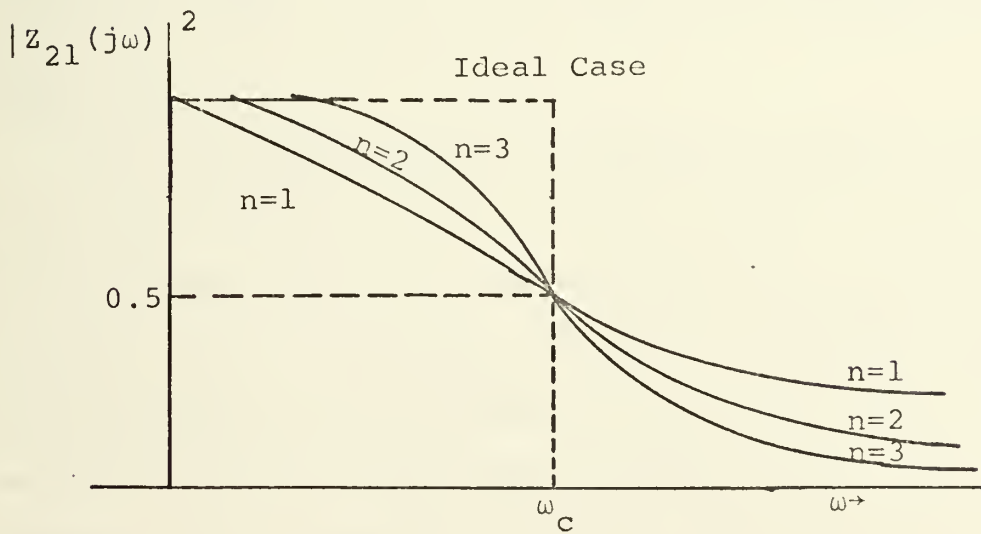


Figure 2. Butterworth Approximation (Not to Scale).



axis is  $\cosh \phi_2$  and whose semi-minor axis is  $\sinh \phi_2$ , where  $\phi_2$  is given by:

$$\phi_2 = \frac{1}{n} \sinh^{-1} (1/\epsilon)$$

Because of the ellipticity of the locus, the Chebyshev filter is referred to as an elliptical filter.

The Bessel approximation, known as the maximally flat time delay case, is characterized by a transfer function magnitude squared.

$$|Z_{21}(j\mu)|^2 = \frac{H^2}{\mu^{2(n+1)} \frac{\pi}{2\mu} [J_{-n-1/2}^2(\mu) + J_{n+1/2}^2(\mu)]}$$

where  $\mu = \omega/t_0 = \omega/\omega_0$

$\omega_0 \triangleq$  bandwidth

and where  $\sqrt{\frac{\pi}{2\mu}} J_{\pm(n+1/2)}(\mu)$  terms are the spherical Bessel functions.

By referring to Table I, transient response characteristics of the Butterworth filter, it can be seen that as the order of the filter increases, the overshoot to a unit step input voltage greatly increases. Table II, transient response characteristics of the Bessel filter, shows that the rise time becomes larger for high-order Bessel filters. The Butterworth-Thompson approximation realization has smaller overshoot than the Butterworth filter and better rise time than the Bessel filter [Ref. 8, p. 506].

Frequency transformation and duality techniques may be used to obtain high-pass, band-pass, or band-stop filter





TABLE I. Butterworth Transient Response Characteristics

Degree n	Percent Overshoot	Risetime
1	0	2.20
2	4.3	2.15
3	8.15	2.29
4	10.9	2.43
5	12.8	2.56

TABLE II. Bessel Transient Response Characteristics

Degree n	Percent Overshoot	Risetime
1	0	2.20
2	0.43	2.73
3	0.75	3.07
4	0.83	3.36
5	0.76	3.58



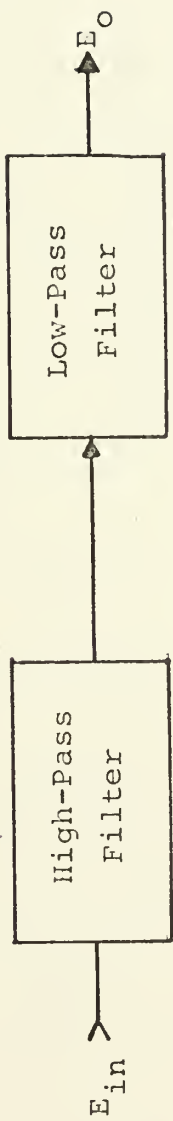
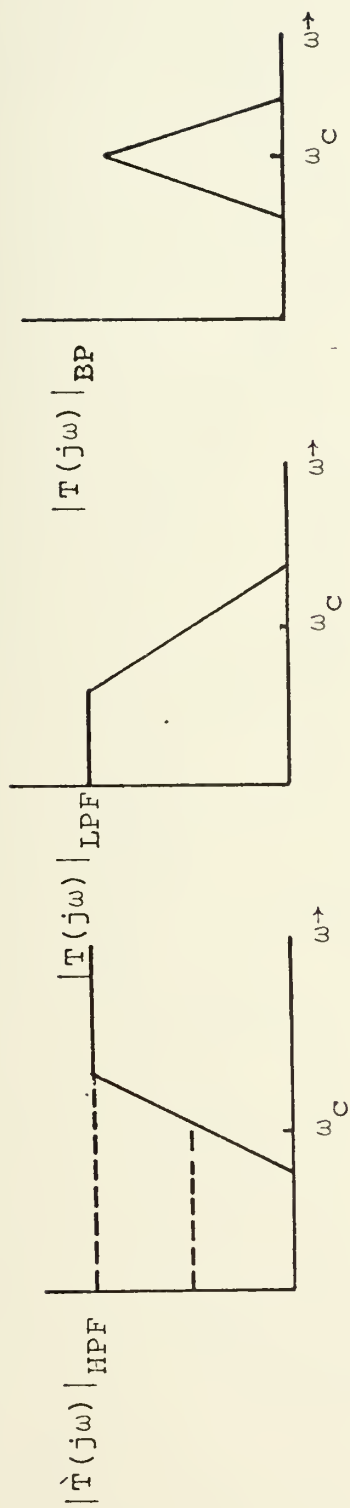
parameters in terms of the prototype low-pass filter parameter. In addition, cascading and concatenation of high-pass and band stop filters permit realizations of band pass and band stop filters respectively (see Figures 3 and 4).

Weinberg, p. 536, points out some basic limitations to the frequency transformation method: excessive number of components, element values widely spread, and susceptibility to parasitics.

In active filter design considerations, several approaches to design have evolved. Tow [Ref. 9] demonstrates the use of conventional passive filter synthesis techniques modified to effect active realizations. His use of the standard building blocks of second-order functions, realized with RC elements and operational amplifiers, permits individual tuning and cascading blocks to realize the required transfer function

Moschytz in a series of articles (June 1967 [Ref. 10], December 1968 [Ref. 11], January 1970 [Ref. 12], June 1970 [Ref. 13], and September 1970 [Ref. 14]) postulates the use of negative impedance converters (NIC), gyrators, operational amplifiers, automatic phase-locked loops, and frequency-emphasizing networks to implement linear active filters. In Ref. 14 he discounts the use of the negative-impedance converter because of practical problems in its realization. Table III, reproduced from page 64 [Ref. 14], gives the characteristics of hybrid integrated circuits. Moschytz emphasizes that the key to hybrid filter design is the high quality and low cost of commercially available monolithic, silicon operational amplifiers. He, page 65 [Ref. 14], notes that "economically competitive, active filters must employ integrated-circuit-processing techniques and, for the sake of filter stability,





$$T(j\omega) \triangleq \frac{E_o(j\omega)}{E_{in}(j\omega)}$$

Figure 3. Cascading Networks to Obtain Bandpass Filter



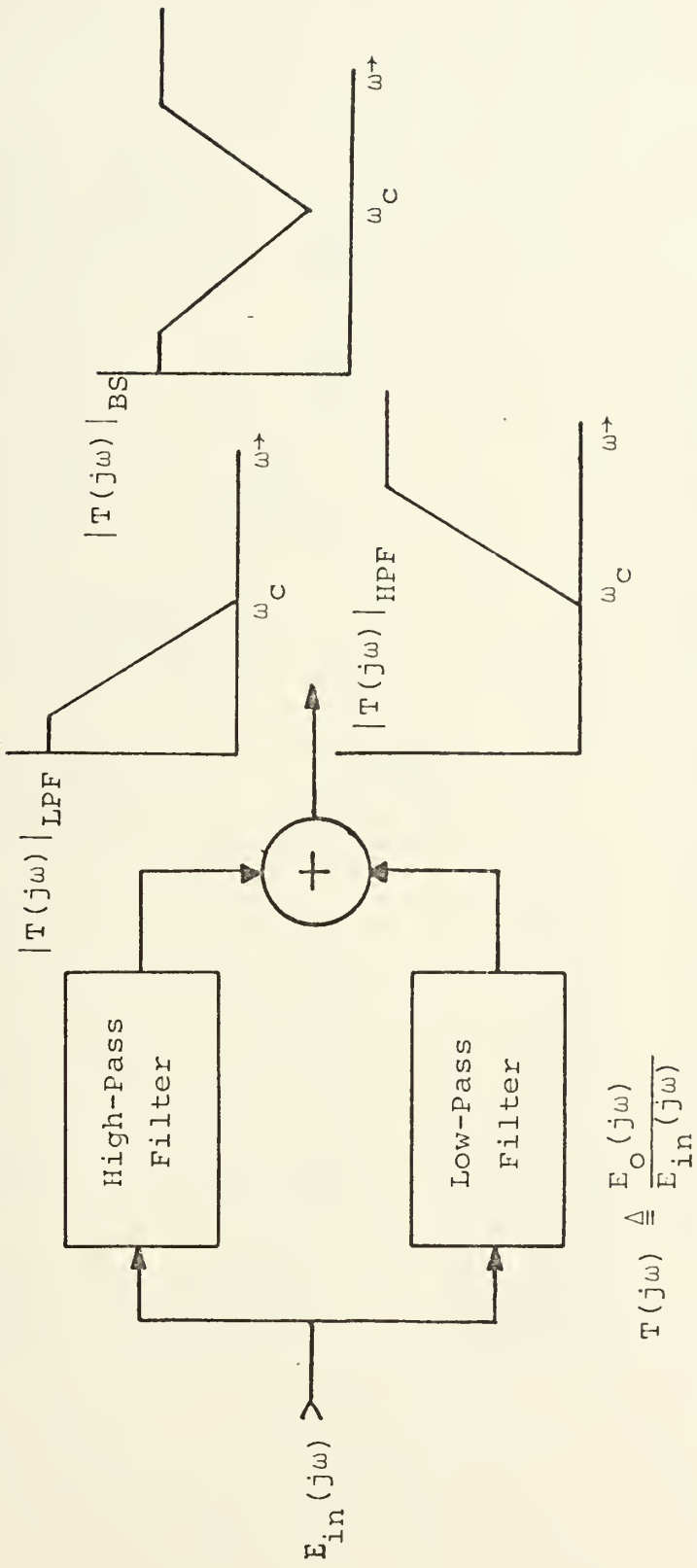


Figure 4. Concatenating Networks to Obtain Band-Stop Filter.





Type	Frequency Range	Maximum Pole Q	$\frac{\Delta f}{f}$ , %	$\frac{\Delta Q}{Q}$ , %	Functional Versatility	Complexity	Power Consumption	Signal Dynamic Range, 20 dB S/N	Compatibility with HIC Technology
Gyrotor <sup>a</sup>	0-350 kHz	500	0.2-0.8	10-25	Excellent (includes bidirectional circuits)	Fair (two gyrotors or floating gyrator per floating inductor)	(Not reported)	(Not reported)	Fair (may require FETs or high-beta p-n-p transistors)
Single-loop op amp	0-100 kHz	20 <sup>c</sup>	0.36-0.5 <sup>d</sup>	5	Good	Good	Good (one op amp) <sup>e</sup>	50 dB <sup>e</sup>	Good
Multiloop <sup>b</sup>	0-100 kHz	500	0.36-0.5 <sup>d</sup>	5	Good	Fair	Fair <sup>c</sup>	50 dB <sup>e</sup>	Good
APLL <sup>a</sup>	0.1 Hz-25 MHz	400	<0.1%/°C		Poor (special-purpose FM filter and discriminator)	Fair	Fair	40-60 dB	Good

\* The characteristics mentioned here may be mutually exclusive.

Notes:

<sup>a</sup> Experimental silicon monolithic.

<sup>b</sup> Op amp: SIC; RC network: tantalum integrated circuit (TIC).

<sup>c</sup> Below 10 kHz  $Q_{max}$  for  $\Delta Q/Q = 5$  percent is 50; from 100 kHz to 1 MHz,  $Q_{min}$  is 5.

<sup>d</sup> 0.36 percent: 5-year life, 10° to 60°C, 95 percent humidity.

<sup>e</sup> 0.5 percent: 20-year life, 0° to 60°C, 95 percent humidity.

<sup>f</sup> Depends on op amp.

TABLE III. Characteristics of Hybrid Integrated Active Filters.



hybrid integrated circuit techniques must be used." To provide higher-Q filters, he recommends [Ref. 10 and 13] cascading of low-Q passive elements to achieve asymptotic behavior with the frequency emphasizing network, an active hybrid circuit, providing the higher -Q response shaping. The use of the automatic phase-locked loop in monolithic integrated circuit form as a frequency selective filter for a conglomerate of FM signals is discussed in Ref. 14.

Welling [Ref. 15] describes the use of conventional passive transfer function blocks in the input and feedback loops of operational amplifiers to realize active filters. Salerno [Ref. 16] utilizes state-variable and signal-flow-graph techniques in filter design with integrators and inverters simulating a given transfer function. Shepard [Ref. 17] uses unity-gain amplifiers with passive R-C filters to realize high-stability active filters. Hueisman [Ref. 18] is an excellent reference for the theory and design of active RC circuits. The Burr-Brown Handbook and Catalog [Ref. 19] and the Application Manual of Philbrick-Nexus [Ref. 20] provide pertinent circuits and some discussion of the theory of active filters.

The importance of monolithic/hybrid integrated circuit filter design utilizing, in many cases, conventional passive filter synthesis techniques has been established.



### C. BASIC MONOLITHIC/HYBRID INTEGRATED-CIRCUIT TECHNOLOGY CONSIDERATIONS

Integrated-circuit monolithic technology has advanced to the state where phase-locked loops [Gribene & Camenzind 1969], retriggerable monostable multivibrators [Gray and Walker 1970, Gray, Anderson and Walker 1970], high performance internally-compensated operational amplifiers [Fullagar], and analog multipliers [Bilotti 1968] have revolutionized filter design. Thin-film and thick-film techniques in hybrid technology have also permitted the realization of high  $-Q$  frequency shaping circuits as Moschytz' frequency emphasizing networks [Ref. 13].

For the types of elements realizable and expected performance of monolithic devices, see Table IV, reproduced from page 111. [Camenzind and Gribene 1969]. For operational amplifier dc characteristics see Table V, reproduced from page 45 [Ref. 12]. Figure 5 summarizes the modes of operation of a non-ideal operational amplifier. Desirable characteristics for a general purpose operational amplifier include low input current, small temperature sensitivity, large current and voltage output capability, high cutoff frequency, high slewing rate, high common mode rejection (if differential), relatively good stability from power supply variations, high input impedance, low output impedance, and high open-loop gain. The characteristics of the monolithic technology which lend themselves to relatively easy implementation of junction or metal oxide field-effect transistors and junction capacitors for non-linear-element use permit implementation of nonlinear active filters on a chip.



Type	Frequency Range	Maximum Pole Q	$\Delta f/f$ , %	$\Delta Q/Q$ , %	Functional Versatility	Complexity	Power Consumption	Signal Dynamic Range, dB S/N	Compatibility with HIC Technology
Gyrator <sup>a</sup>	0-350 kHz	500	0.2-0.8	10-25	Excellent (includes bidirectional circuits)	Fair (two gyrators or floating inductor)	(Not reported)	(Not reported)	Fair (may require FETs or high-beta p-n-p transistors)
Single-loop <sup>b</sup> op amp	0-100 kHz	20 <sup>c</sup>	0.36-0.5 <sup>d</sup>	5	Good	Good	Good (one op amp) <sup>e</sup>	50 dB <sup>e</sup>	Good
Multi-loop <sup>b</sup>	0-100 kHz	500	0.36-0.5 <sup>d</sup>	5	Good	Fair	Fair <sup>e</sup>	50 dB <sup>e</sup>	Good
APLL <sup>c</sup>	0.1 Hz-25 MHz	400	<0.1%/°C		Poor (special-purpose FM filter and discriminator)	Fair	Fair	40-60 dB	Good

\* The characteristics mentioned here may be mutually exclusive.

- Notes:
- <sup>a</sup> Experimental silicon monolithic.
- <sup>b</sup> Op amp: SIC; RC network: tantalum integrated circuit (TIC).
- <sup>c</sup> Below 10 kHz  $Q_{max}$  for  $\Delta Q/Q = 5$  percent is 50; from 100 kHz to 1 MHz,  $Q_{max}$  is 5.
- <sup>d</sup> 0.30 percent: 5-year life, 10° to 60°C, 95 percent humidity, 0.5 percent; 20-year life, 0° to 60°C, 95 percent humidity.
- <sup>e</sup> Depends on op amp.

TABLE IV. Typical Performance of Integrated Circuit Components.





	Inverting Mode	Noninverting Mode
Ideal closed-loop gain	$\alpha_I = -\frac{R_F}{R_G}$	$\alpha_N = \frac{R_F + R_G}{R_G}$
Forward gain	$A_I \approx \frac{A_o}{(1 + \epsilon_o)(1 + \beta_o \epsilon_i)}$	$A_N \approx \frac{A_o}{1 + \epsilon_o'}$
Feedback factor	$\beta_I = \beta_o \frac{1 + \beta_o \epsilon_i}{1 + 2\beta_o \epsilon_i}$	$\beta_N = \frac{\beta_o}{1 + 2\beta_o \epsilon_i}$
Loop gain	$A_I \beta_I \approx \frac{A_o \beta_o}{(1 + \epsilon_o)(1 + 2\beta_o \epsilon_i)}$	$A_N \beta_N \approx \frac{A_o \beta_o}{(1 + \epsilon_o')(1 + 2\beta_o \epsilon_i)}$
Gain error	$E_I = \frac{1}{A_I \beta_I} - \left( \frac{1}{A_I \beta_I} \right)^2 + \dots \approx \frac{1}{A_I \beta_I}$	$E_N = \frac{1}{A_N \beta_N} - \left( \frac{1}{A_N \beta_N} \right)^2 + \dots \approx \frac{1}{A_N \beta_N}$
Closed-loop gain	$G_I = \alpha_I \frac{A_I \beta_I}{1 + A_I \beta_I} \approx \alpha_I (1 - E_I)$	$G_N = \alpha_N \frac{A_N \beta_N}{1 + A_N \beta_N} \approx \alpha_N (1 - E_N)$
Feedback resistor for minimum gain error	$R_{F E_{I,min}} = \left[ \frac{R_i R_o}{2} (1 - \alpha_I) \right]^{1/2}$	$R_{F E_{N,min}} = \left[ \frac{R_i R_o}{2} (\alpha_N - 1) \right]^{1/2}$
Input impedance	$(Z_{in})_I \approx R_i \left( 1 + \frac{\alpha_I}{A_o} \right)$	$(Z_{in})_N \approx A_N \beta_N R_i$
Output impedance	$(Z_o)_I \approx \frac{R_o}{A_I \beta_I}$	$(Z_o)_N \approx \frac{R_o}{A_N \beta_N}$

Nomenclature Definitions (see Figure 5)

$\beta_o \triangleq$  Feedback Factor of Ideal Amplifier

$$= \frac{R_G}{R_G + R_F}$$

$$\epsilon_o \triangleq R_o / R_F$$

$$\epsilon_i \triangleq R_F / R_i$$

$$\epsilon_o' \triangleq (R_o / R_F) (1 - \beta_o)$$

TABLE V. Operational Amplifier DC Characteristics (First Column is Inverting Mode, Second - Non-inverting).



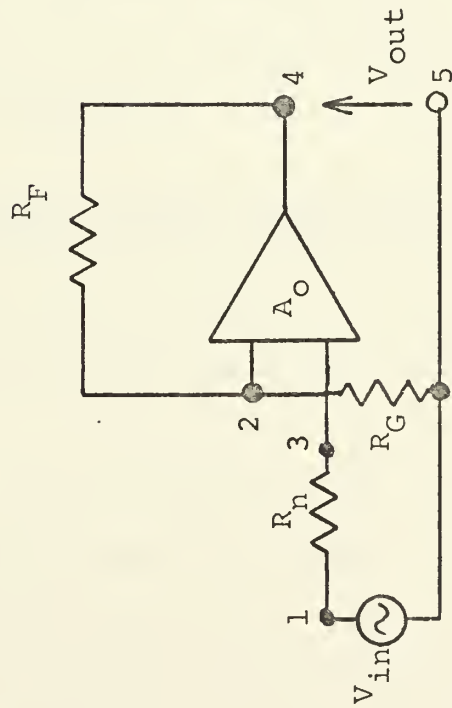
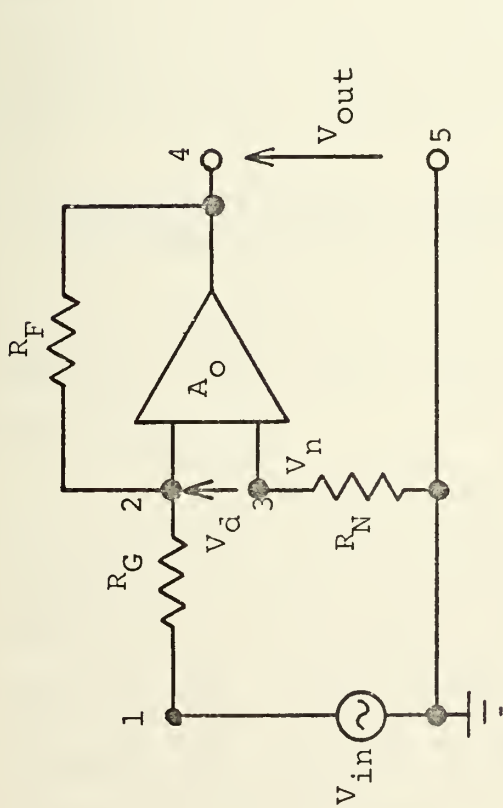
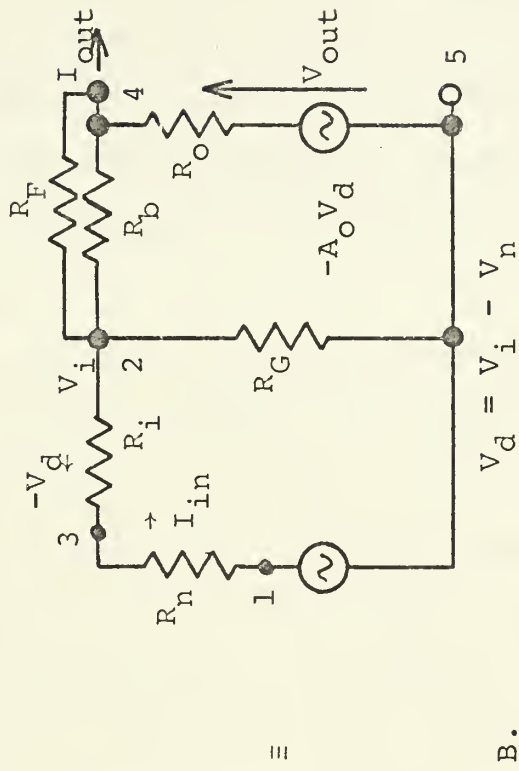
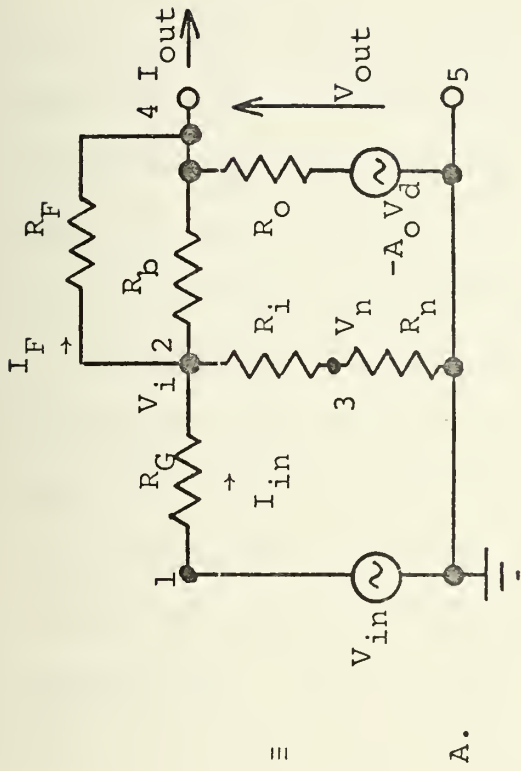


Figure 5. Nonideal Operational Amplifier with Equivalent Circuit Diagram. A - Inverting Mode. B - Noninverting Mode.



Incorporation of thin-film techniques and several monolithic chips leads to hybrid circuitry which has the advantages of wider ranges of component values and reduction of parasitic effects, but has the disadvantages of increased cost, increased number of bonding operations required, lower yield, and less reliability.

Integrated circuits, in general, have the advantages of providing: high density of active elements for a given package size, good temperature tracking because of good thermal coupling, close matching of components, consistent topology of devices, and the availability of a large class of nonlinearities. Some of the disadvantages of integrated circuits are: the lack of wide range of component values, limited number of devices available, limited power output, sensitivity to parasitics, large absolute value tolerance, and, especially for filtering, the lack of inductors.

#### D. DESIGN OF HYBRID INTEGRATED-CIRCUIT NONLINEAR ACTIVE FILTERS UTILIZING FREQUENCY RESPONSE SPECIFICATIONS

The approach to design that each class of nonlinear filters: low-pass, high-pass, band-pass, and band-stop will take is the following:

1. A given class of filter consistent with the general frequency response specification will be chosen. An arbitrary resistor will be chosen as the parameter  $\alpha$ , the nonlinear resistance, and the transfer function for the parameter plane computer program will be obtained. A preliminary sensitivity analysis for each resistor would permit an optimal choice of the resistor for the nonlinear resistance.



2. The linear R-C operational amplifier filter will be constructed utilizing values of components derived from active filter synthesis techniques.

3. The nonlinear resistance characteristic, as a function of frequency, will be obtained experimentally for the particular field-effect transistor. Previously the nonlinear-device controller will have been programmed to provide the general behavior necessary to go from the high-resistance state to the low-resistance state as frequency is increased or vice-versa. An  $\alpha$  characteristic, experimentally derived, will be obtained.

4. The  $\alpha$  characteristic will then be superimposed on the PARTFl computer analysis Bode plots and the predicted frequency response of the nonlinear filter obtained.

5. The frequency response of the nonlinear filter will be measured and compared to the results of 4. In some cases, particularly the low-pass filter, additional frequency response data will be taken. The principle of superposition will be tested by superimposing two frequencies in a specified frequency range. The transient response of the filter will be monitored.

Note: It is recognized that the normal approach to design would require that the specified frequency response be superimposed on the parameter plane Bode plots first, and then the required frequency-dependent nonlinearity obtained. The synthesis approach as set forth here was predicated on accepting the nonlinear characteristic available and then proceeding with the analysis. It is felt that no loss of the applicability of the synthesis technique obtains.





### III. NONLINEAR DEVICE CONSIDERATIONS

#### A. INTRODUCTION

Although monolithic/hybrid integrated circuit technology provides the use of NPN/PNP transistors, field effect transistors, diodes, variable-capacitance diodes, tunnel diodes, and other nonlinear devices, only the discrete field-effect transistor will be investigated in this thesis. For a complete description of integrated circuit components available with attendant theoretical discussions, see Warner; Lynn, Meyer, and Hamilton; Camenzind; and Hibberd. All of the above components have potential use as voltage-controlled or frequency-dependent nonlinearities for active filters.

The mutator, an element for transforming a nonlinear resistor into a nonlinear inductor or a nonlinear capacitor, is presented in [Ref. 21, Chua, 1968] and [22, Chua, 1969]. The gyrator, a member of the mutator family, transforms a nonlinear capacitor into a nonlinear inductor, or vice-versa.

In addition, the reflector and scalar [Refs. 21 and 22] permit reflecting and scaling an  $i-v$ ,  $\phi-i$ , or  $q-v$  characteristic in the plane of consideration. Using these circuits, a nonlinear resistor can be transformed into another nonlinear resistor, a nonlinear capacitor, or a nonlinear inductor of specified characteristics.



## B. JUNCTION AND INSULATED GATE FIELD-EFFECT TRANSISTOR

There are two main types of field-effect transistors; the junction field-effect transistor (referred to as JFET) and the insulated-gate field-effect transistor (referred to as IGFET). The insulated-gate FET is also referred to as the metal-oxide-semiconductor FET (MOSFET). For a pictorial representation of the junction FET, see Figure 6; the enhancement IGFET is depicted in Figure 7; the depletion IGFET is shown in Figure 8.

FET's may also be characterized by their mode of operation: Type-A-depletion; Type B-depletion/enhancement; and Type C-enhancement only. Figure 9 illustrates the transfer characteristic of these modes [Motorola Application Note 211A].

The doping of the channel, whether n-type or p-type impurity, also causes further classification of FET's. Conventional methods are used to determine the polarities of terminal voltages and currents for an FET; i.e. an n-channel FET has positive drain-to-source voltage, with positive  $I_D$ , and  $V_{GS}$  negative for the depletion mode. The p-channel FET has negative drain-to-source voltage, with negative  $I_D$ , and  $V_{GS}$  positive for the depletion mode or negative for the enhancement mode. Thorough description of the theory of operation of these devices is included in chapter 14, Millman and Halkias [Ref. 23], and in chapters 9 and 10 in Gray and Searle [Ref. 24]. The principle that permits the use of the FET as a voltage-dependent nonlinearity is that in the region of operation before pinch-off occurs, the drain current varies linearly



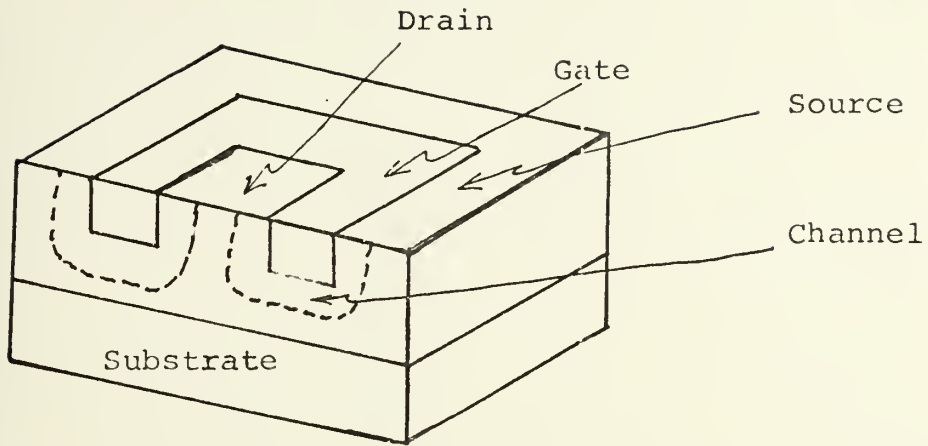


Figure 6. Junction Field-Effect Transistor.

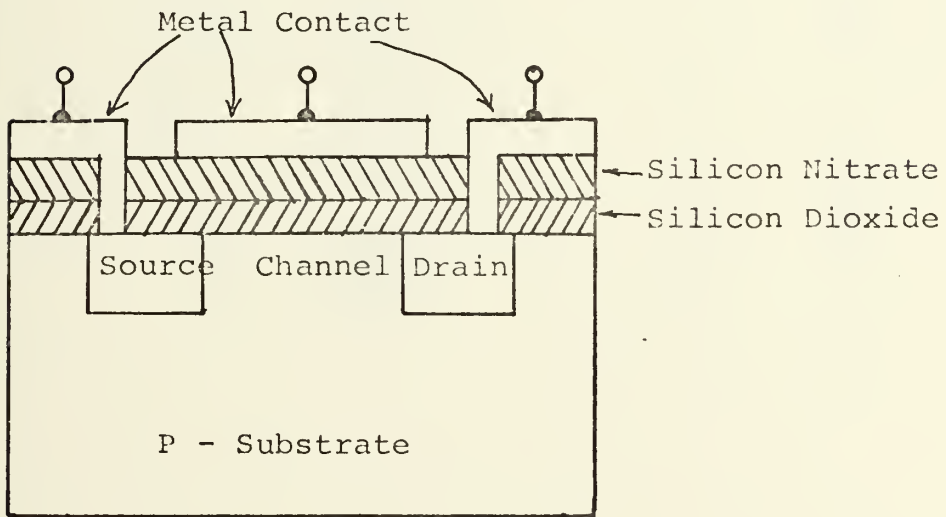


Figure 7. Enhancement IGFET.



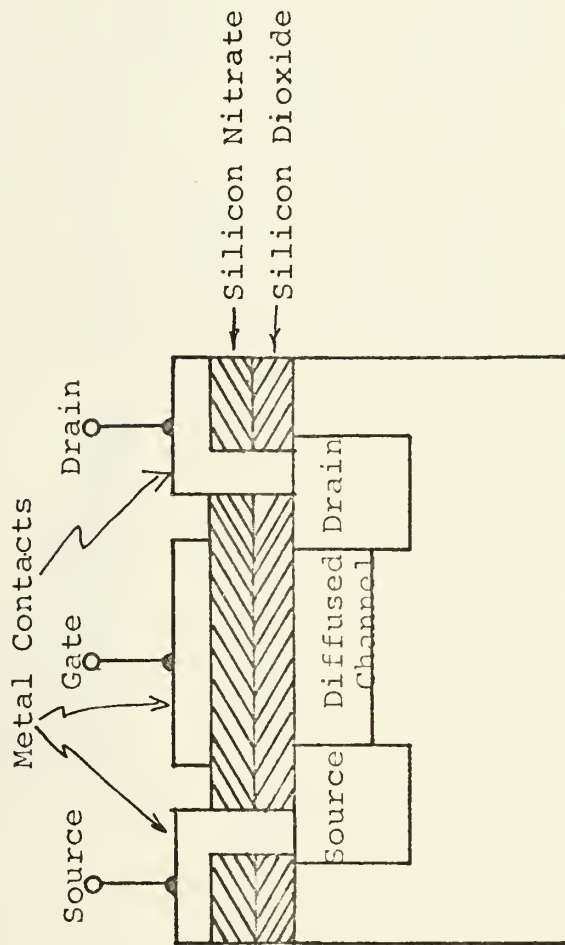


Figure 8. Depletion IGFET.





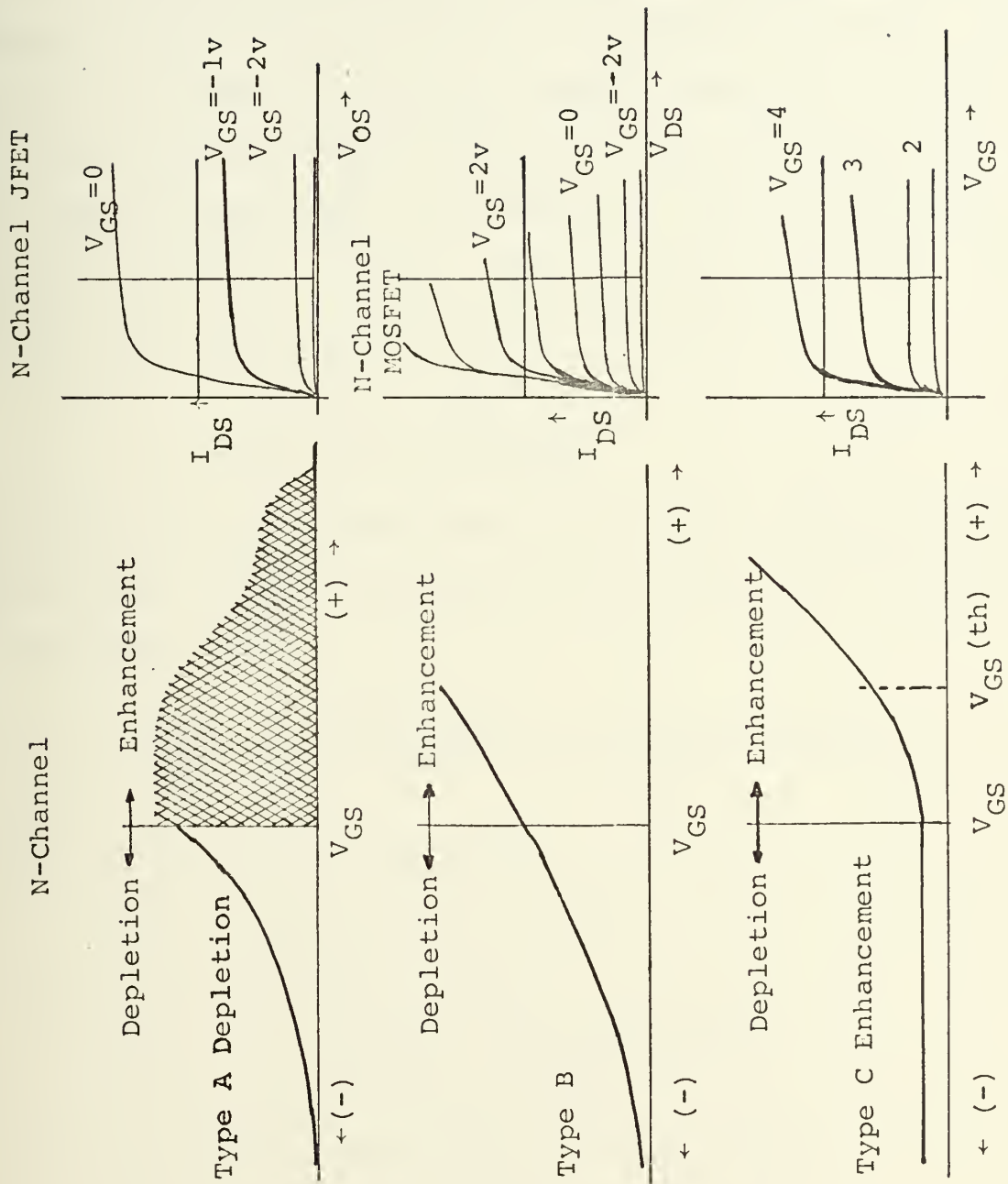


Figure 9. Transfer Characteristics of FET's.



with drain-source voltage (triode region of operation). The electric field produced by the back-biased gate-source junction or the electric field across the dielectric between gate and channel causes the resistivity of the channel to vary. Thus a plot of a family of  $I_{DS}-V_{DS}$  curves, with  $V_{GS}$  as a parameter, will be a set of straight lines, all passing through the origin; in addition, the slope of a particular line will be determined by the gate-source voltage. Gosling [Sept. 1965, Ref. 25], cites the value of drain-source resistance as:

$$R_{DS} = \frac{R_0}{\{1 - (V_{GS}/W_0)^{\frac{1}{2}}\}}$$

where  $R_0$  and  $W_0$  are predetermined constants and  $V_{GS}$  is the gate-source voltage. Equation 14-5, [Ref. 23] cites the conductance to be:

$$\frac{I_D}{V_{DS}} = \frac{1}{R_{DS}} = \frac{2aweN_D\mu_n}{L} [1 - (V_{GS}/V_p)^{\frac{1}{2}}] \quad (\text{JFET})$$

where  $V_p \triangleq$  pinch-off voltage

$V_{GS} \triangleq$  gate-to-source voltage

$L =$  length of channel

$N_D =$  donor density [electrons/cm<sup>3</sup>]

$W =$  perpendicular distance to 'a'

$a =$  zero drain current channel width

$e =$  electronic charge

$\mu_n =$  donor mobility

Area =  $2aw$ , channel area at zero drain current.



Reference 24, p. 343, shows, when  $V_{DS} \ll V_{GS}$ ; for the MOSFET:

$$R_{DS} = \frac{WL}{h\mu_e \epsilon} \frac{1}{V_{GS}}$$

where  $L$  = length of channel  
 $W$  = thickness of oxide layer  
 $h$  = width of channel  
 $\epsilon$  = dielectric permittivity of the oxide layer  
 $\mu_e$  = electron mobility

and for the JFET [Ref. 24, p. 354] when  $V_{DS} \ll V_{GS}$ :

$$G = G_o \left[ 1 - \left( \frac{V_{GS}}{V_p} \right)^{\frac{1}{2}} \right]$$

where  $G_o = \frac{2q\mu_e N_o ha}{L}$

$$N_o = N_D$$

$q$  = electron charge

$h$  = height of channel

$a$  = zero drain current halfwidth

A typical depletion junction FET is the 2N3819 (n-channel), or the 2N3820 (p-channel). Experimental plots of the triode region of JFET type 2N3819 are shown in Figure 10. Photographs of characteristic curves for specified FET's are shown in Figures 11 and 12. Note that at zero gate-source voltage, drain current is maximum and that current decreases as gate-source voltage is increased, for a given drain-source voltage. Note also that the n-channel FET, 2N3819, has greater current flow for a given  $V_{DS}/V_{GS}$  combination than the 2N3820.



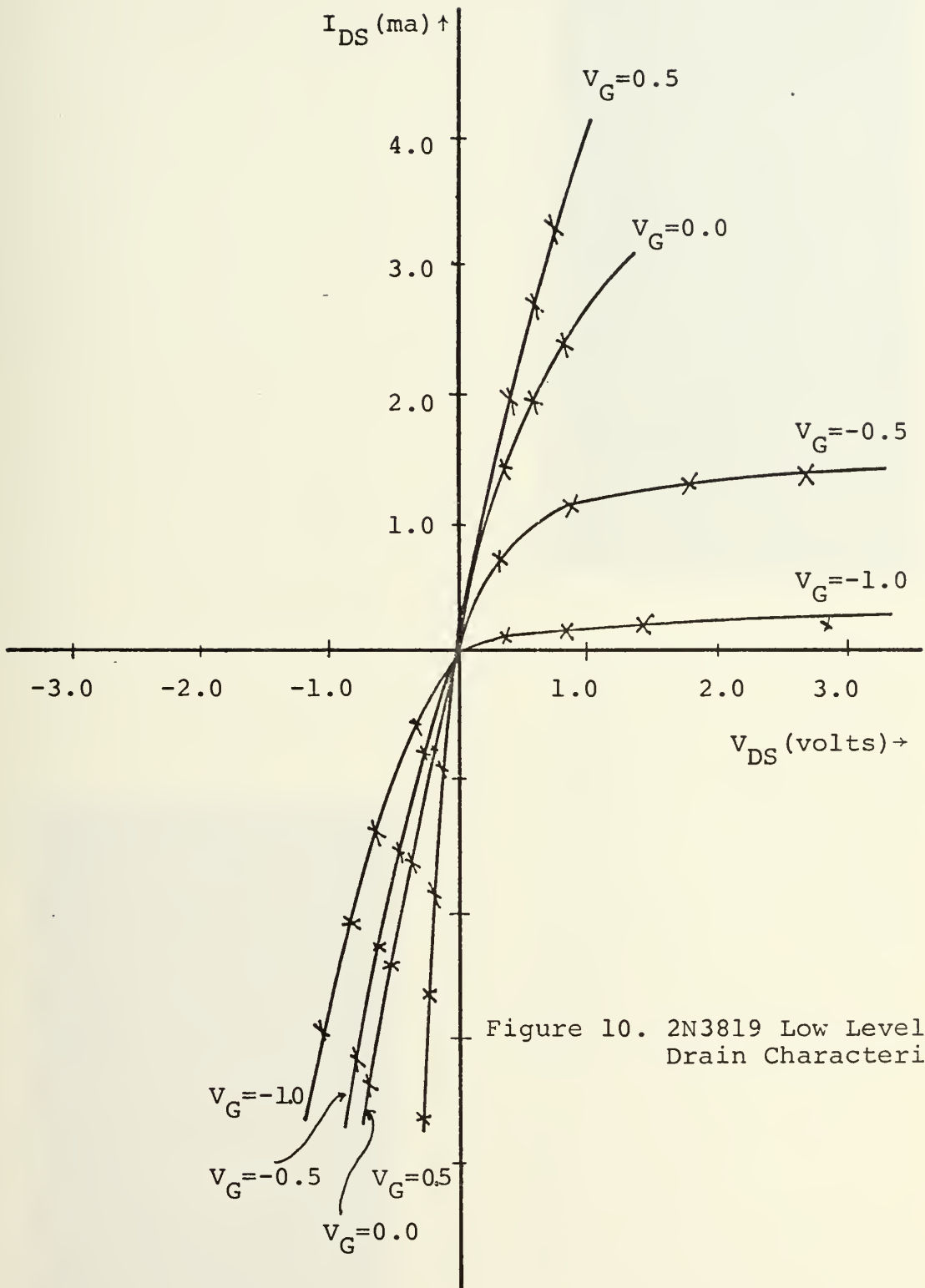


Figure 10. 2N3819 Low Level Drain Characteristic





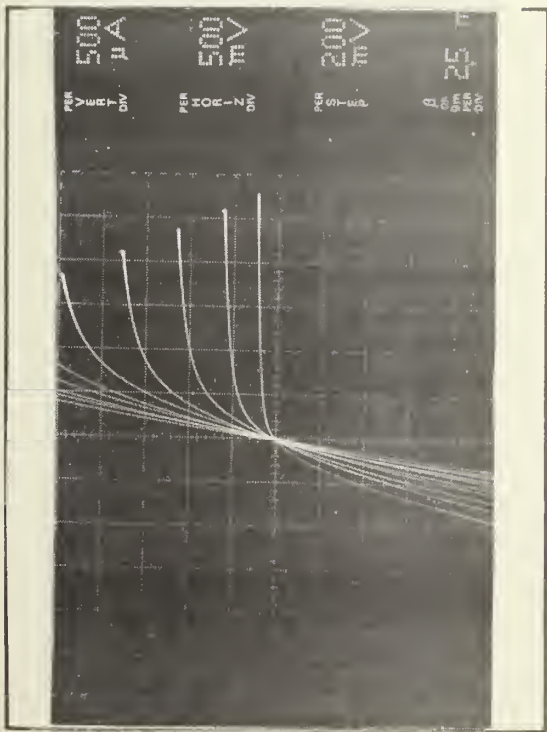
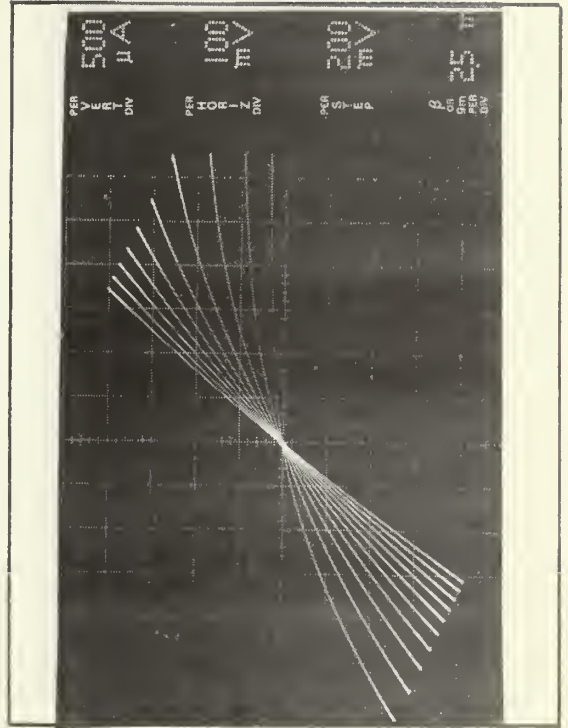


Figure 11. 2N3819 Low Level Drain  
 Characteristic Photographs  
 $I_{DS}$  vs.  $V_{DS}$ ; parameter is  
 $V_{GS}$ .





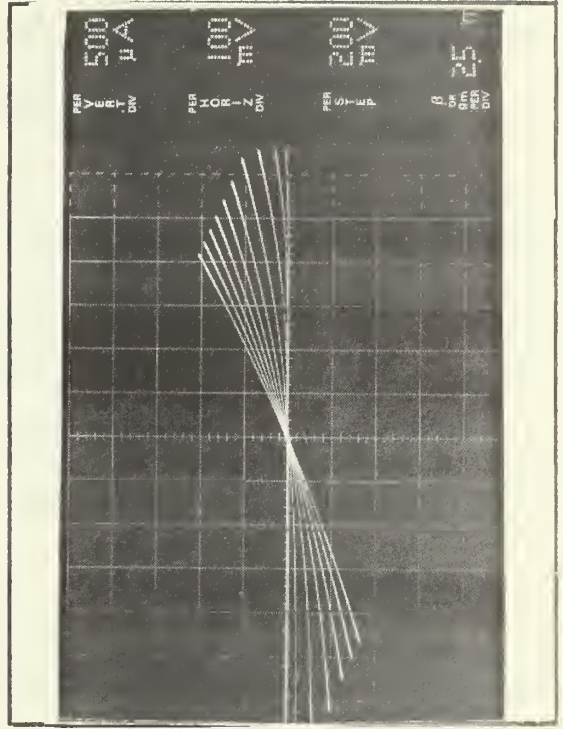
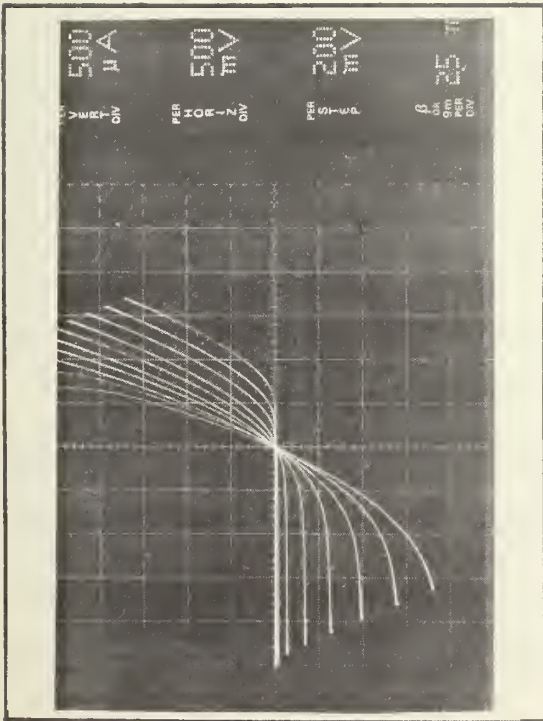


Figure 12. 2N3820 Low Level Drain  
 Characteristic Photographs  
 $I_{DS}$  vs.  $V_{DS}$   $\cdot V_{GS}$  is the  
 parameter.



A typical depletion-type insulated-gate FET is the 3N138. Experimental plots of the triode region are shown in Figure 13. Photographs of operating conditions of the 3N138 are shown in Figure 14.

A typical enhancement-type insulated-gate FET is the 3N172. Low level drain characteristics are shown in Figure 15. Note that when  $V_{GS}$  is zero little drain current flows and as the electric field is enhanced by increasing the gate-source voltage the resistivity of the channel is decreased and current increases for a given  $V_{DS}$ .

Some of the advantages of the use of the FET as a nonlinear resistor are: the gate, in typical operation, draws no current; the mechanism for determining the resistivity is voltage-dependent; the FET is amenable to monolithic-hybrid integrated circuit technology, the FET is a unipolar type device; and the FET has no offset voltage or current.

One of the major disadvantages of the use of multiple discrete FET's in filter circuits is the poor tracking of parameters between units. A solution to this problem is effected by constructing multiple-FET's on a chip, either for monolithic or hybrid circuit use. Christensen and Wollesen present state-of-the-art techniques for the solution of this problem.

Another disadvantage of the FET is the relatively low dynamic range of  $V_{DS}$  for linear resistivity. A feedback scheme has been utilized to increase the dynamic range while retaining the linear  $V_{DS}/I_{DS}$  characteristic desired. Schematic diagrams for the conventionally-connected FET and the feed-back-connected



$V_g = 0.405$   
 $V_g = -1.25$

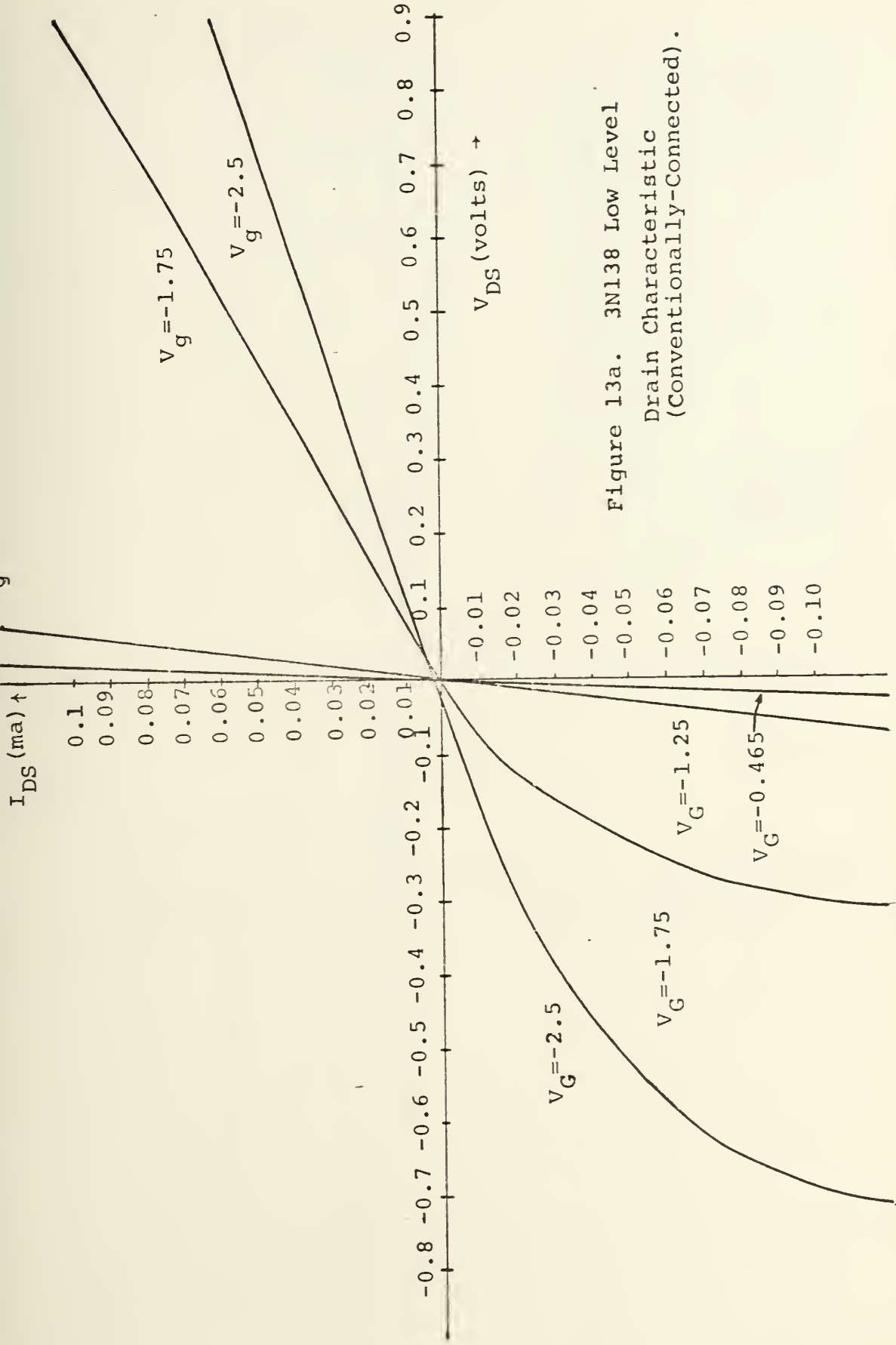


Figure 13a. 3N138 Low Level  
Drain Characteristic  
(Conventionally-Connected).





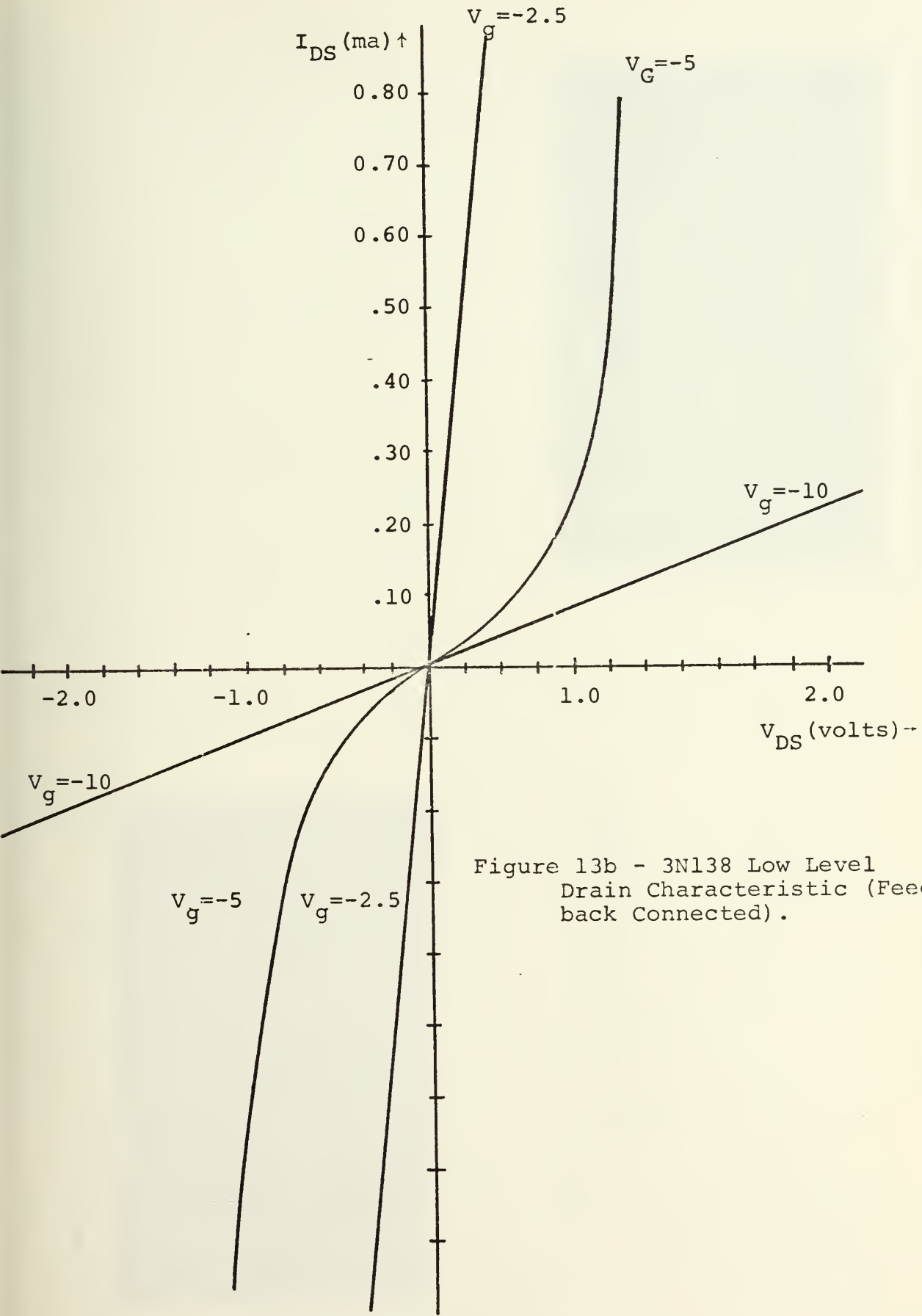


Figure 13b - 3N138 Low Level Drain Characteristic (Feedback Connected).



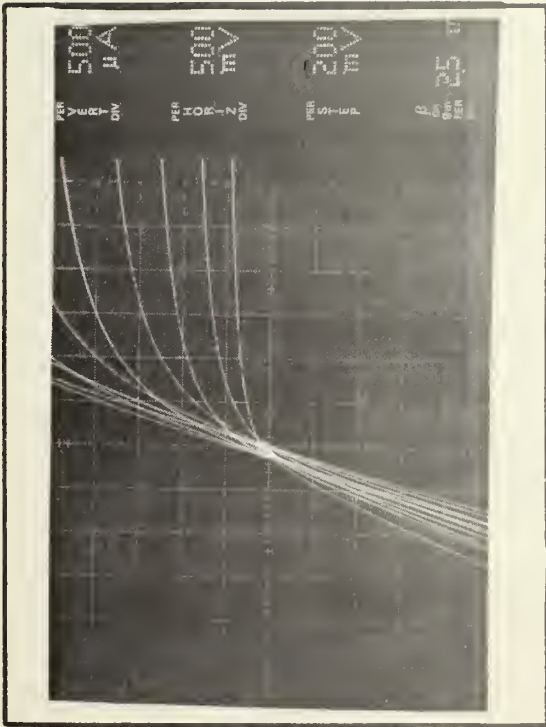
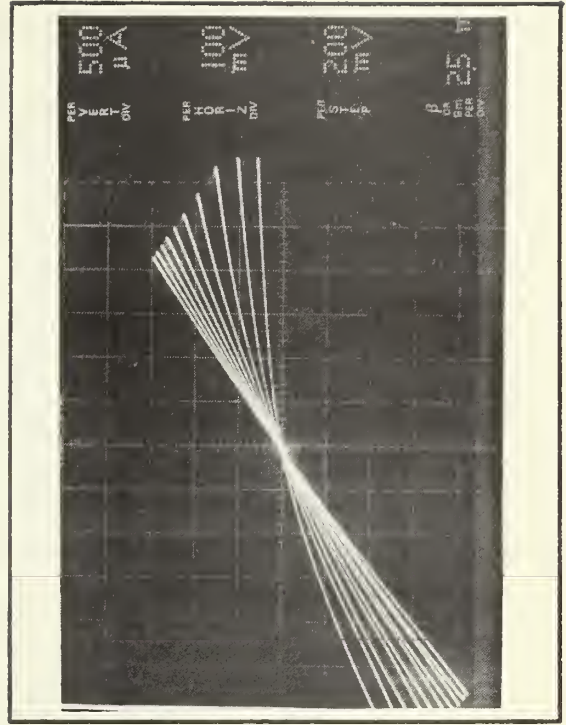


Figure 14. 3N138 Low Level Drain  
Characteristic Photographs  
 $I_{DS}$  vs  $V_{DS}$ ;  $V_{GS}$  is the  
parameter.





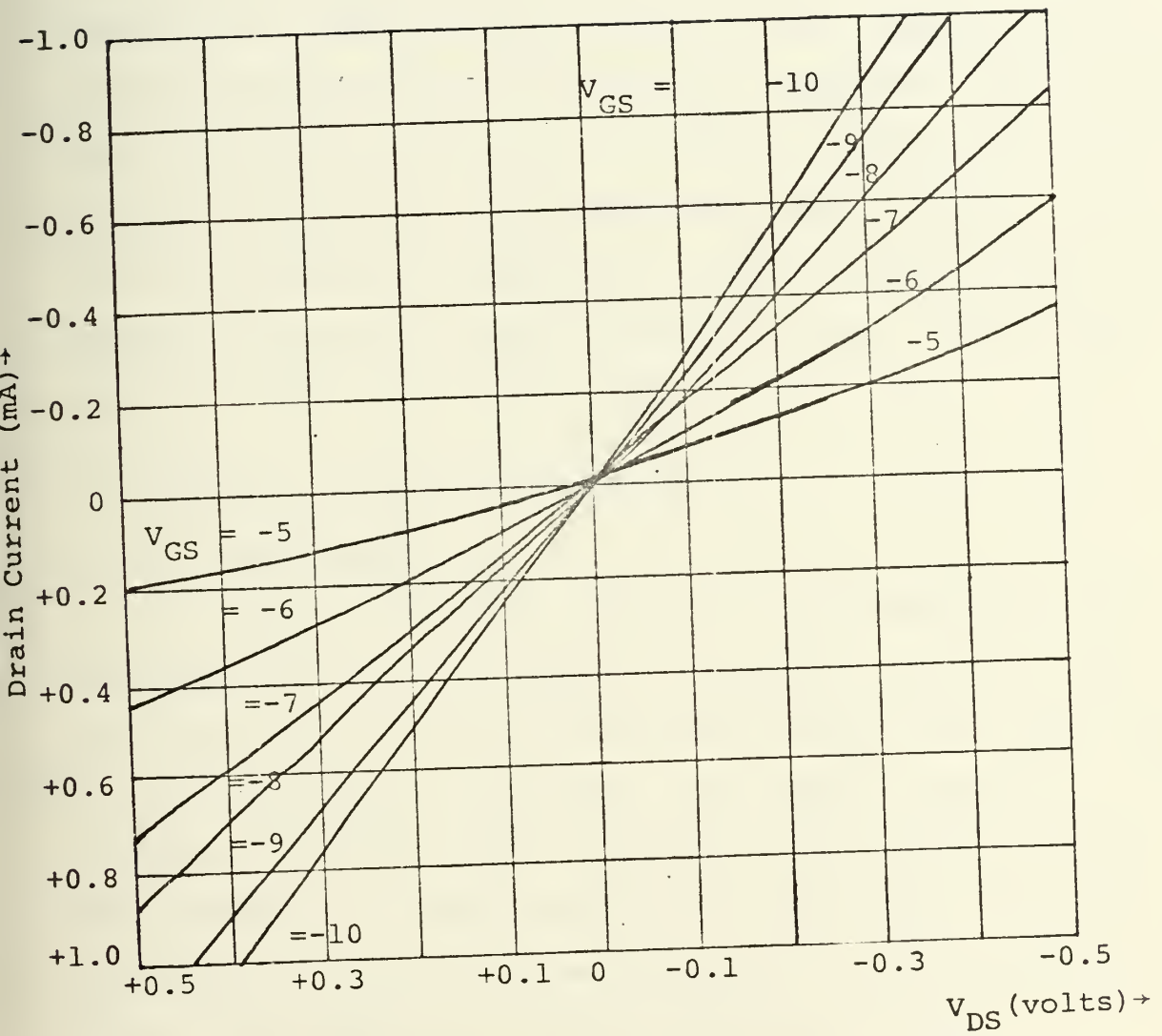


Figure 15. 3N172 Low Level Characteristics.



are shown in Figures 16 and 17 respectively. A comparison of the feedback--connected FET (Figure 18-2N381) and Figures 19, 20, 21 and 22-3N138) with the conventionally-connected FET (Figure 12-2N3819) and (Figure 14-3N138) should lead to the following conclusions. For limited  $V_{GS}$  in the case of the feedback-connected FET, the linearity of the device is improved for larger dynamic ranges of  $V_{DS}$ . But as the gate-source voltage continues to increase, quadratic type curvature is noted (see Figure 21). This, of course, will lead to harmonic distortion in the nonlinear filter circuits. The use of field-effect transistor in circuit applications is discussed thoroughly in Gosling [Sept. 1965-Ref. 25, Ref. 26], Morgan, Martin, Neu, and Crawford.

## C. VOLTAGE CONTROLLED ATTENUATORS

### 1. Introduction

There are two main types of FET voltage-controlled attenuators in use: the first, discussed by Gosling in Ref. 25, refers to the class of attenuators using the triode region of remote pinch-off transistors; the second, presented in this thesis and elsewhere [RCA Transistor Manual 1969], utilizes the transition of resistance from the pre-pinch-off region, the region of relatively low resistance, to the post-pinch-off region, the region of relatively high resistance.

### 2. Triode Region FET Voltage-Controlled Attenuator

Gosling, et al., make use of the linear  $I_{DS}-V_{DS}$  characteristics obtained in the triode region of FET operation. He cites the useful range of  $R_{DS}$  to be no more than a 10:1 ratio, and approximates the value of  $R_{DS}$  to be  $R_{DS} = R_O \exp$





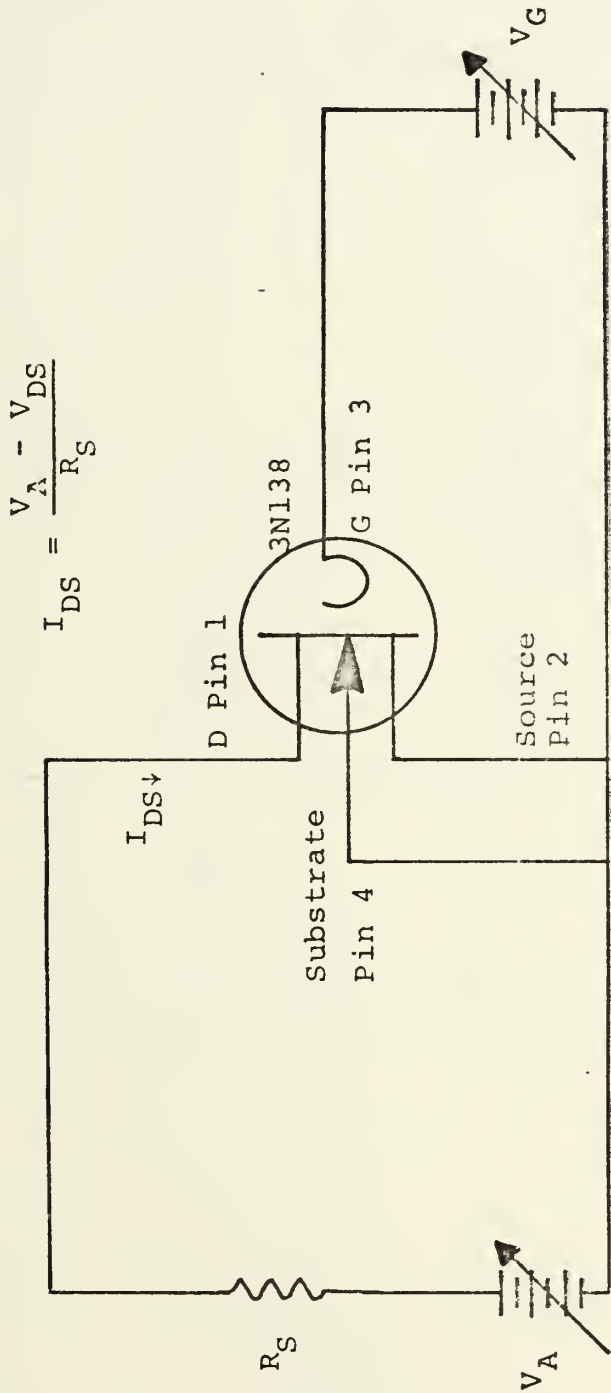


Figure 16. Conventionally-Connected 3N138 Test Circuit Schematic.



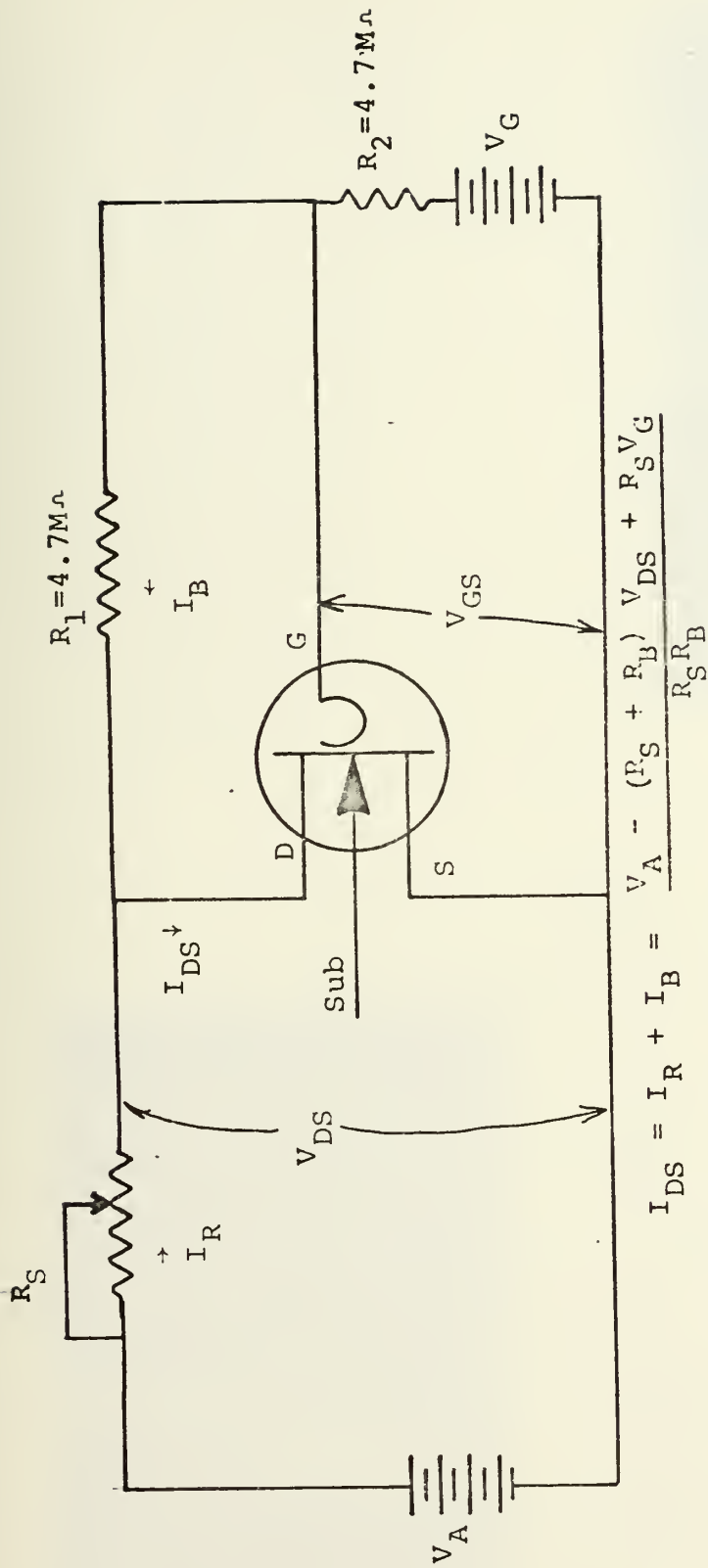


Figure 17. Feedback-Connected 3N138 Test Circuit Schematic.

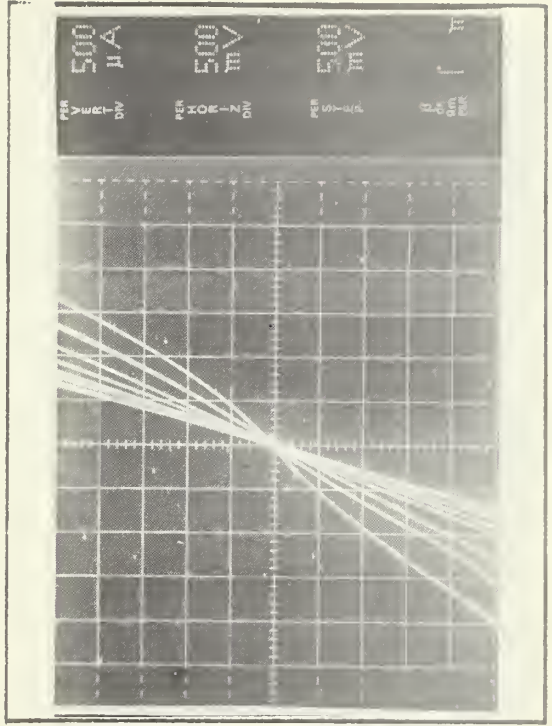




Figure 18. (Above) Feedback-Connected 2N3819 Low Level Characteristic Photographs.  $I_{DS}$  vs.  $V_{GS}$  is parameter.

Figure 19 (Below)

Feedback-Connected 3N138 Low Level Characteristic Photograph.  $I_{DS}$  vs.  $V_{DS} \cdot V_{GS}$  is parameter.





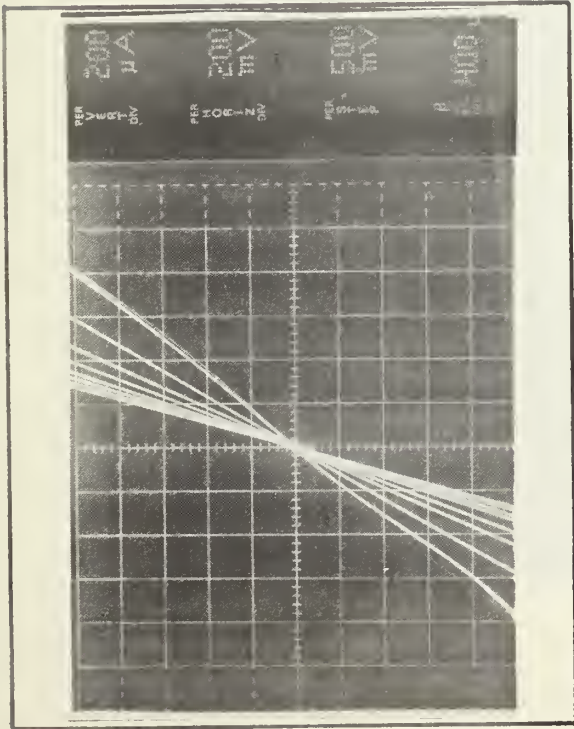


Figure 21 (Below) Feedback-Connected  
3N138 Low Level Characteristic  
 $I_{DS}$  vs.  $V_{DS} \cdot V_G$  is the parameter.

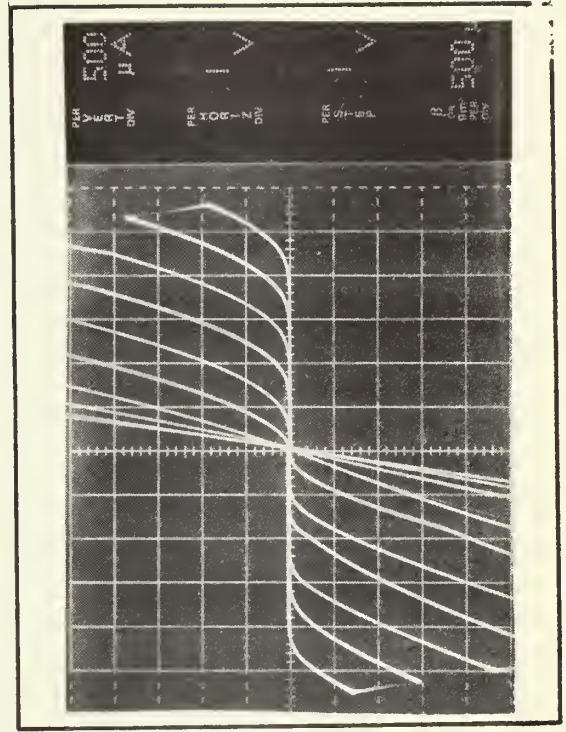


Figure 20 (Above) Feedback-Connected  
3N138 Low Level Characteristic  $I_{DS}$  vs.  
 $V_{DS} \cdot V_G$  is the parameter.





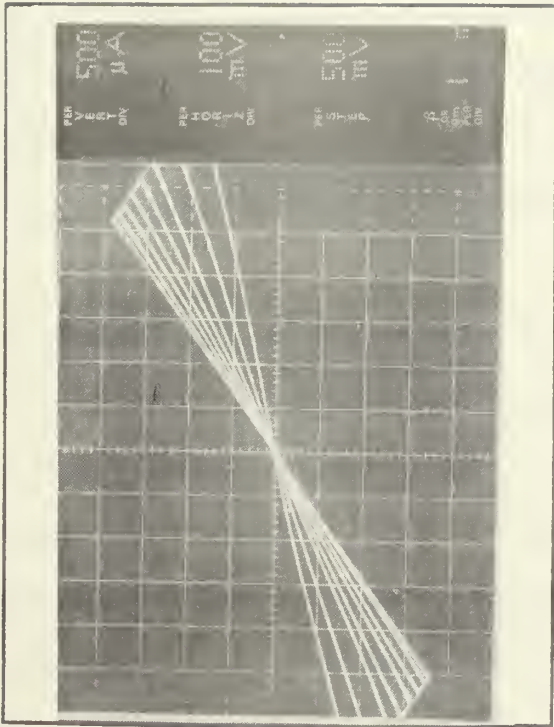


Figure 22 (Above) Feedback-Connected  
3N138 Low Level Characteristic  
Photograph  $I_{DS}$  vs.  $V_{DS}$  is the  
parameter.



$(\lambda V_{GS})$ , where  $\lambda$  and  $R_O$  are constants. He derives a relationship for the attenuation factor  $A$ , to be

$$\frac{E_{out}}{E_{in}} \triangleq A = \frac{\exp(\phi)}{1 + \exp(\phi)}$$

$$\text{where } \phi = \lambda V_{GS} + \log \frac{R_O}{R_1} .$$

The schematic diagram of the basic attenuator is shown in Figure 23. He determines the ratio of maximum attenuation factor,  $A_{max}$ , to minimum attenuation factor,  $A_{min}$ , to be

$$\frac{A_{max}}{A_{min}} = \frac{m}{1 + (m-1)A_{min}}$$

where  $m \triangleq$  ratio of maximum to minimum drain-source resistance. Figures 24 and 25, reproduced from [Ref. 25, p. 115], demonstrate the operation of the attenuator for varying series resistance size and harmonic distortion effects respectively.

The advantages of this type of attenuator are small signal distortion due to pinch-off transition and a nearly linear relationship between attenuation factor,  $A$ , and control voltage.

The disadvantages of this type of voltage-controlled attenuator are the range of the attenuation ratio is limited, the gate-source voltage (control) is limited in range, and the drain-source voltage range is limited.

### 3. Feedback-Connected FET Voltage-Controlled Attenuators

The use of the feedback-connected FET results in a larger dynamic range of  $V_{DS}$  and  $R_{DS}$ . For a series resistance of 100 k $\Omega$ , the input voltage to the attenuator was varied from



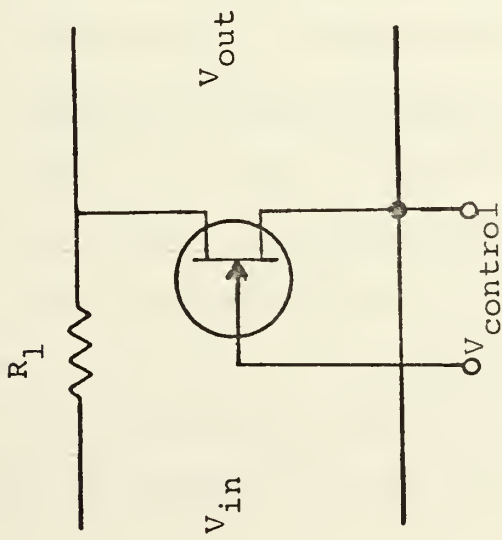
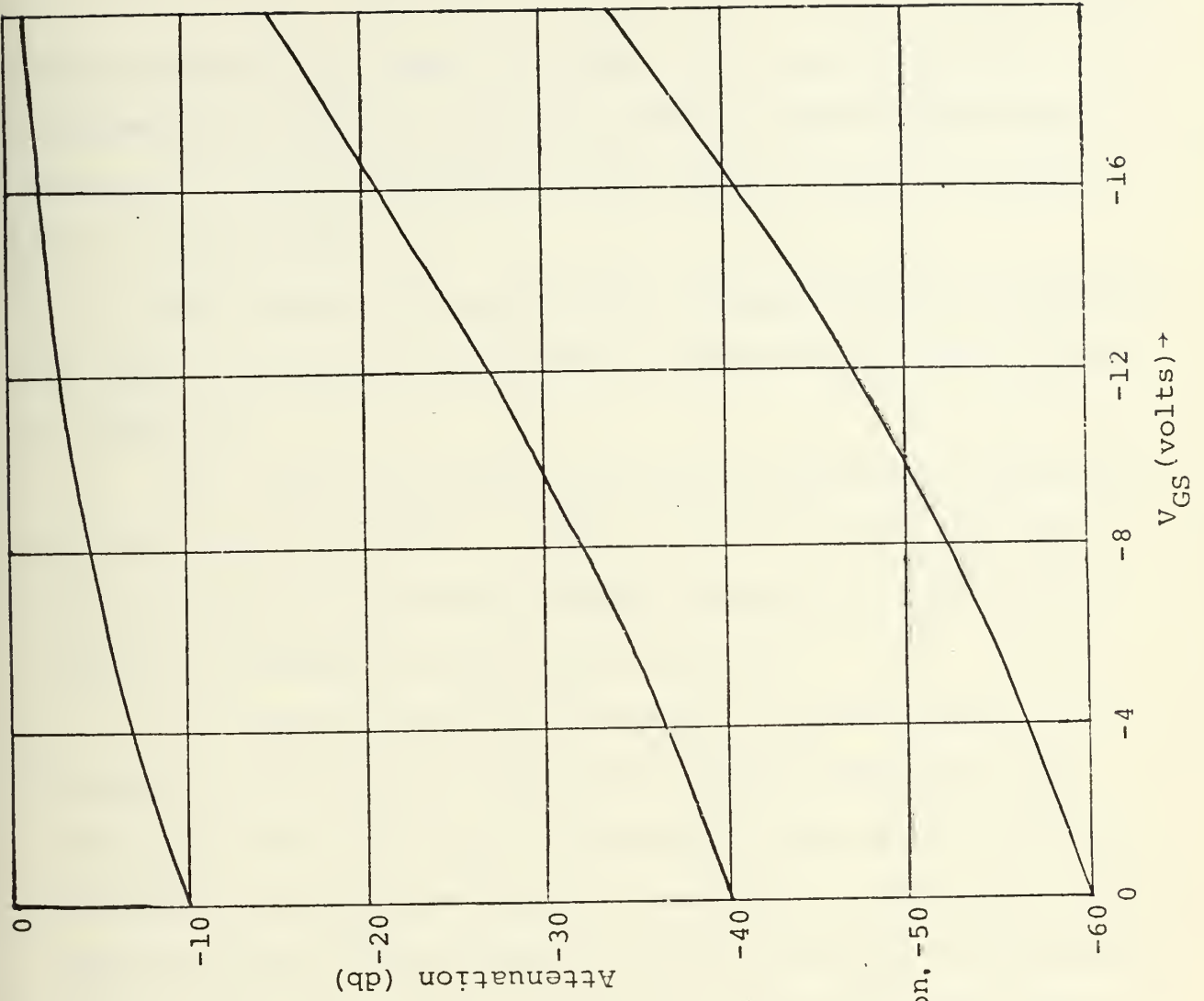


Figure 23. Voltage-Controlled FET Attenuator Circuit Schematic.

Figure 24. (Right) Attenuator Characteristics for Different Values of zero-bias Attenuation, -50





300 mv - 3v rms. The plots of attenuation versus control gate-source voltage, are shown in Figure 26. The attenuator schematic is shown in Figure 27 together with the pertinent formulae. Table VI summarizes the range of  $R_{DS}$  for the FET for a 3v rms input.

The feedback-connected FET voltage attenuator operation is shown for varying frequencies of operation at 780 mv input in Figure 28.

The effect of change in series resistance is shown for  $R_s = 20k$  and  $R_s = 100k$  in Figure 29. As in Gosling [Ref. 25], the effect of series resistance changes is most noticeable at low values of gate-source voltage.

In each of the three families of curves shown in Figures 26, 28, and 29, noticeable harmonic distortion was observed in the  $-6v < V_{GS} - 4v$  region of gate-source voltage. The amount of distortion was not measured. In each case, the improvement over conventionally-connected FET's in the dynamic ranges of  $V_{DS}$ ,  $R_{DS}$ , and  $V_{GS}$  operation was noted. The improvement in linearity can be observed in Figure 19.

#### 4. MOSFET Voltage-Controlled Attenuators

Figure 30 shows the schematic of the MOSFET, conventionally-connected, voltage-controlled attenuator. Figures 31, 32, and 33 characterize the MOSFET voltage-controlled attenuator, and Table VII summarizes attenuation factors and values of  $R_{DS}$  available with this configuration. It can be seen that the MOSFET has more change in the attenuation





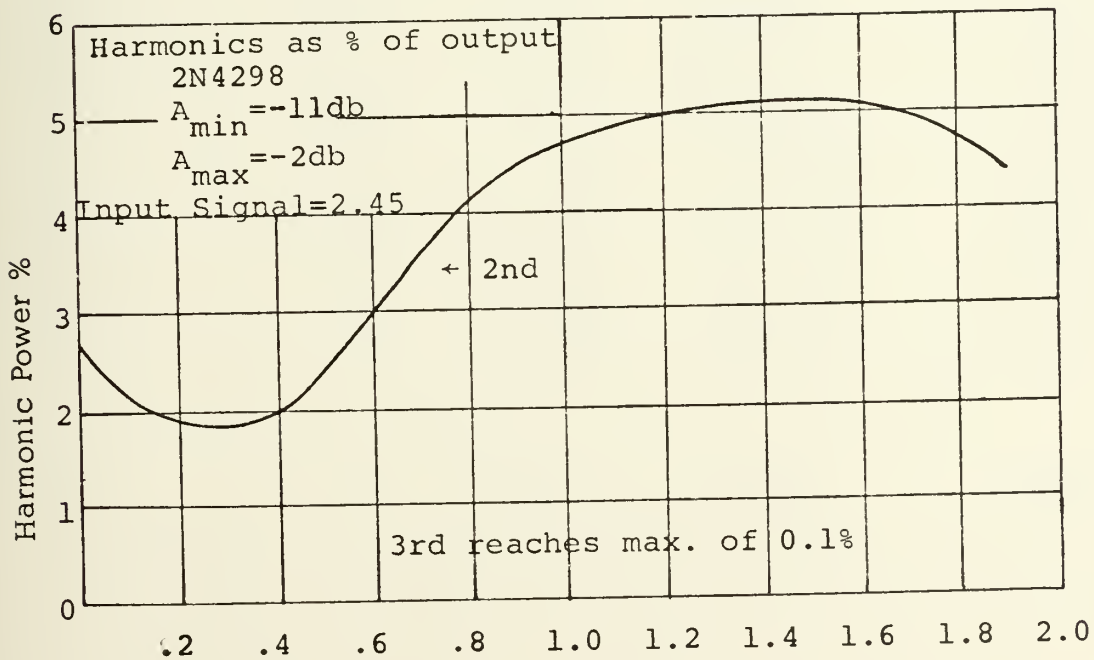
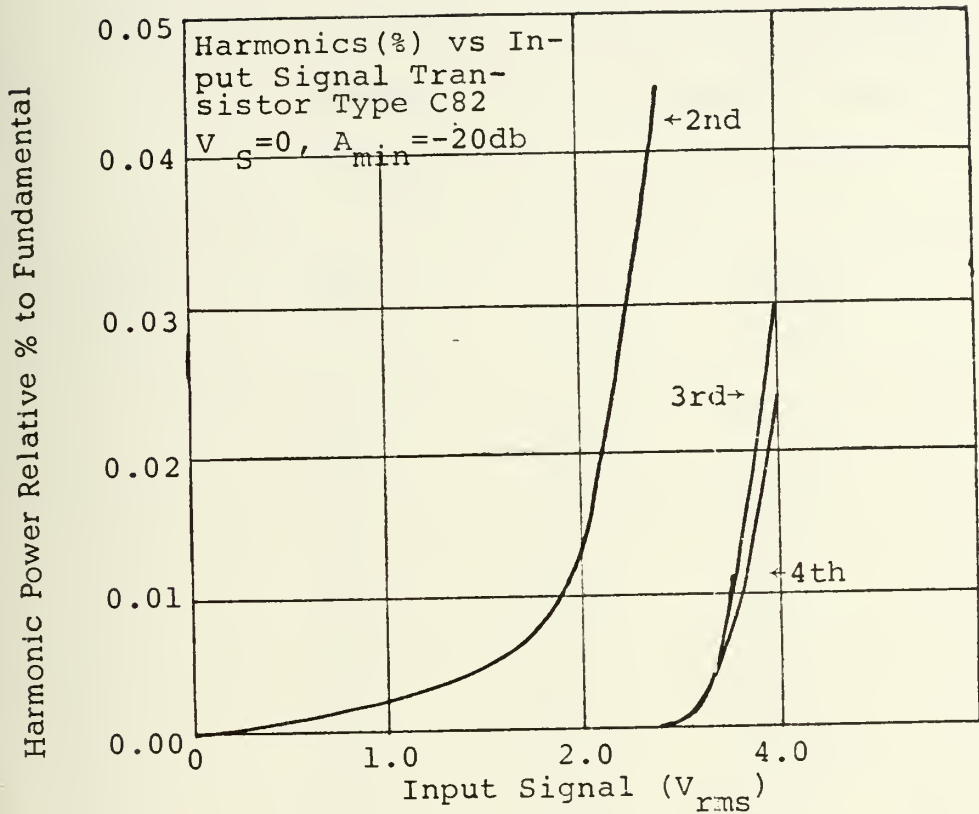


Figure 25. Distortion Effects in Voltage-Controlled FET Attenuators.



TABLE VI. Attenuation Factors and Resistance ( $R_{DS}$ )  
 Values for 3N138 (Feedback-connected)  
 Voltage-Controlled Attenuator.

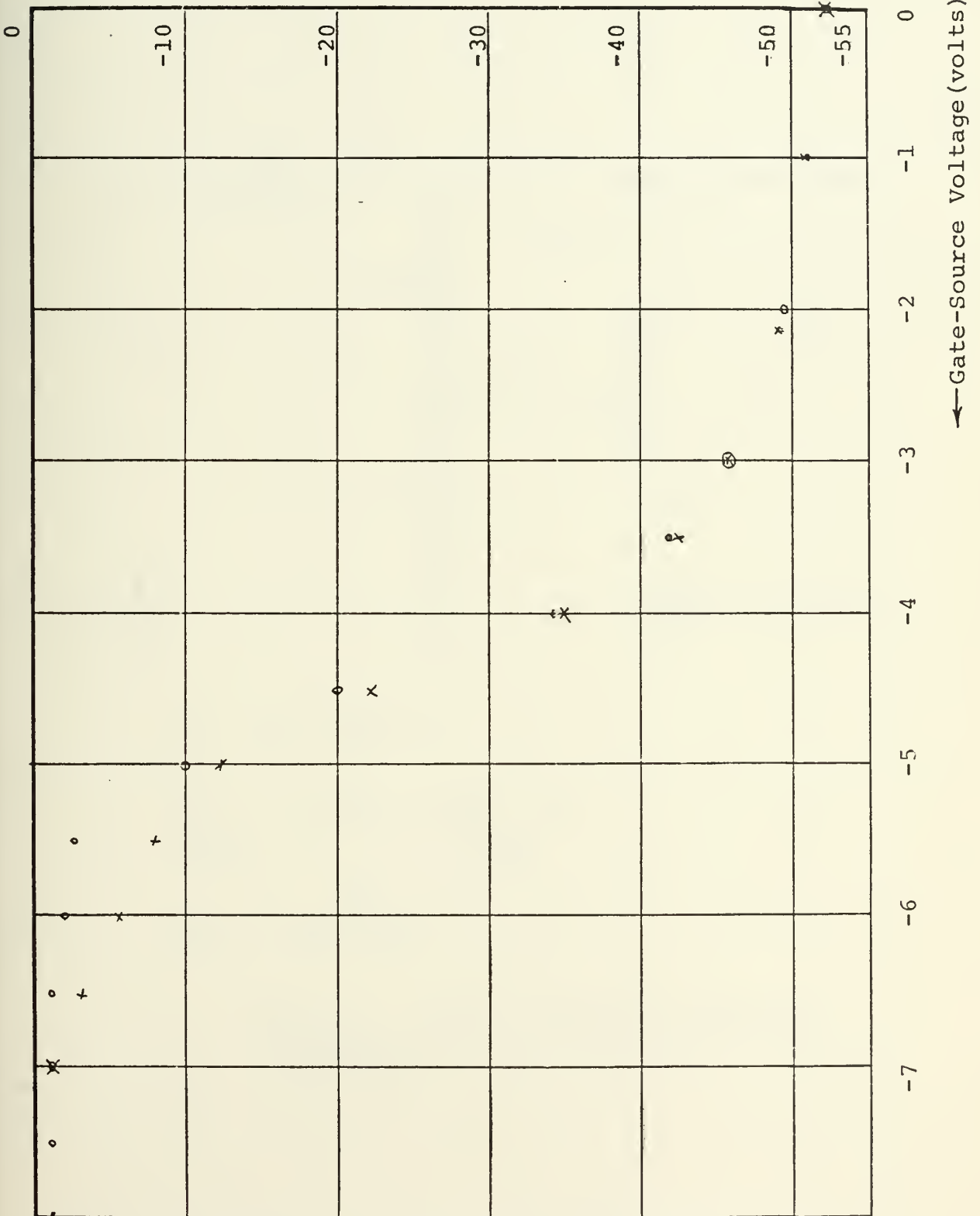
(Volts) $-V_G$	(db) -A	-A/20	(ohms) $R_{DS}$	$R_{DS}/R_O$
0	52.5	2.625	237.7	1.0
0.5	51.5	2.575	266.8	1.12
1.0	50.8	2.54	289.2	1.22
1.5	50.2	2.51	310.	1.30
2.0	49.5	2.475	336.	1.41
2.5	48.0	2.40	399.7	1.68
3.0	46.2	2.31	492.2	2.07
3.5	42.2	2.11	782.31	3.29
4.0	34.7	1.735	1875.3	7.89
4.5	22.5	1.125	8106.87	34.10
5.0	12.5	0.625	31085.2	130.8
5.5	8.0	0.40	66142.53	278.3
6.0	5.7	0.285	107.81K $\Omega$	453.6
6.5	3.5	0.175	201.6K $\Omega$	848.13
7.0	2.5	0.125	300 K $\Omega$	1262.1
7.5	1.5	0.075	530.4K $\Omega$	2231.4
8.0	1.2	0.060	675.0K $\Omega$	2839.7
↓	↓	↓	↓	↓
10.0	1.2	0.06	675.0K	2839.7



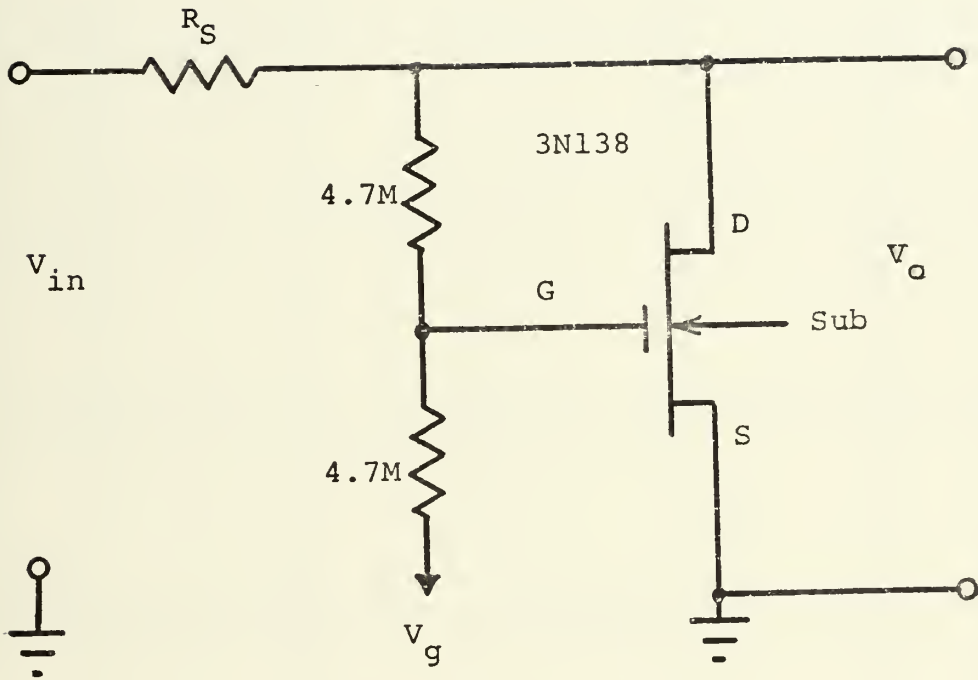
Figure 26. 3N138, Feedback-Connected, Voltage-Controlled Attenuator Characteristics, Input Voltage is the parameter.

x -  $V_{IN} = 2.48v$  rms      0 -  $V_{IN} = 248$  mv rms

Attenuation (db) +







$$20 \log \frac{V_{out}}{V_{in}} \triangleq A$$

$$\frac{V_{in}}{V_{out}} = 10^{-A/20} = \frac{R_{DS} + R_S}{R_{DS}}$$

$$R_{DS} = \frac{R_S}{10^{-A/20} - 1}$$

Figure 27. 3N138, Feedback-Connected, Voltage-Controlled Attenuator Circuit Schematic.





Figure 28. 3N138, Feedback-Connected, Voltage-Controlled Attenuator Characteristics, Input Frequency is the parameter.

'x' denotes 400 Hz Input frequency.  
 'o' denotes 5000 Hz Input Frequency.

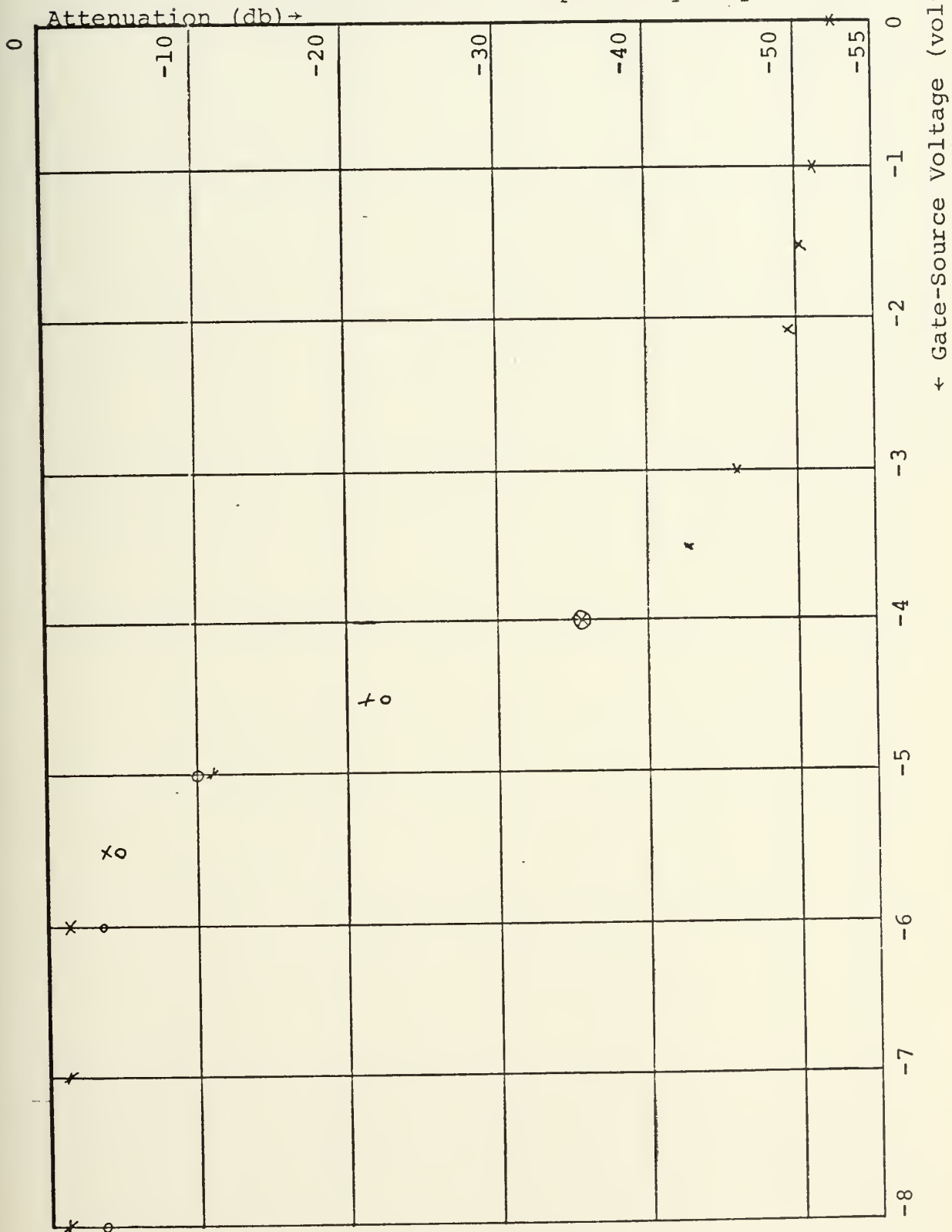
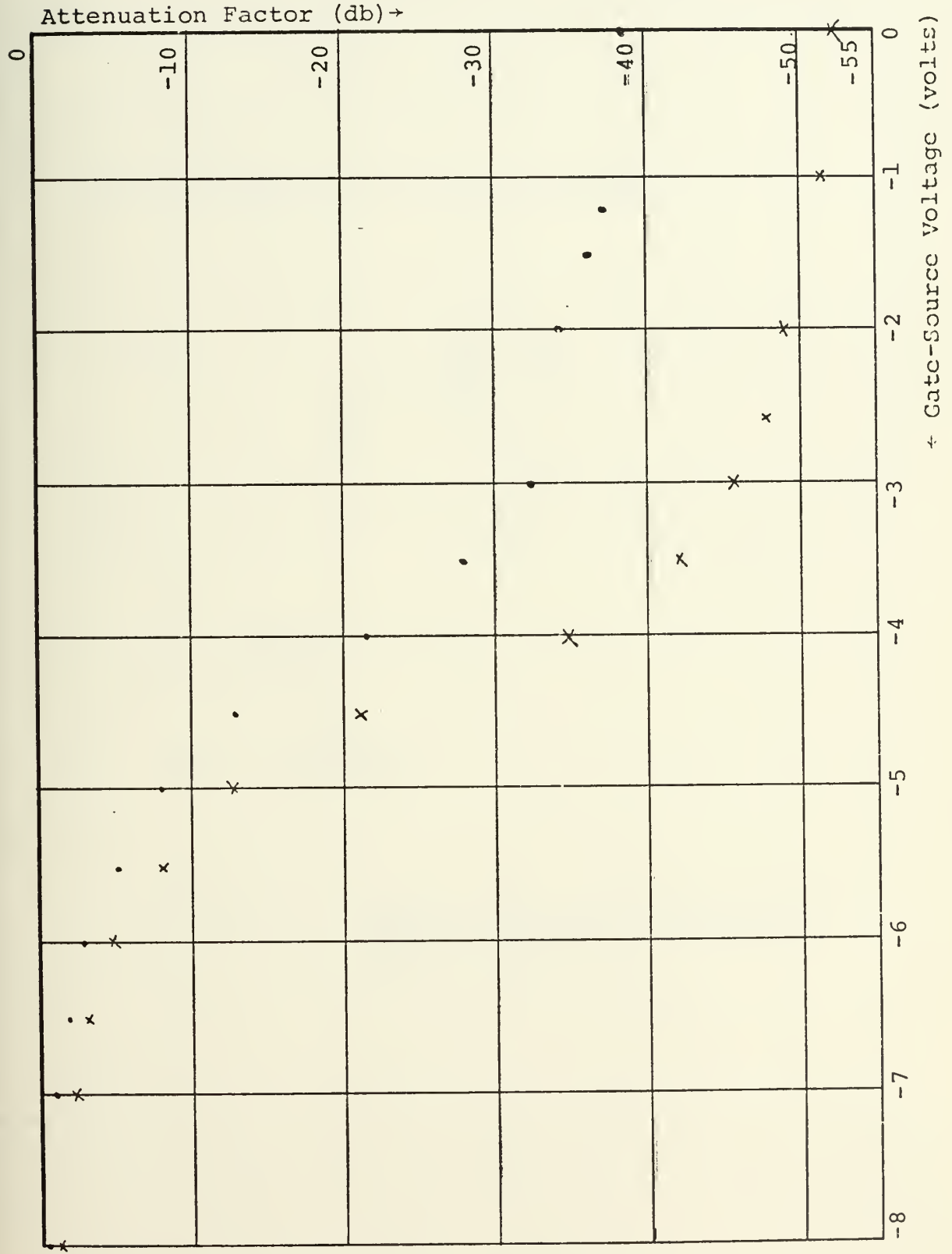


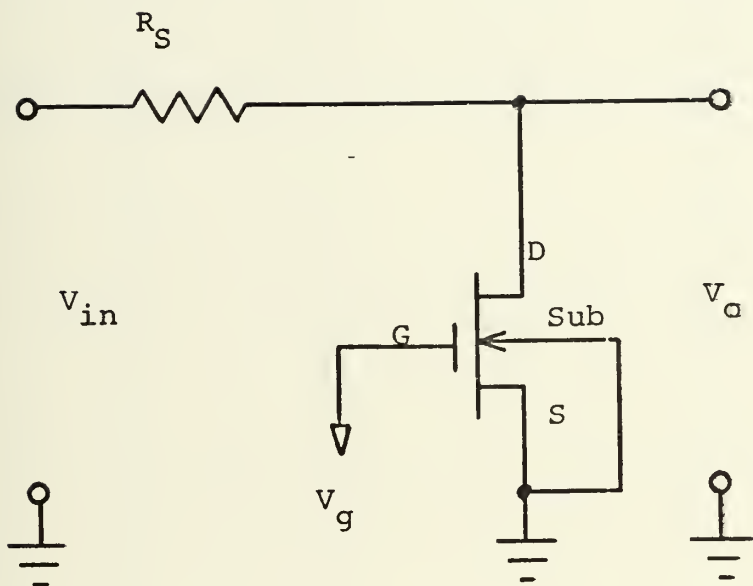


Figure 29. 3N138, Feedback-Connected, Voltage-Controlled Attenuator Characteristics, Series Resistance is the parameter.

x -  $R_S = 100\text{ k}$       • -  $R_{in} = 20\text{ k}$







$$20 \log \frac{V_{out}}{V_{in}} \triangleq A$$

$$R_{DS} = \frac{R_S}{10^{-A/20} - 1}$$

Figure 30. 3N138, Conventionally-Connected, Voltage-Controlled Attenuator Circuit Schematic.



Figure 31. 3N138, Conventionally-Connected, Voltage-Controlled Attenuator Characteristics, Input Voltage is the parameter.

x - 2.78 v rms input.    • - 278. mv rms input.

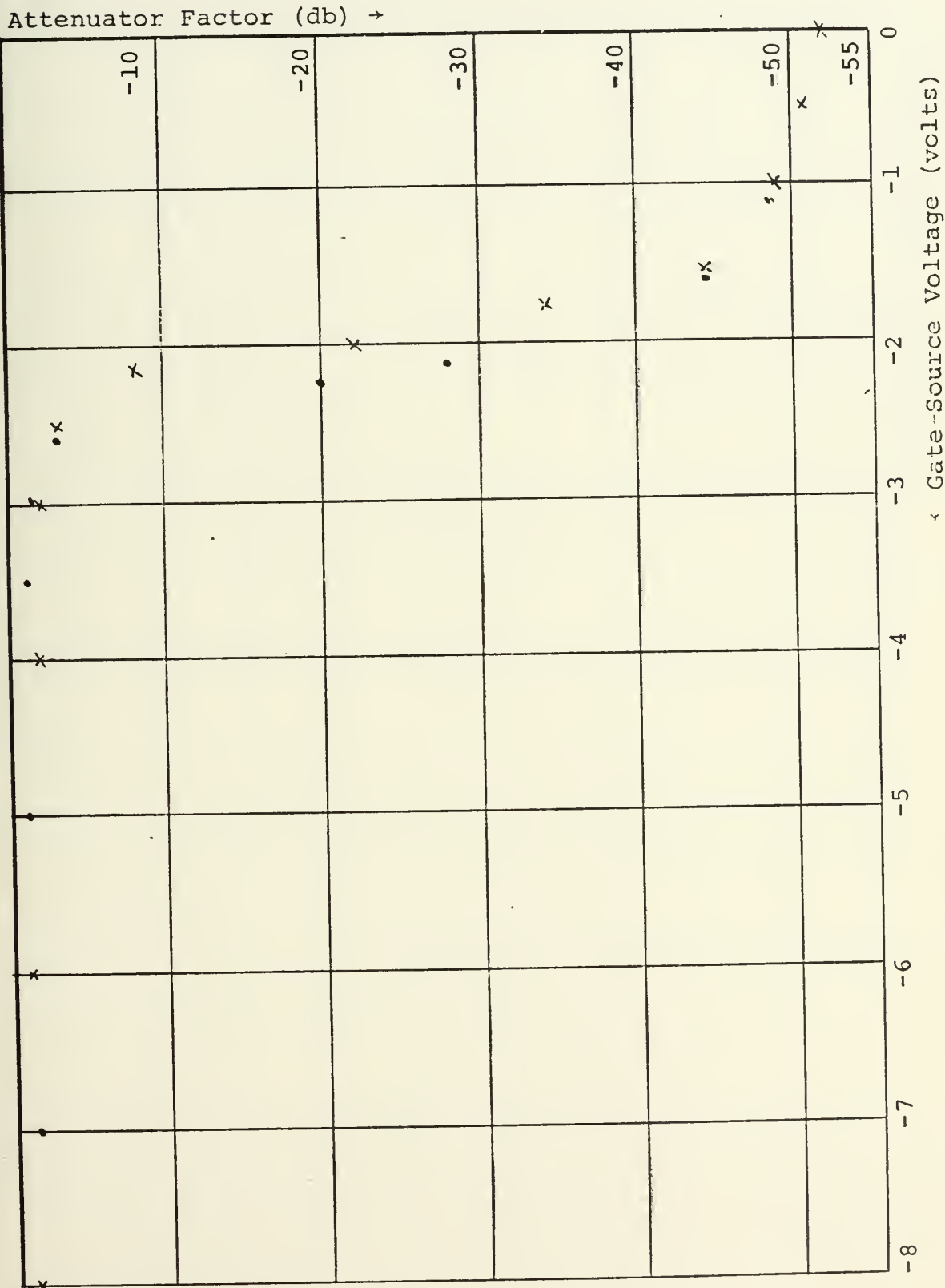






Figure 32. 3N138, Conventionally-Connected, Voltage-Controlled Attenuator Characteristics. Input Frequency is a parameter.

'x' - 400 Hz, '.' - 1000 Hz, and 'o' - 5000 Hz

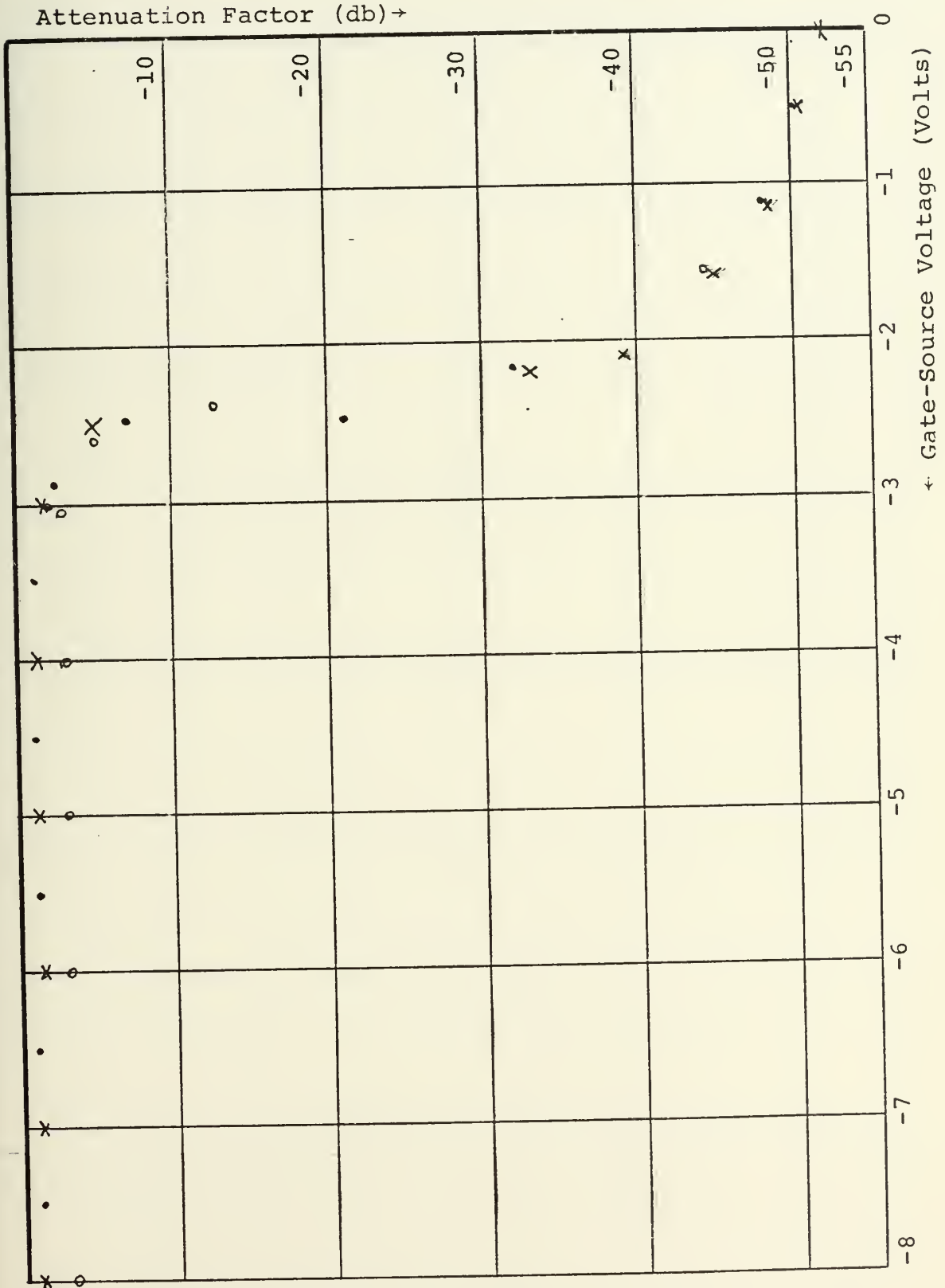




Figure 33. 3N138, Conventionally-Connected, Voltage-Controlled Attenuator Characteristic. Series Resistance is the parameter.

'x' -  $R_S = 20\text{ k}$  . '.' -  $R_S = 100\text{ k}$  .

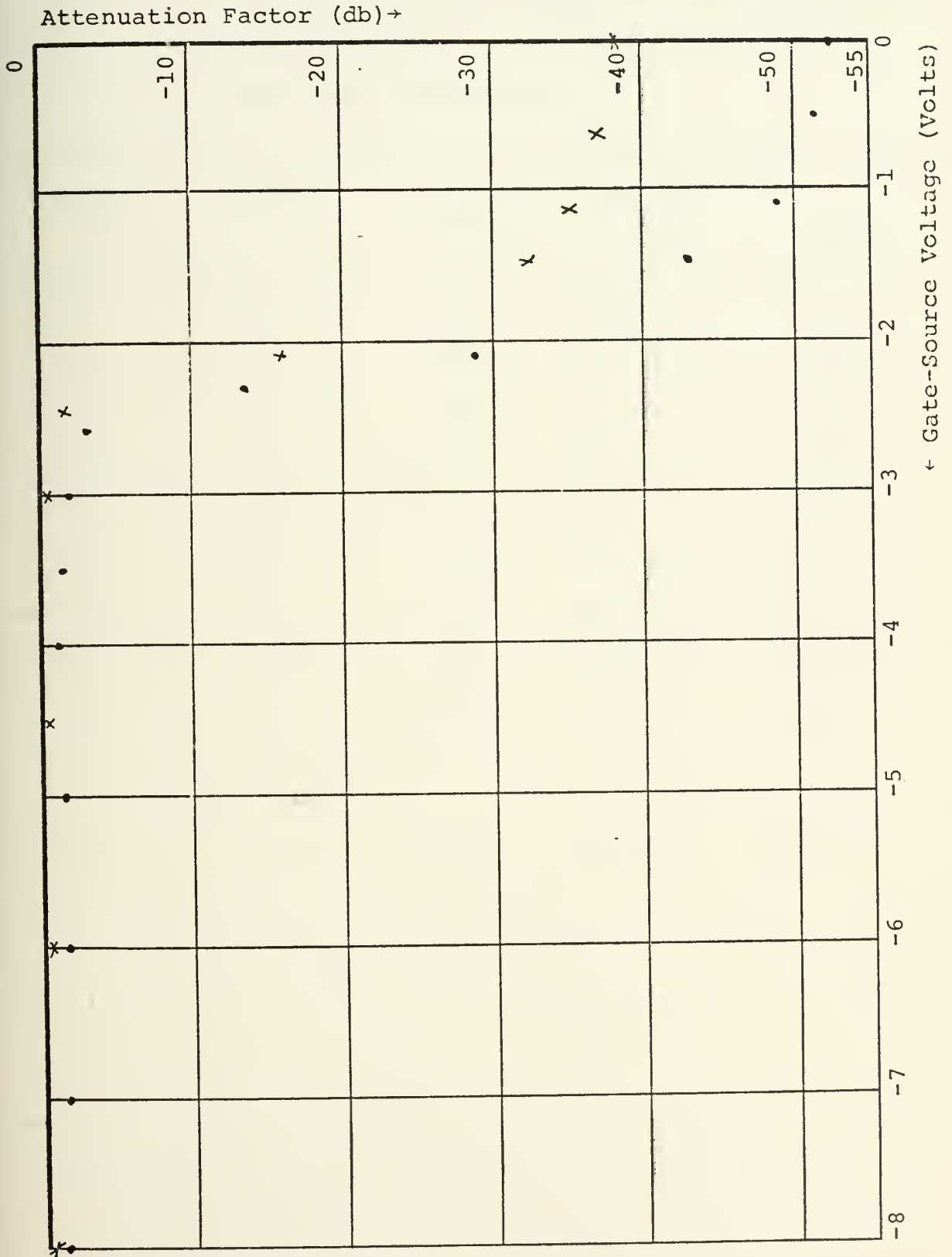




TABLE VII. Attenuation Factors and Resistance ( $R_{DS}$ ) Values for 3N138 (Conventionally-connected) Voltage-Controlled Attenuator.

(Volts) $-V_G$	(db) $-A$	$-A/20$	(ohms) $R_{DS}$	$R_{DS}/R_O$
0	52.0	2.60	251.82	1.059
0.5	51.8	2.59	257.70	1.084
1.0	49.0	2.45	356.08	1.50
1.5	44.7	2.235	585.51	2.46
2.0	22.0	1.1	8628.6	36.3
2.5	3.2	0.16	224.5K $\Omega$	944.5
3.0	2.0	0.10	386.2K $\Omega$	1624.7
4.0	1.8	0.09	434.27K $\Omega$	1827.0
5.0	1.0	0.05	819.55K $\Omega$	3447.8
↓	↓	↓	↓	↓
10.0	1.0	0.05	819.55K $\Omega$	3447.8



characteristic for high gate-to-source voltage then the feedback-connected MOSFET. At gate voltages in the region of -3 to -4v, negative clipping of the signal was noted. No other distortion effects were observed, however. The MOSFET attenuator is relatively insensitive to  $V_{DS}$ , although  $V_{DS}$  effects the pinch-off voltage level. The magnitude of series resistance effects the pinch-off voltage value as well as the zero gate-source voltage  $R_{DS}$  values. Harmonic distortion was not measured but no anomalies, other than negative peak clipping for certain gate-source voltages, were noted in the waveshape of the signal.

A comparison of the drain-source resistance as a function of gate-source voltage for the MOSFET and feedback-connected MOSFET voltage-controlled attenuator can be obtained by referring to Figures 34 and 35. It can be seen that neither configuration has a linear  $R_{DS}$  characteristic; neither has a normalized logarithmic characteristic. Ranges of values of  $R_{DS}$  expected for feedback-connected MOSFET attenuators range from 200-675k $\Omega$ . For the conventionally-connected MOSFET attenuator the range of  $R_{DS}$  is from 200 $\Omega$ -800k $\Omega$ .

##### 5. JFET Voltage-Controlled Attenuators

Figure 36 characterizes the attenuation factor characteristic for a 2N3819 JFET voltage-controlled attenuator.

#### D. FREQUENCY DEPENDENT ATTENUATORS

In order to use the parameter plane computer analysis techniques for nonlinear active filter synthesis, one must have an experimentally-derived frequency-dependent  $\alpha(\omega)$ . This character will then be superimposed on the  $\alpha$ -family Bode





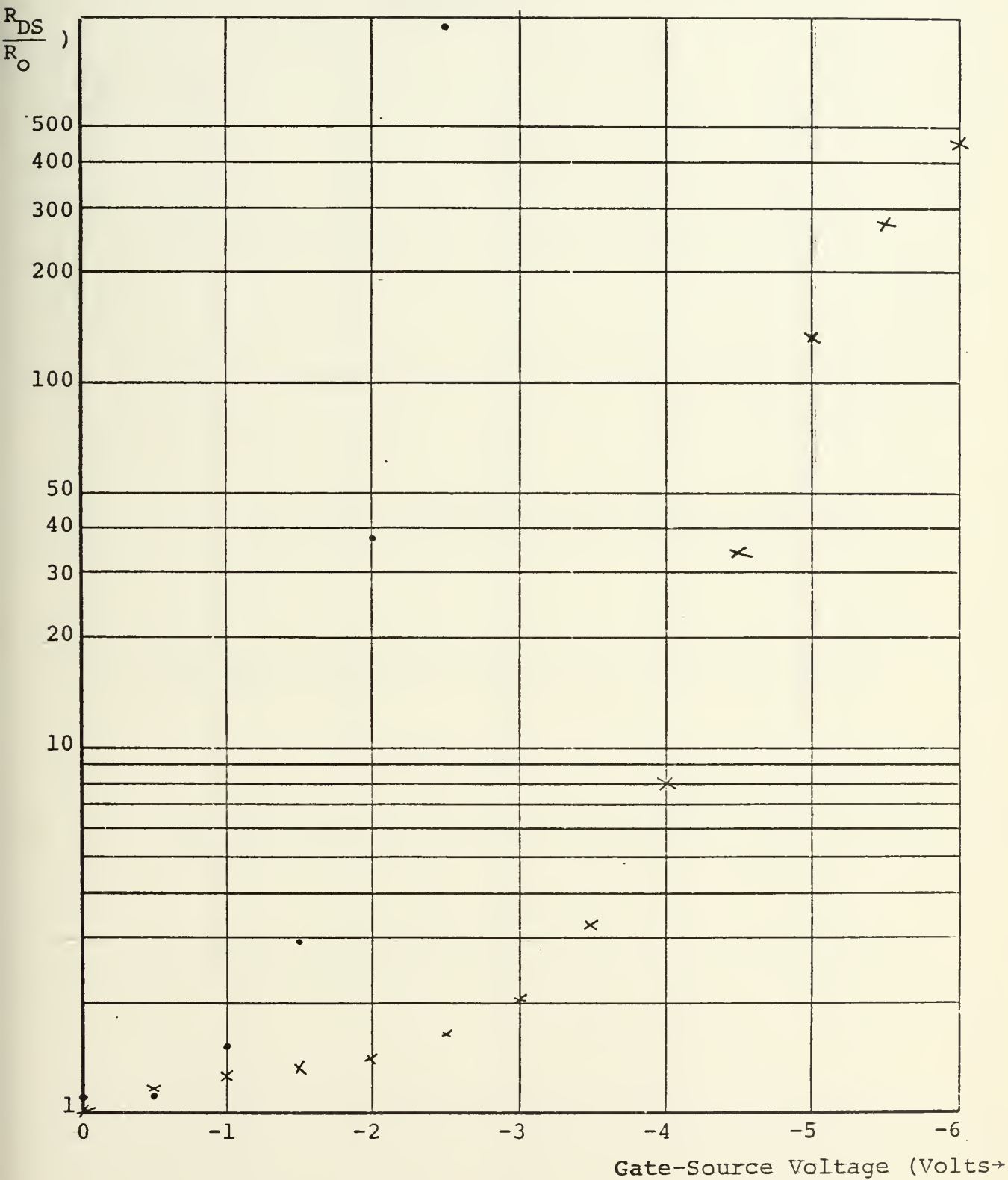


Figure 34. 3N138 Drain-Source Resistance Characteristic, Log Plot '.' - Conventionally-Connected; 'x' - Feed-back-Connected.



Figure 35. 3N138 Drain-Source Resistance Characteristic. Linear Plot ('x' - Feedback-Connected, '.' - Conventionally-Connected)

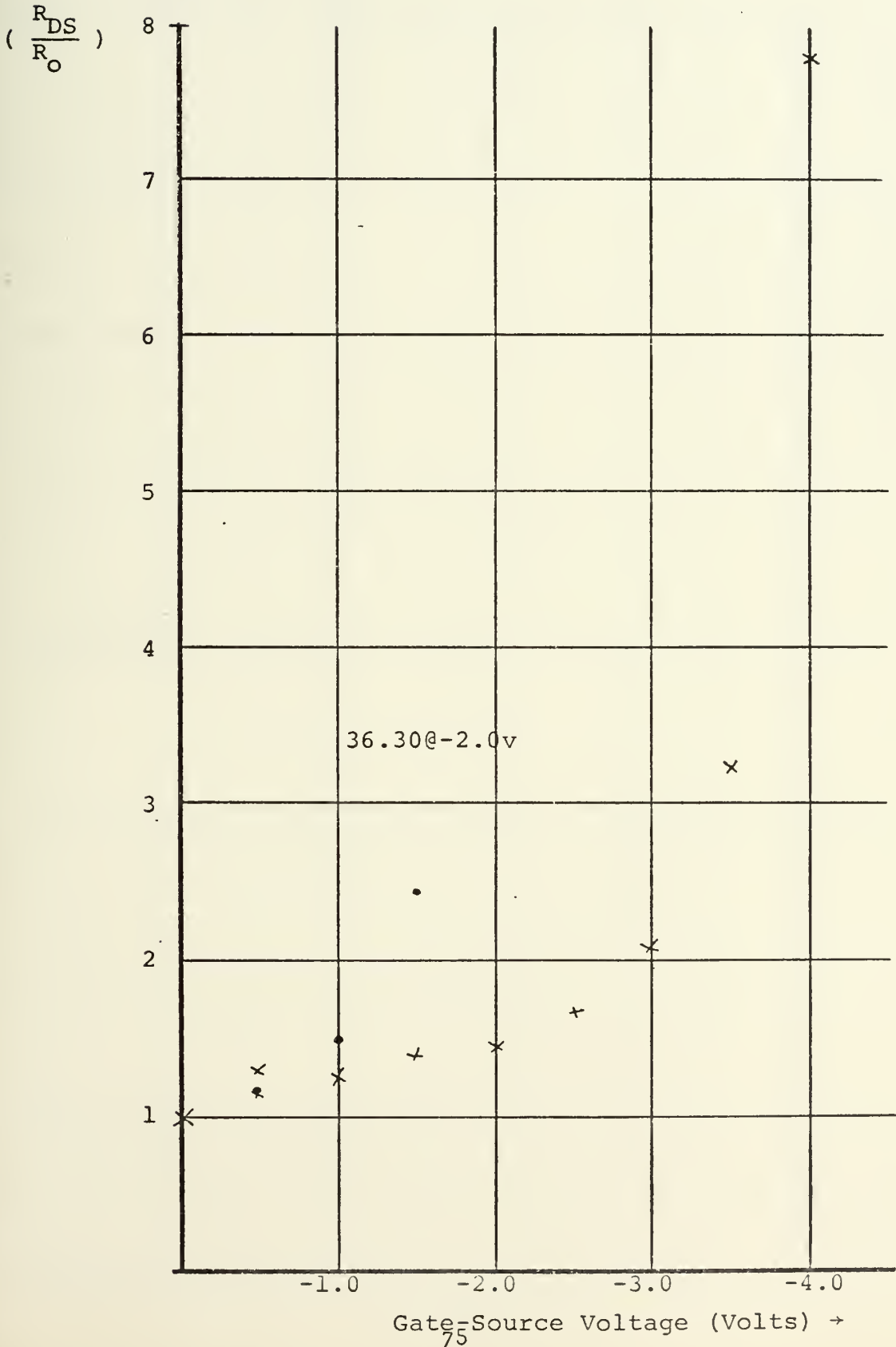
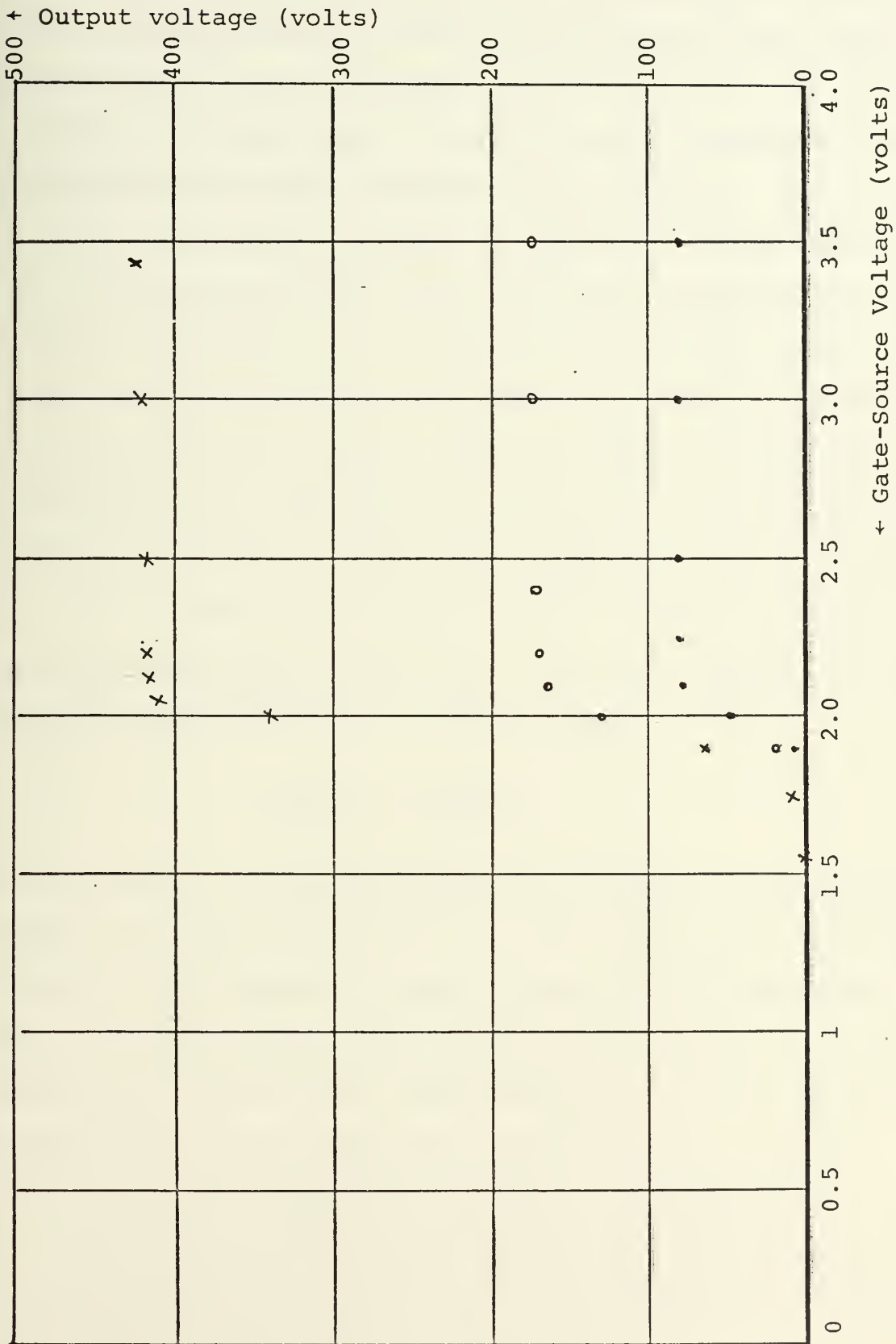




Figure 36. 2N3819, Conventionally-Connected, Voltage Controlled Attenuator Characteristic. Input voltage is the parameter ('x' - 500 mv rms, 'o' - 200 mv rms, '.' - 100 mv rms input)





plots generated by the parameter plane computer programs yielding the frequency response of the nonlinear active filter. This  $\alpha$ -characteristic is measured by operating the FET in series with a known resistance; simultaneously, the gate-source voltage, and hence  $R_{DS}$ , is provided by the nonlinear controller which is essentially a frequency discriminator. The schematic of the test circuit is shown in Figure 37. By definition this is a frequency-dependent FET attenuator, since the attenuation factor is measured for a given frequency input. Low-pass and high-pass characteristics are easily provided by one FET and its associated controller. For a band-pass or band-stop characteristics, cascading or concatenation of high-pass and low-pass filters, as previously discussed, may be utilized.

To introduce the parameter plane analysis techniques; let  $\alpha = R_{DS}$ , where  $R_{DS} = g(f(\omega_{in}))$ . Then the transfer function for the parameter plane analysis becomes:

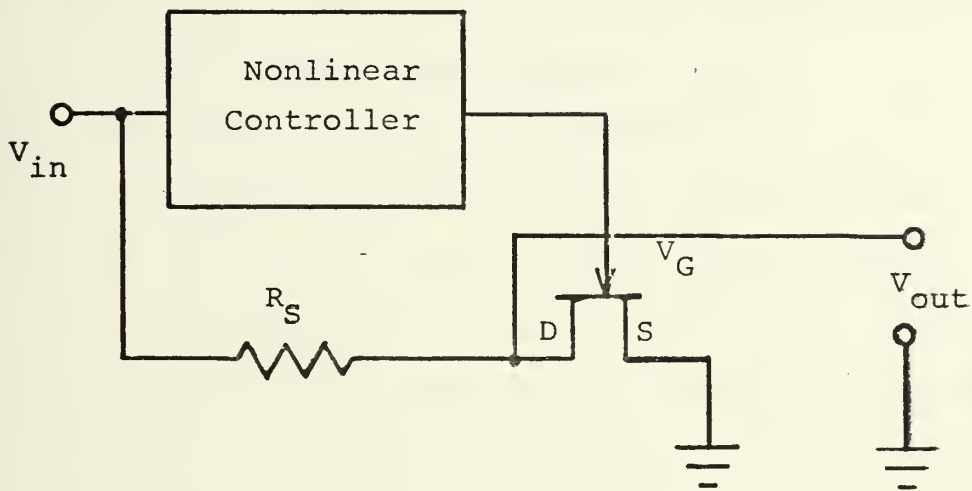
$$|T(j\omega)| = \frac{\alpha(\omega)}{R_S + \alpha(\omega)}$$

The parameter plane solution yields a family of Bode plots drawn for a specified set of  $\alpha$ 's; the specified frequency response superimposed on those curves permits specifications of the frequency-dependent nonlinear resistance, or alternatively and equivalently, superimposition of the frequency-dependent nonlinear resistance characteristic provides immediately the frequency response of the attenuator.

A slide-rule and computer analytical solution of the low-pass attenuator case leads to the curves depicted in Figures







$$V_G = f(\omega_{in})$$

$$R_{DS} = g(f(\omega_{in}))$$

$$\therefore \frac{E_o}{E_{in}} = \frac{g(f(\omega_{in}))}{R_S + g(f(\omega_{in}))}$$

$f, g$  are single-valued functions of  $\omega_{in}$  and  $f(\omega_{in})$  respectively

Figure 37. Frequency-Dependent FET Attenuator Circuit Schematic.



38 and 39 respectively. The desired frequency response characteristic was obtained by measuring the particular FET and controller attenuation-factor as a function of frequency. Superimposing the  $\alpha$ -characteristic on the Bode plots led immediately to the frequency response shown.

Four different combinations of FET's and controllers manifested themselves in the low-pass characteristic of Figures 40, 41, and 42; the high-pass case is shown in Figure 43. The controller used for the filters shown in Figures 39, 40, 41, and 42, is the phase shift dc-chopper discriminator discussed in III-B below. The controller used for the attenuator in Figure 43 is the filter-discriminator discussed III-D.



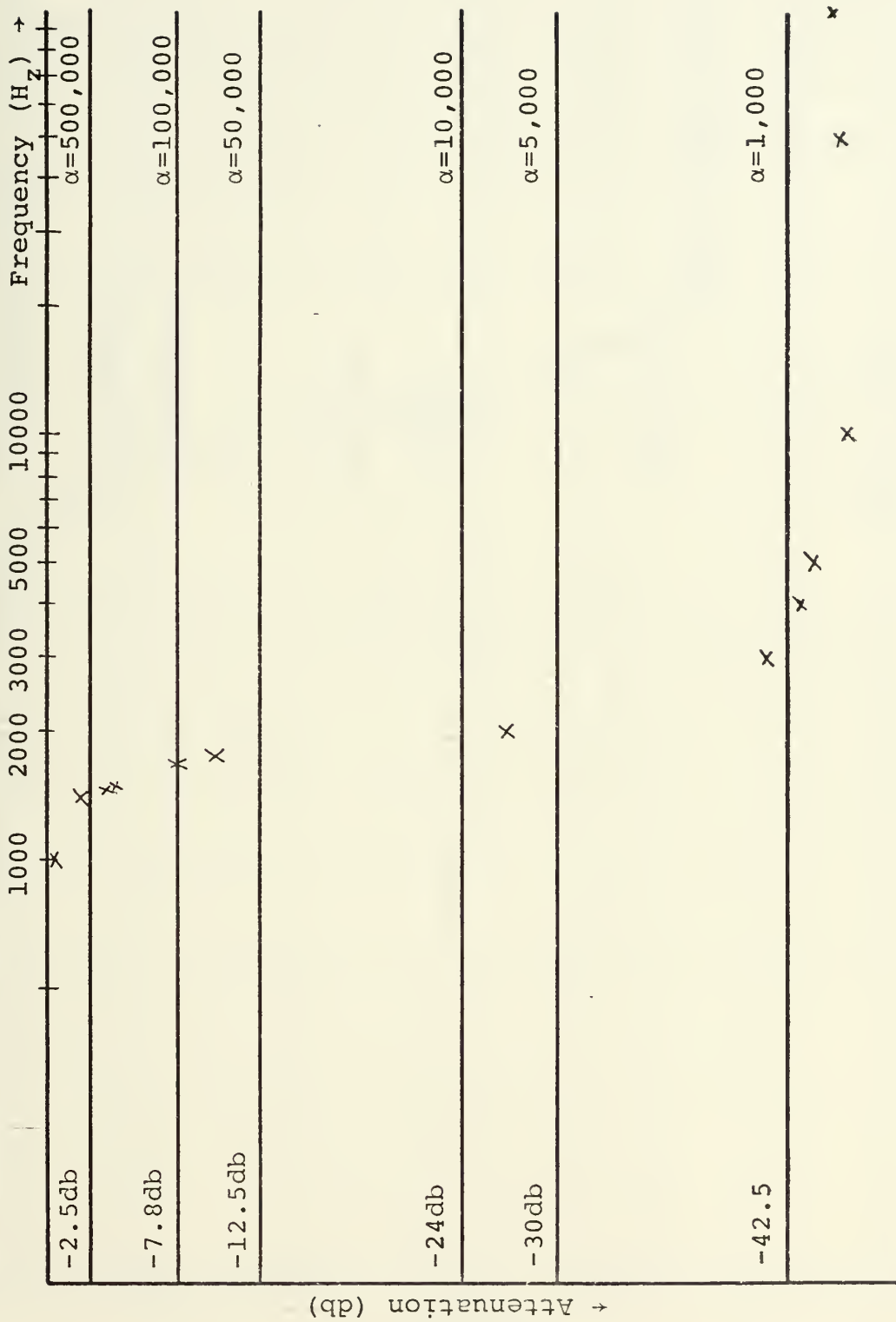


Figure 38. Slide Rule Analytic Solution for Parameter Plane Frequency-Dependent Attenuator



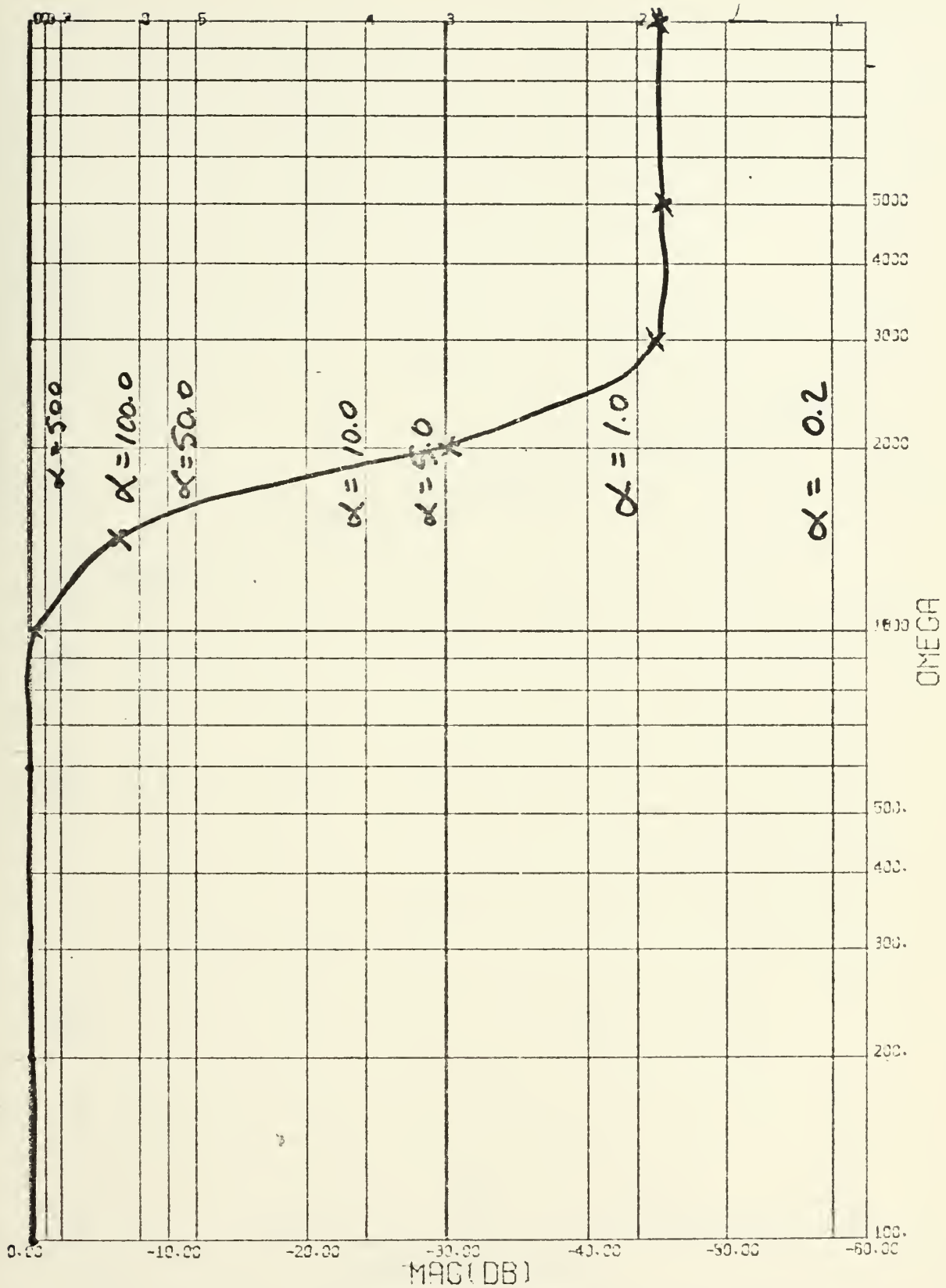


Figure 39. Parameter Plane Computer Solution for Frequency-Dependent Attenuator.





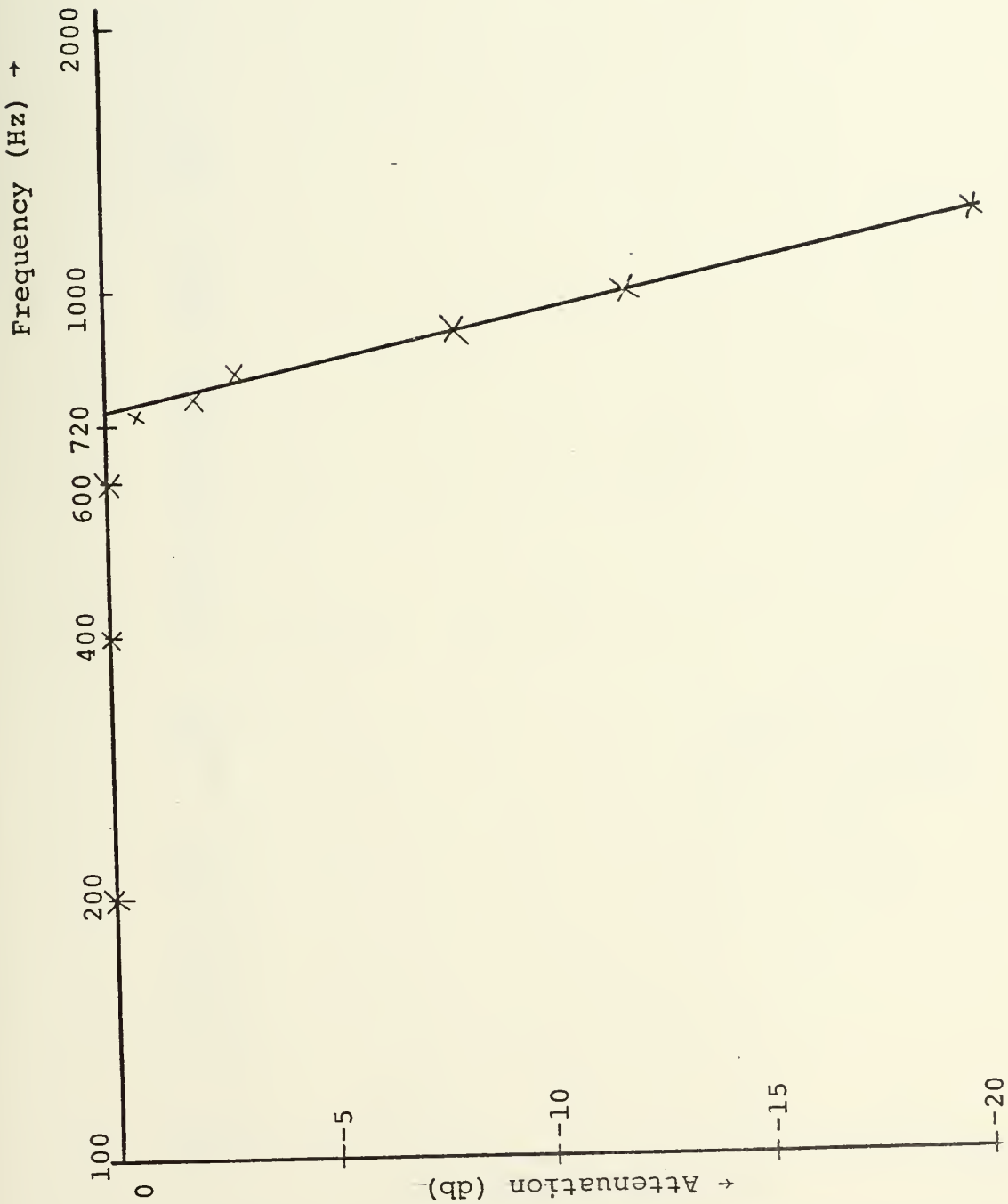


Figure 40. 2N3819 Low-Pass Frequency-Dependent Attenuator Characteristic.



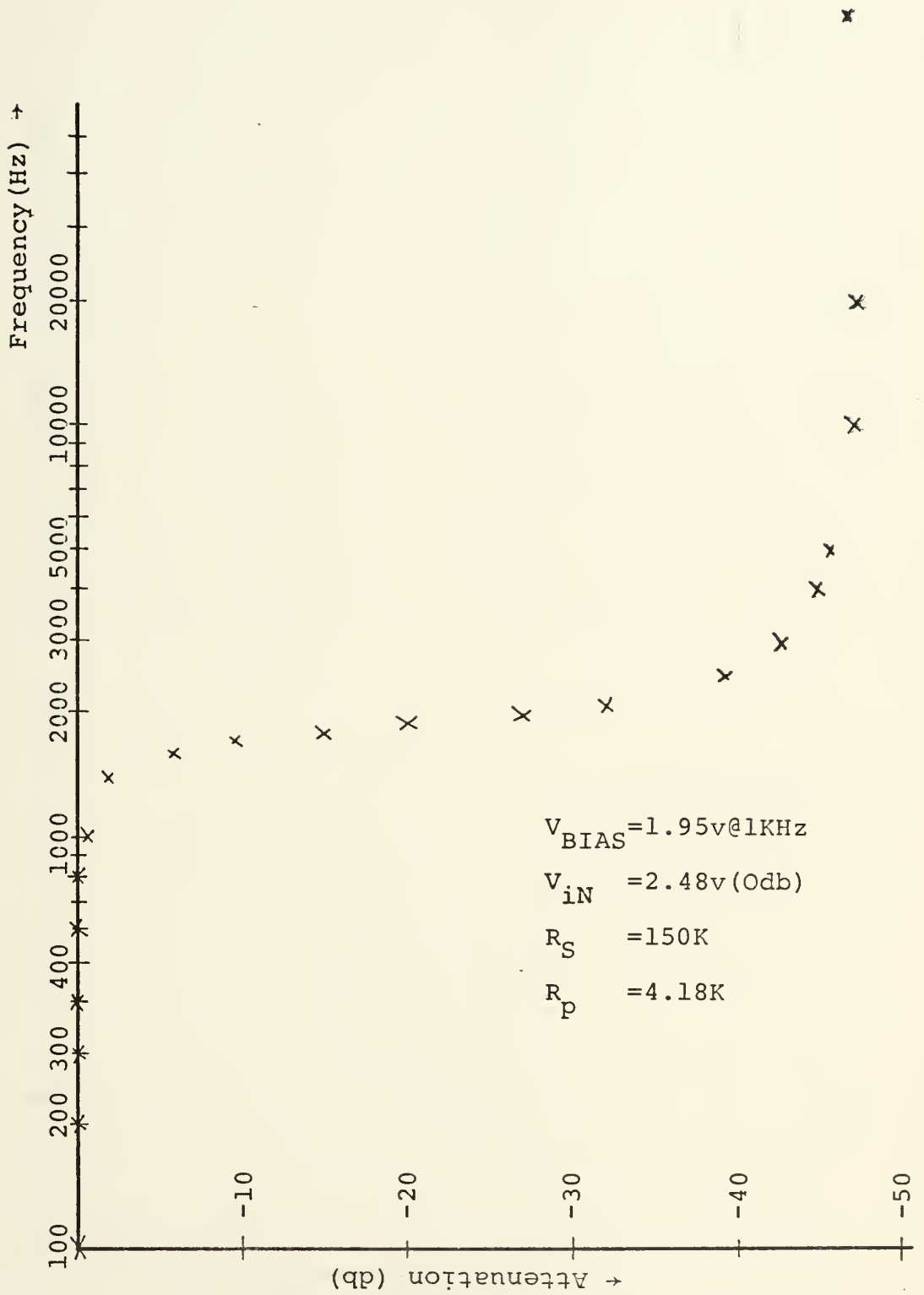


Figure 41. 3N141 Low-Pass Frequency-Dependent Attenuator Characteristic.



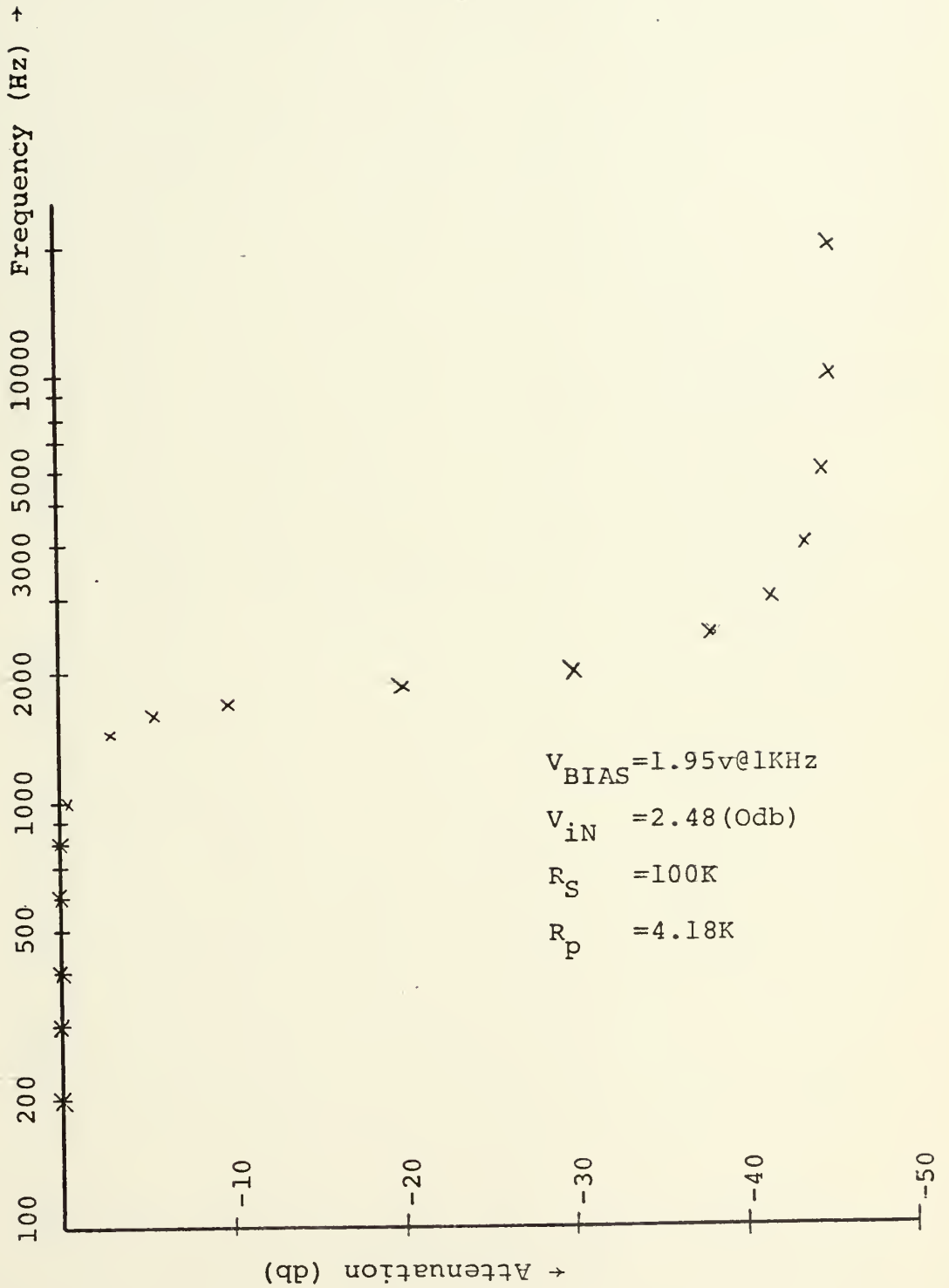


Figure 42. 3N141 Low-Pass Frequency-Dependent Attenuator Characteristic.



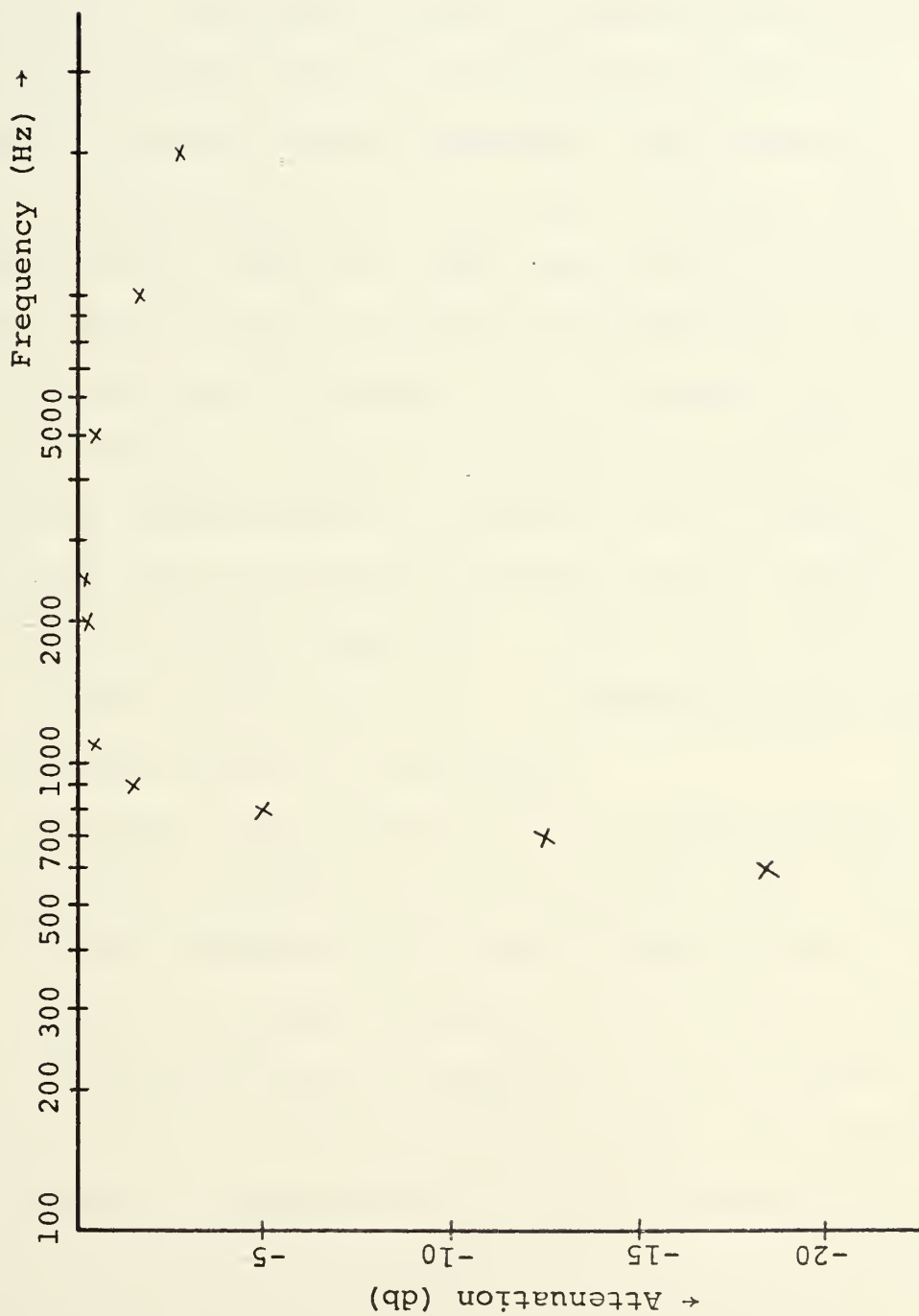


Figure 43. 3N141 High-Pass Frequency-Dependent Attenuator Characteristic.





#### IV. NONLINEAR DEVICE CONTROLLER

##### A. INTRODUCTION

To control a nonlinear element or device usually requires either a prescribed voltage or current whose values are determined by another varying parameter. For instance, to produce a frequency-dependent nonlinear resistance, one could use a field-effect transistor whose gate-source d-c control voltage is obtained from a frequency discriminator (see Figure 44 for the basic block diagram). Or, to produce a nonlinear capacitance which is a function of some designated voltage, one could use a back-biased p-n junction, i.e. a varactor, in conjunction with the nonlinear device control voltage obtained from a voltage comparator. Chua, [Refs. 21 and 22] provides a complete description of the ramifications of the nonlinear element control realizations.

To be suitable for nonlinear active filter use, the nonlinear element controller should be capable of: (1) wide frequency range utilization; (2) large dynamic range of voltage/current inputs; (3) minimal parasitic effects; and (4) amenability to monolithic/hybrid integrated circuit construction techniques. If the controller cannot produce the required control values as a prescribed function of the varying parameter, the nonlinear element values will not be consistent with design specifications. Thus, the superimposition of the



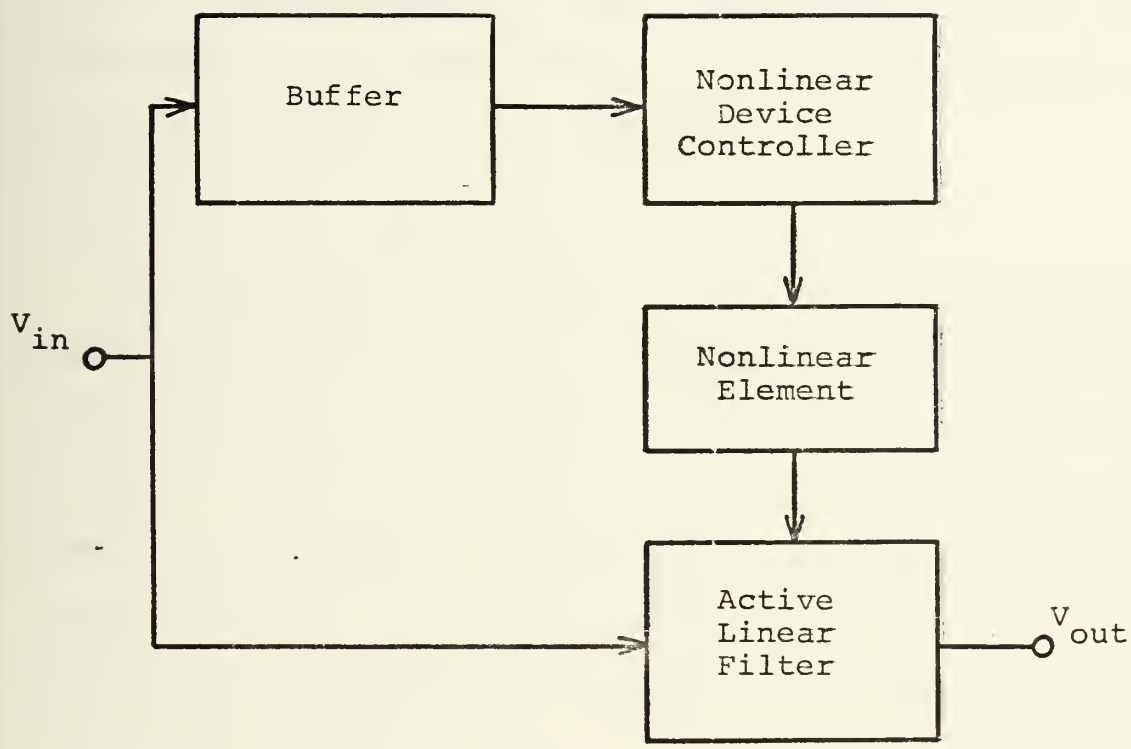


Figure 44. Block Diagram of Basic Nonlinear Device Controller.



specified nonlinear element locus on the parameter plane curves would not permit accurate prediction of the frequency response of the nonlinear active filter. The following paragraphs describe three physical realizations of the frequency-dependent nonlinear resistance controller. The discussion will emphasize the advantages and limitations of each design in terms of the criteria set forth in this paragraph.

#### B. PHASE SHIFT DISCRIMINATOR

The phase shift discriminator as a frequency-sensitive nonlinear device controller is achieved by having a phase-shift amplifier in cascade with a dc-chopper phase-sensitive circuit. In the phase-sensitive amplifier the amount of phase shift is proportional to the incoming frequency; the dc-chopper circuit produces a dc voltage proportional to the phase difference between the output of the phase-shifter amplifier and the incoming signal. Figure 45 illustrates the basic block diagram of the phase shift discriminator controller, and Figure 46 shows the schematic of a typical realization of this discriminator [Delpeck 1966].

The experimental phase response of the phase-shifter is shown in Figure 47 and can be compared to a linear ac analysis simulation computed by using the IBM 360 ECAP program with

$$\omega_{REF} = \frac{1}{R_S C_S} .$$

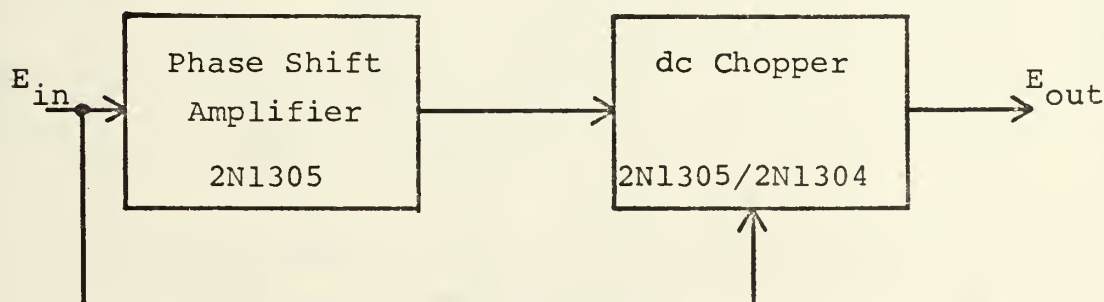
The discriminator characteristics are plotted in Figures 48, 49, and 50. The following conclusions may be noted:



(1) the discriminator does not provide a linear output as a function of frequency: (2) the frequency range of the discriminator is limited: (3) the output characteristic is affected by the amplitude of the incoming signal: (4) the output voltage is sensitive to component value changes; and (5) the amplitude of the d-c output voltage is small when compared to the input voltage, i.e. the conversion gain is small.

The phase shift discriminator is amenable to monolithic/hybrid integrated circuit construction techniques. The phase shift discriminator provides a "floating" output across the output capacitance, however. AC grounding by means of a large filter capacitor was attempted and found useful, but because of this disadvantage, its lack of linearity, its low output voltage, and other previously mentioned disadvantages, this discriminator was not chosen as the frequency-selective non-linear device controller.

FIGURE 45. Block Diagram of Phase Sensitive Discriminator







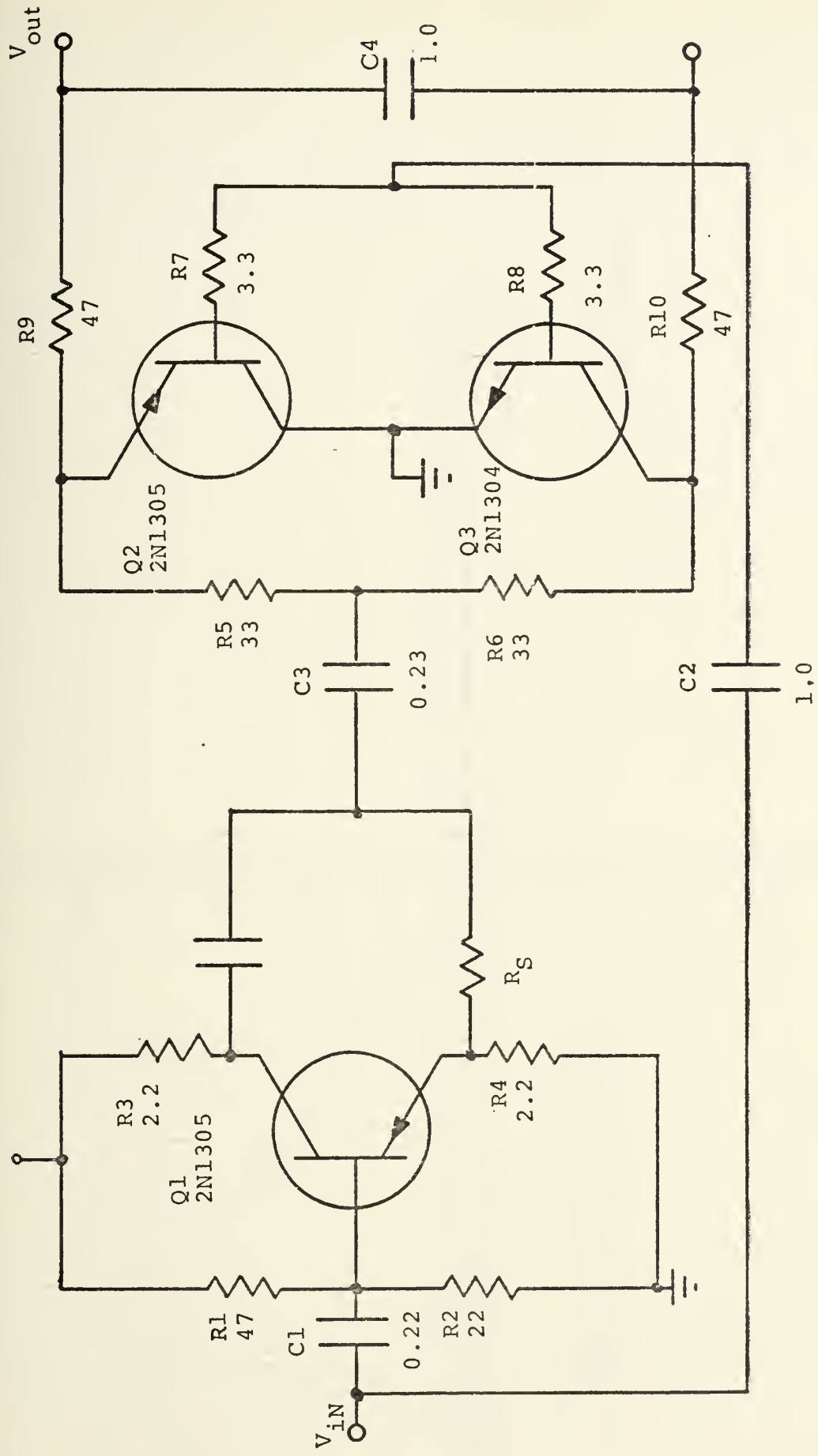


Figure 46. Phase-Sensitive Discriminator Circuit Schematic (all R's are  $K\Omega$ , all C's are  $\mu\text{fds}$ ).



Phase Angle (Degrees)

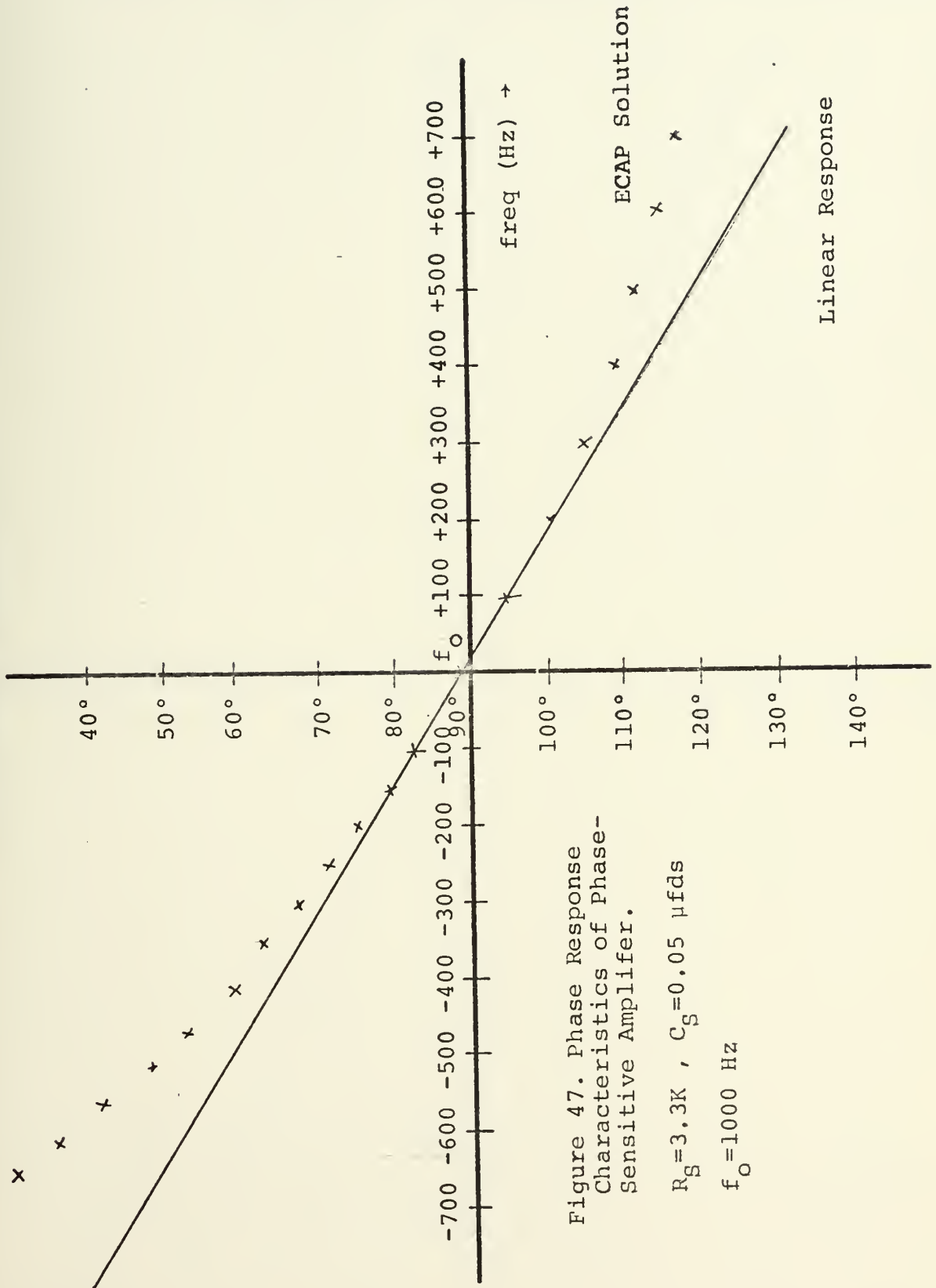


Figure 47. Phase Response Characteristics of Phase-Sensitive Amplifier.

$R_G = 3.3K$  ,  $C_S = 0.05 \mu\text{fds}$   
 $f_O = 1000 \text{ Hz}$



Figure 48. Phase Sensitive Discriminator Characteristic  
 $f_o = 1\text{KHz}$ .  $V_{in} = 778\text{mv rms}$ .

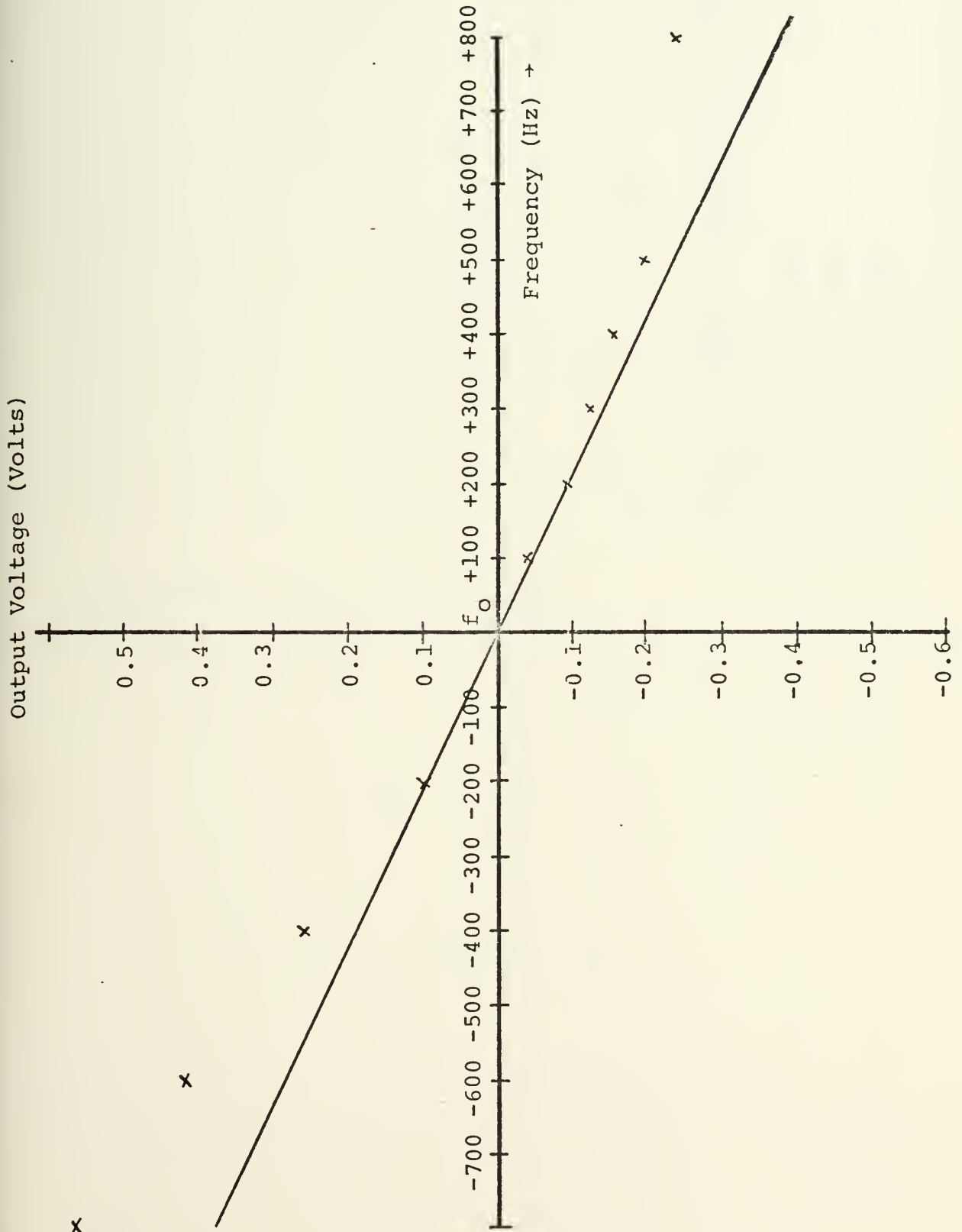
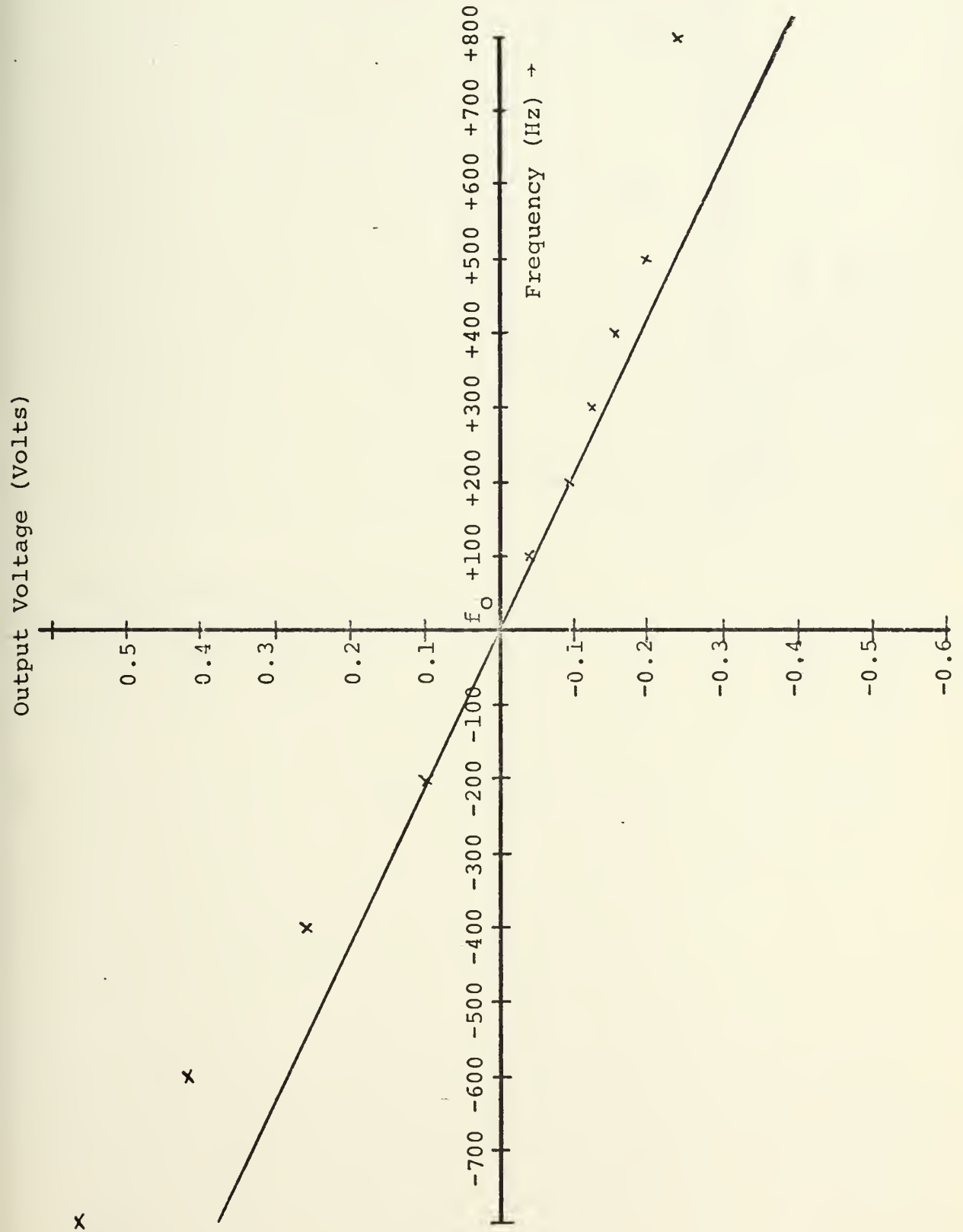




Figure 48. Phase Sensitive Discriminator Characteristic  
 $f_o = 1\text{KHz}$ .  $V_{in} = 778\text{mv rms}$ .







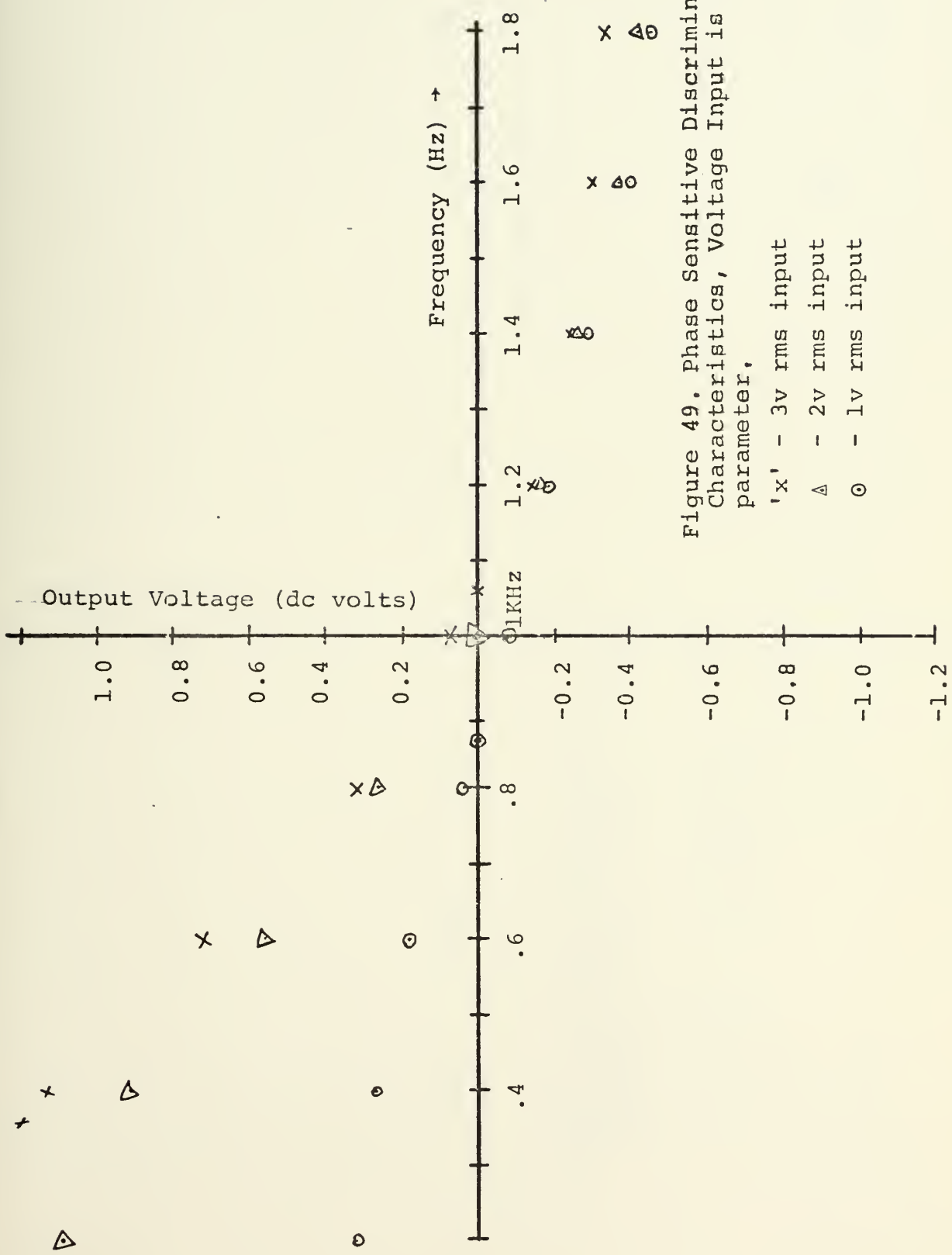


Figure 49. Phase Sensitive Discriminator Characteristics, Voltage Input is the parameter.

- 'x' - 3v rms input
- Δ - 2v rms input
- ⊙ - 1v rms input



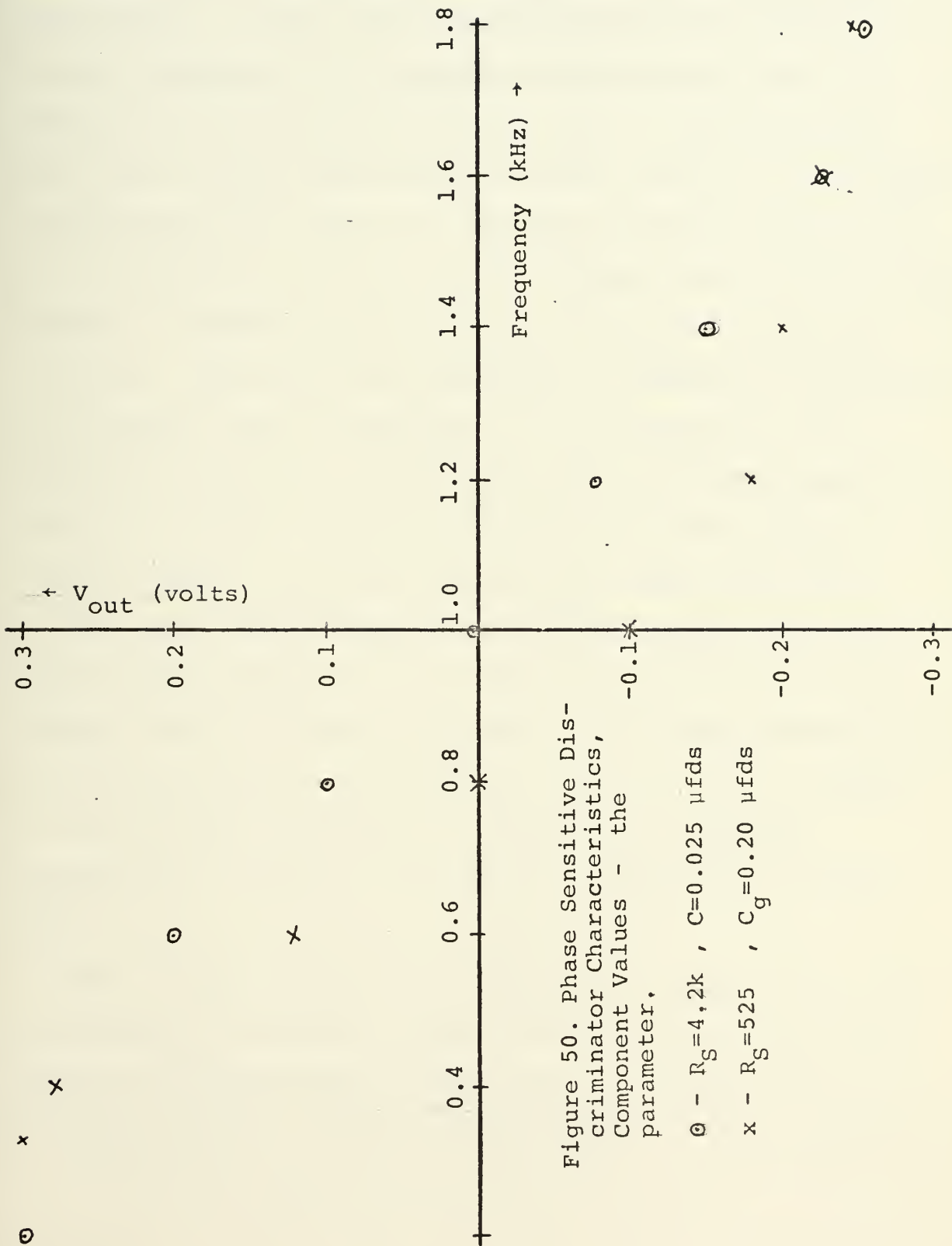


Figure 50. Phase Sensitive Discriminator Characteristics, Component Values - the parameter.

⊙ -  $R_S=4,2k$  ,  $C=0.025 \mu\text{fds}$

x -  $R_S=525$  ,  $C_g=0.20 \mu\text{fds}$



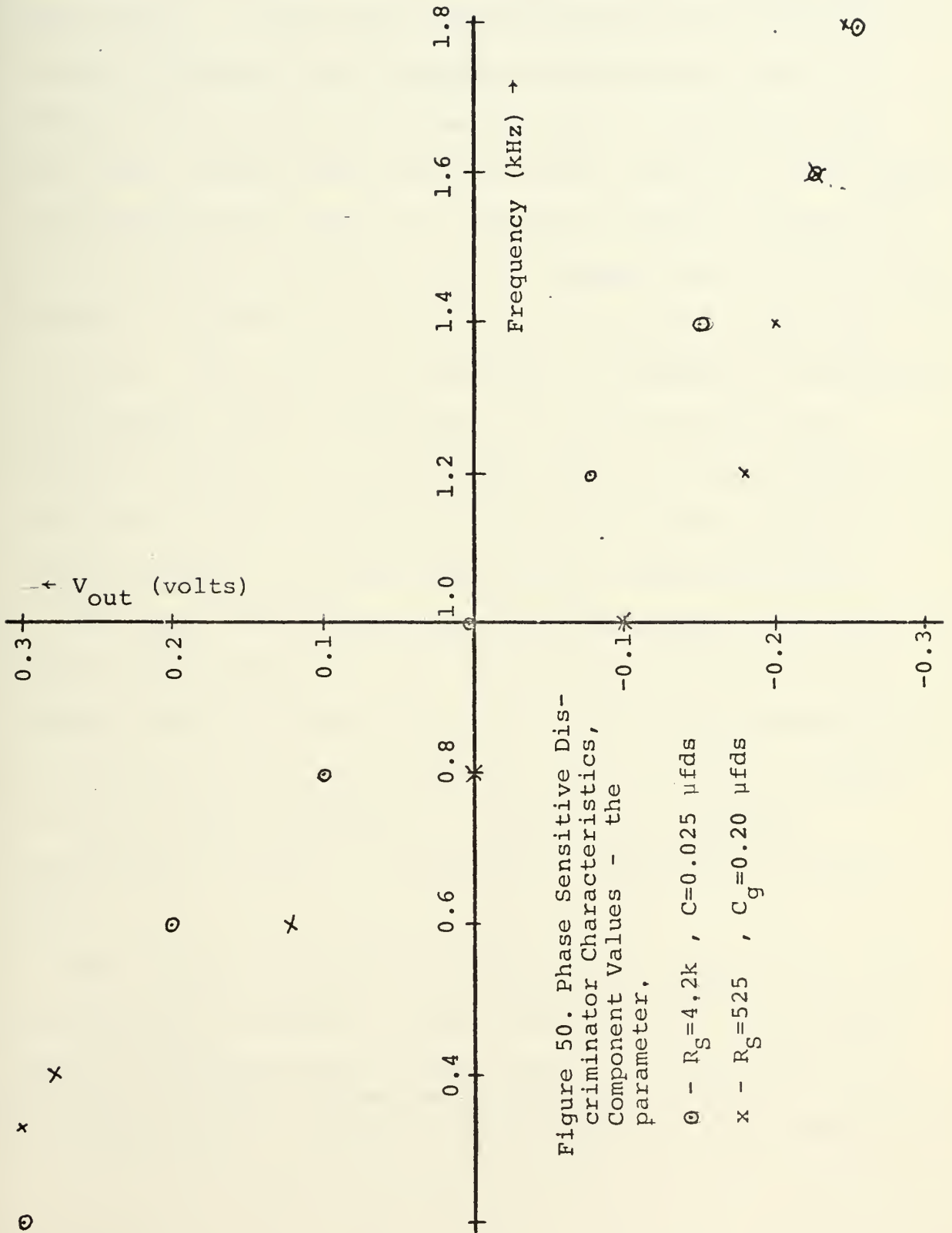


Figure 50. Phase Sensitive Discriminator Characteristics, Component Values - the parameter.

⊙ -  $R_S = 4.2k$  ,  $C = 0.025 \mu fds$

x -  $R_S = 525$  ,  $C_g = 0.20 \mu fds$



### C. RETRIGGERABLE MONOSTABLE MULTIVIBRATOR/INTEGRATOR

The retriggerable monostable multivibrator/integrator is available as an integrated circuit package (Fairchild part number 9601). It has the typical advantages of integrated circuit technology; its principal disadvantage is that it requires at least a two-volt signal into a fifty-ohm load. This input current requirement loads the output of most conventional operational amplifier voltage followers, requiring the use of a booster transistor in the feedback loop of the op-amp follower. The 9601 has the inherent reliability of binary circuitry. Requiring a few peripheral components to determine the frequency range of operation, this discriminator has excellent linearity. In addition, since the 9601 requires a square-wave input, analog signals must be passed through limiting stages to provide the requisite input waveshape.

The basic block diagram of the retriggerable monostable multivibrator/integrator as a frequency-selective nonlinear voltage control is shown in Figure 51. The basic block diagram of the integrated-circuit one-shot (9601) is given in Figure 52. The circuit schematic of the 9601 as a frequency discriminator is shown in Figure 53. [Fairchild IC Catalog 1970].

The low-pass network R2-C2 filters the output of the 9601; the controller produces a linear output voltage curve proportional to frequency over a range and at a sensitivity set by the Rx-Cx network. Figure 54 demonstrates the high quality of





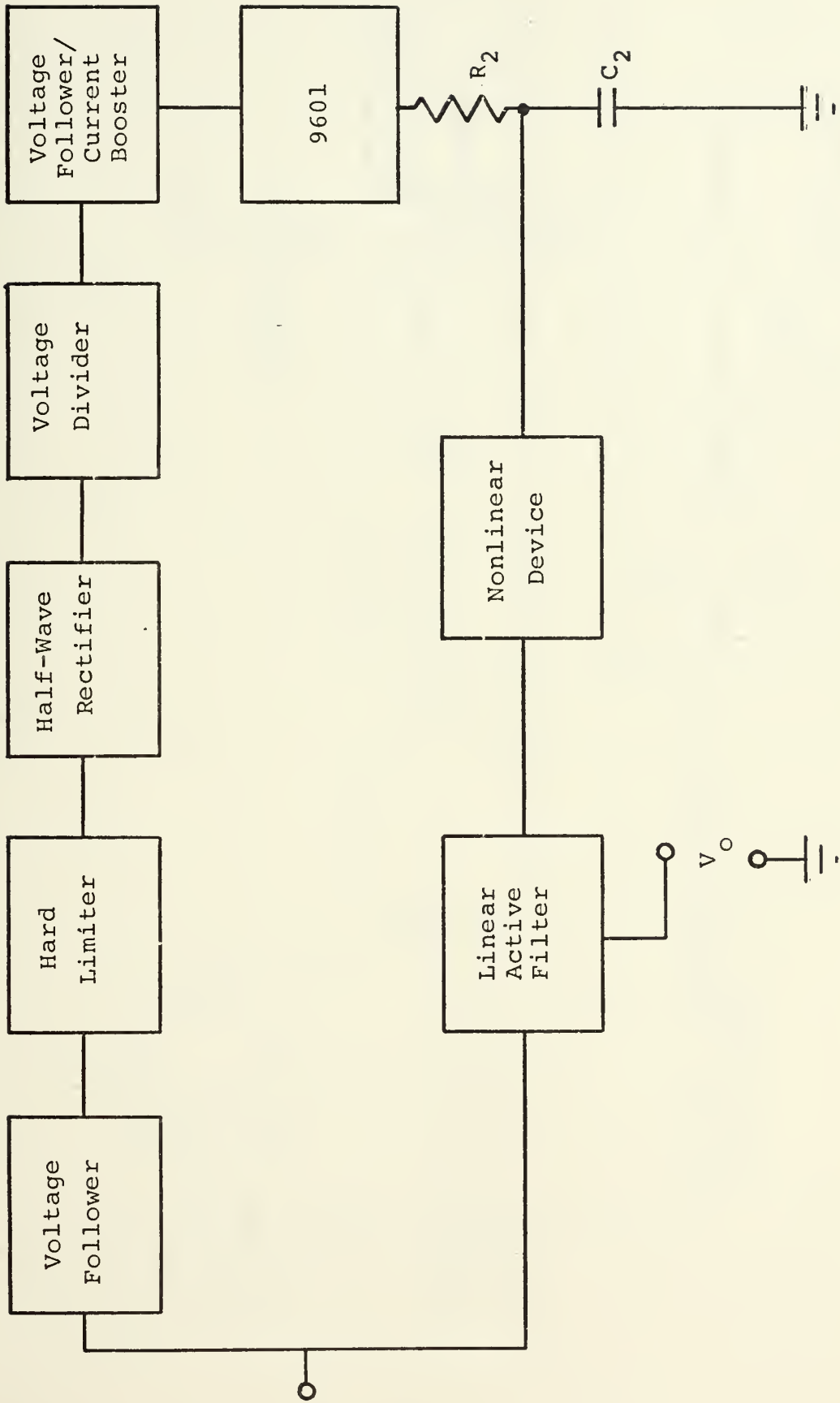


Figure 51. Retriggerable Monostable Multibrator/  
Integrator Controller Block Diagram.



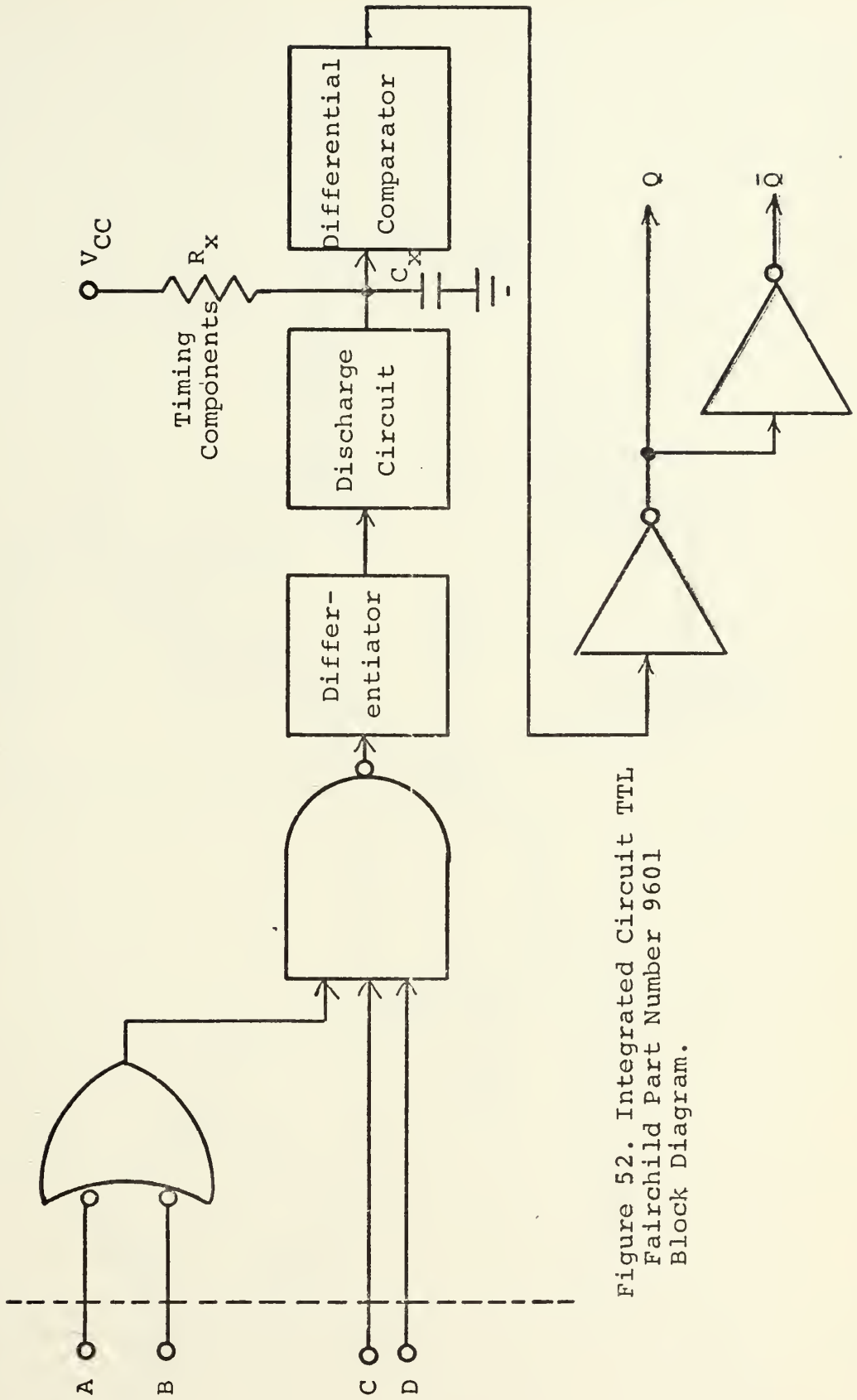


Figure 52. Integrated Circuit TTL Fairchild Part Number 9601 Block Diagram.



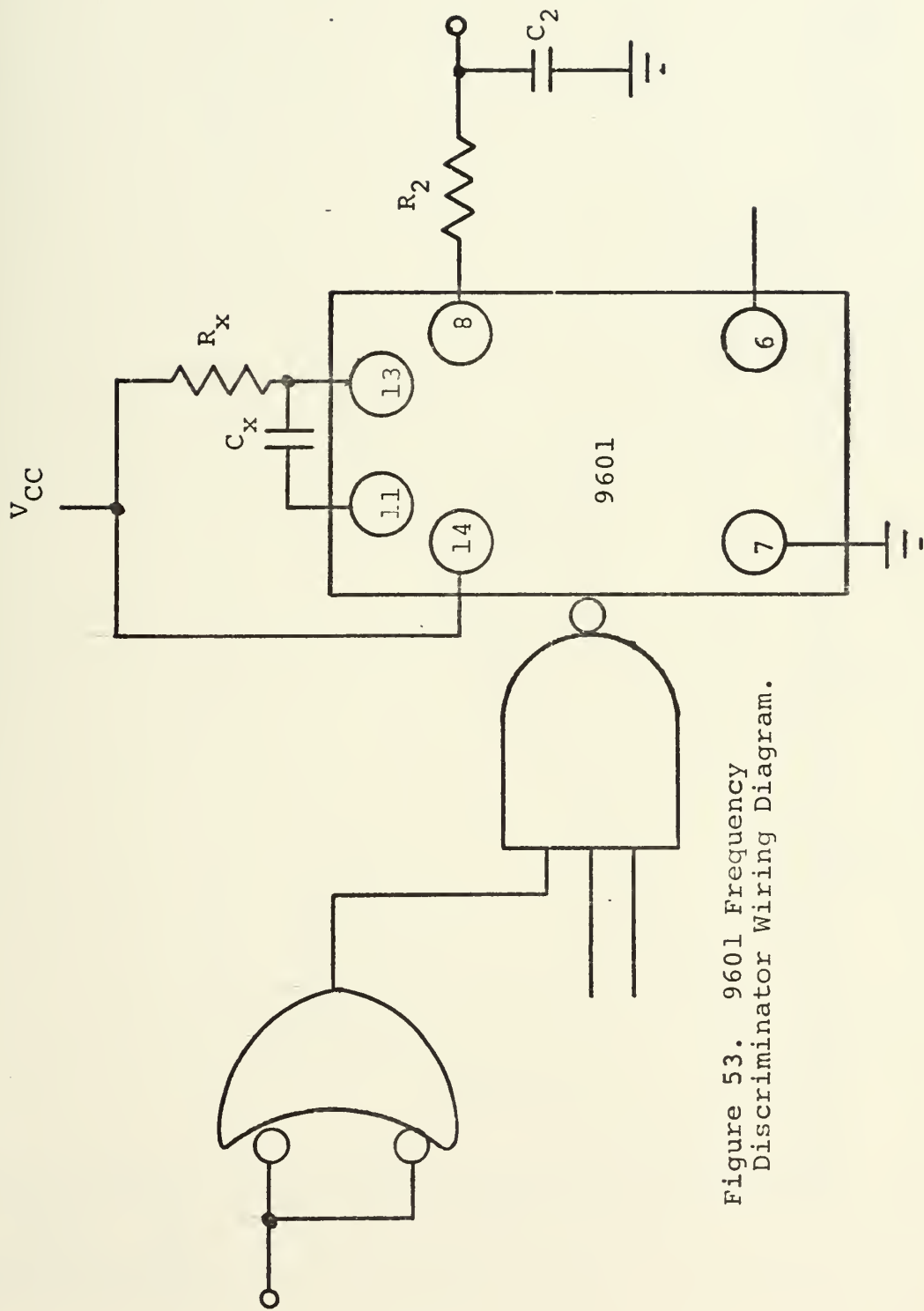


Figure 53. 9601 Frequency Discriminator Wiring Diagram.



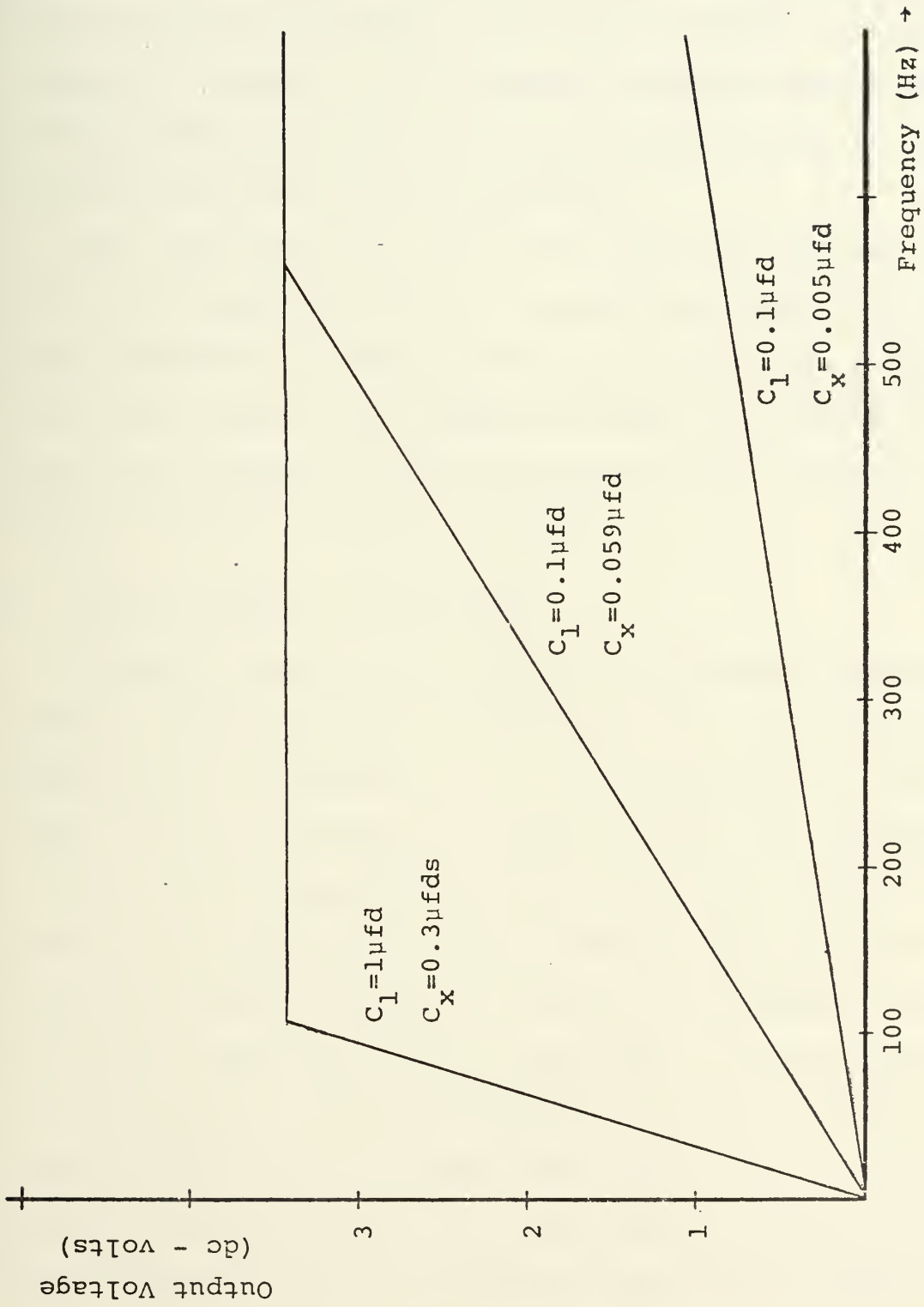


Figure 54. 9601 Frequency Discriminator Characteristic.





linearity available. The selection of frequency range and output voltage sensitivity is determined by the Rx-Cx time-constant. Clearly this controller is amenable to integrated circuit/hybrid technology; this factor, combined with its excellent linearity, wide frequency range and excellent output voltage sensitivity, make it very attractive as a frequency-selective nonlinear device controller.

The requirement for a 2-3 volt square-wave signal into a 50-ohm load makes additional circuitry necessary. In addition, when preceded by a hard limiter, as required for changing the analog signal to the requisite square wave input, the controller provides consistent output voltages over a wide range of input voltages (26 mv-10v).

#### D. ACTIVE FILTER DISCRIMINATOR

A simple scheme, relatively easy to implement in monolithic/hybrid integrated-circuit technology is the use of either a high-pass or a low-pass filter, half-wave rectifier, and low-pass filter to provide a d-c output voltage versus frequency, in the range of frequencies of interest. The filter is operated on the skirt of the filter response, where the rate of change of output voltage as a function of frequency can be set by the number of poles in the filter. The frequency range is determined by the cutoff frequency of the filter and the order of the filter. A simplified block diagram of this system is shown in Figure 55. The output voltage of the filter discriminator may then be combined with a bias voltage or



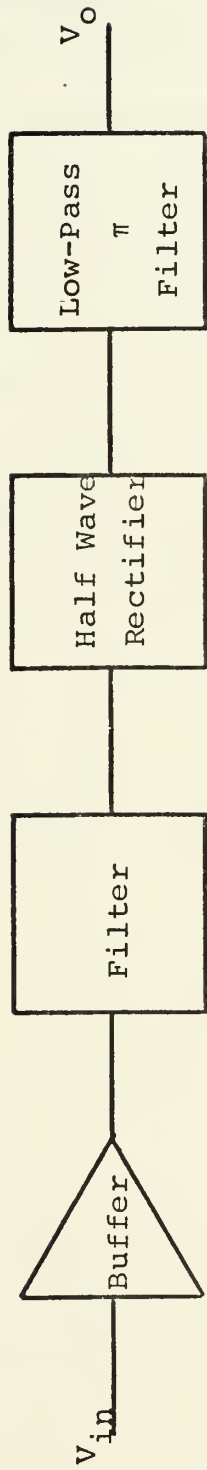


Figure 55. Filter Discriminator Block Diagram.



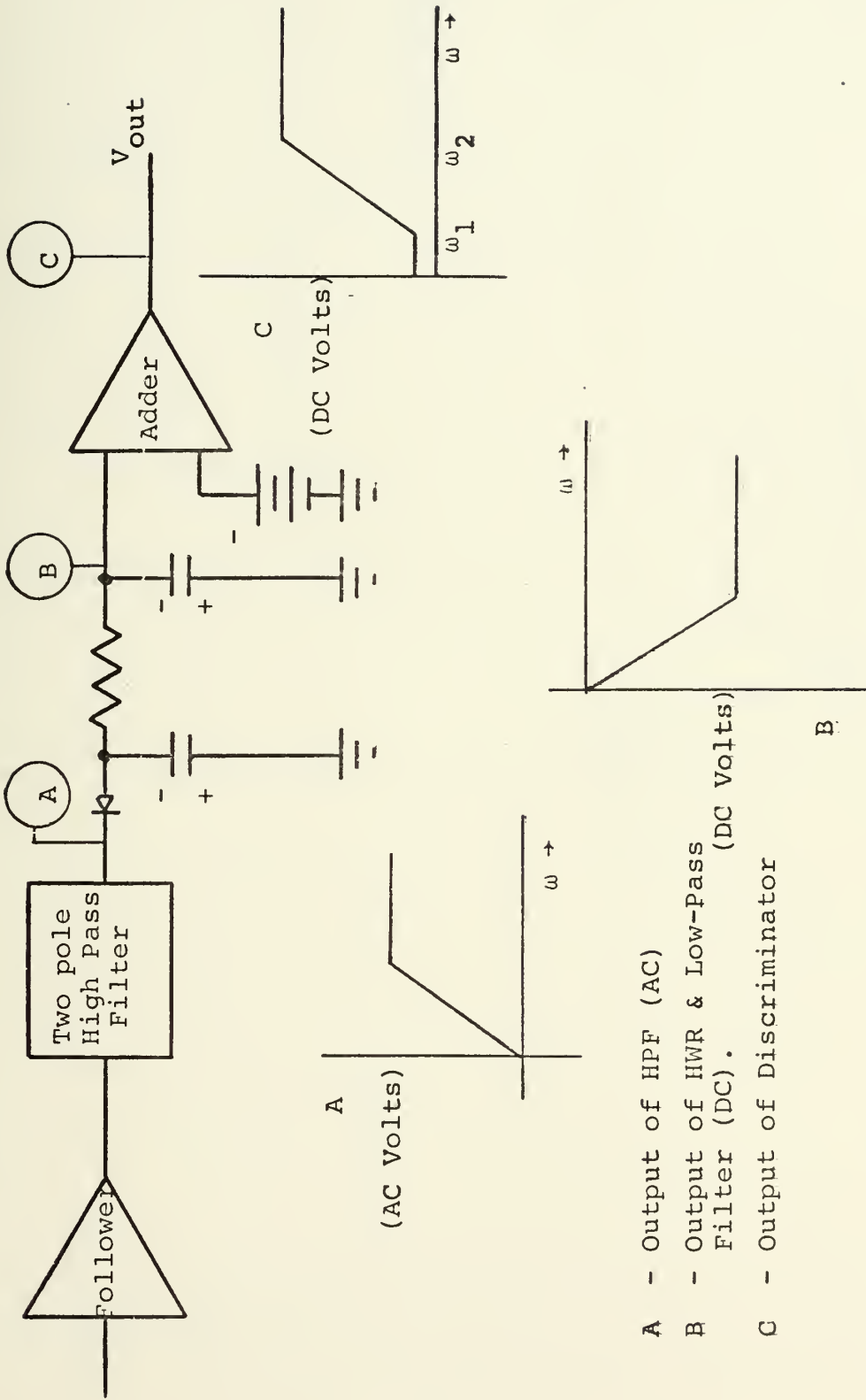
other logic voltage to produce the required control voltage as a function of frequency (see Figure 56 for examples).. The bias voltage was determined for the particular device chosen, in this case for a field-effect transistor.

This controller has the advantage of system simplicity but requires additional components, readily available with monolithic/hybrid integrated circuit technology. It has adaptability in that the filter shaping can take any form consistent with realization of linear active filters. Further flexibility is achieved by the summer circuit. The controller's principal disadvantage is its amplitude dependence, i.e., the output voltage is also determined by the amplitude of the signal input. This effect could be reduced by the use of AGC or limiting. Neither was tried.

Since an R-c pi-filter was chosen to smooth the output from the half-wave rectifier, one would assume the output voltage to be affected by the load. Figure 57 shows the effect of loading on the output characteristic. This is not considered to be a limitation as it is expected that the input impedance of the summer will remain relatively constant as a function of frequency.

Figure 58 shows the effect of a d-c bias voltage; it is possible with this control device and the filter characteristic to realize any voltage-frequency relationship desired.





- A - Output of HPF (AC)
- B - Output of HWR & Low-Pass Filter (DC).
- C - Output of Discriminator

Figure 56a. Control Voltage Examples.  
 Example 1. Linearly rising DC Voltage as a function of frequency ( $\omega_1 < \omega < \omega_2$ ).





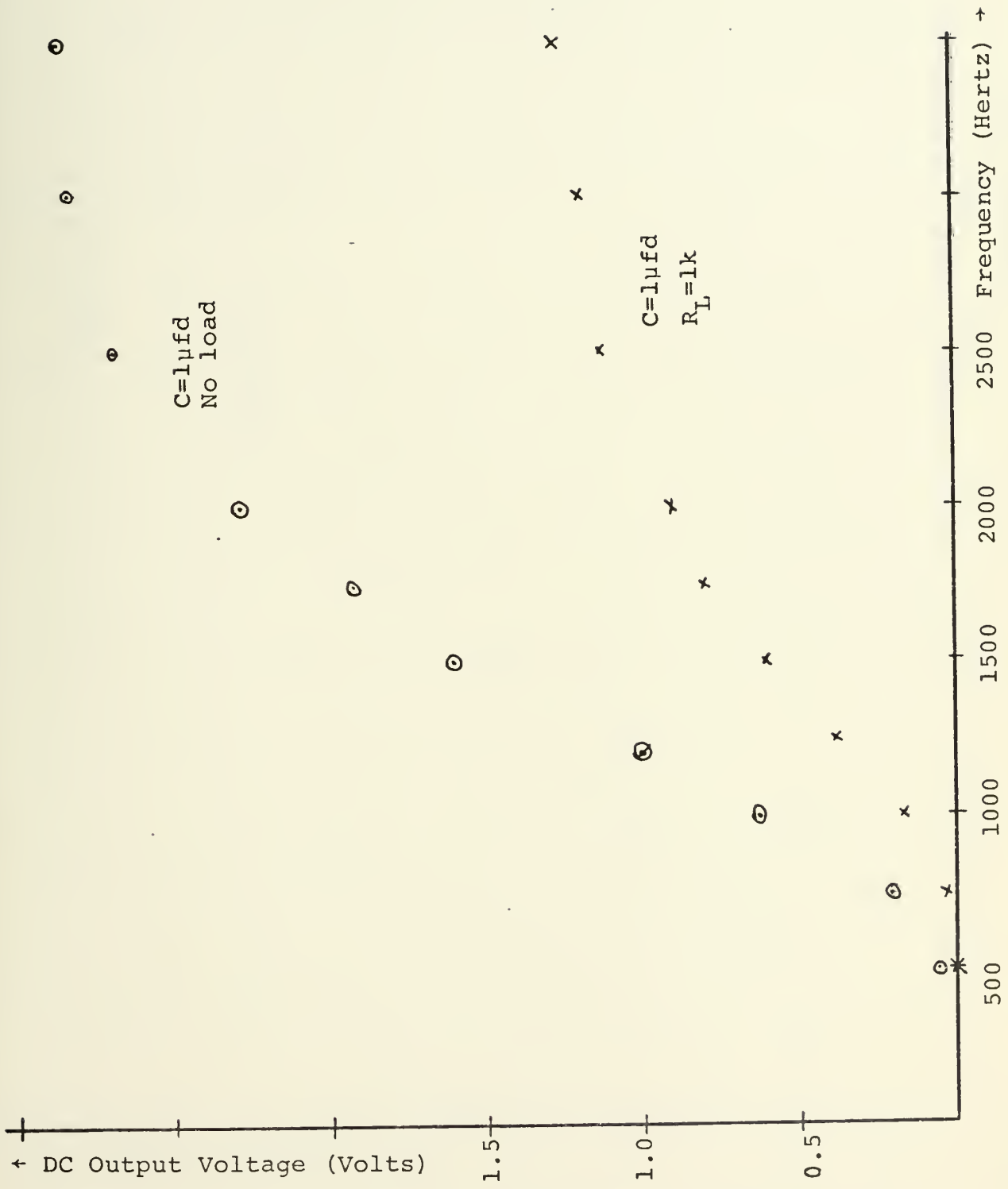


Figure 57. Filter Discriminator,  $R_{LOAD}$ =Parameter.



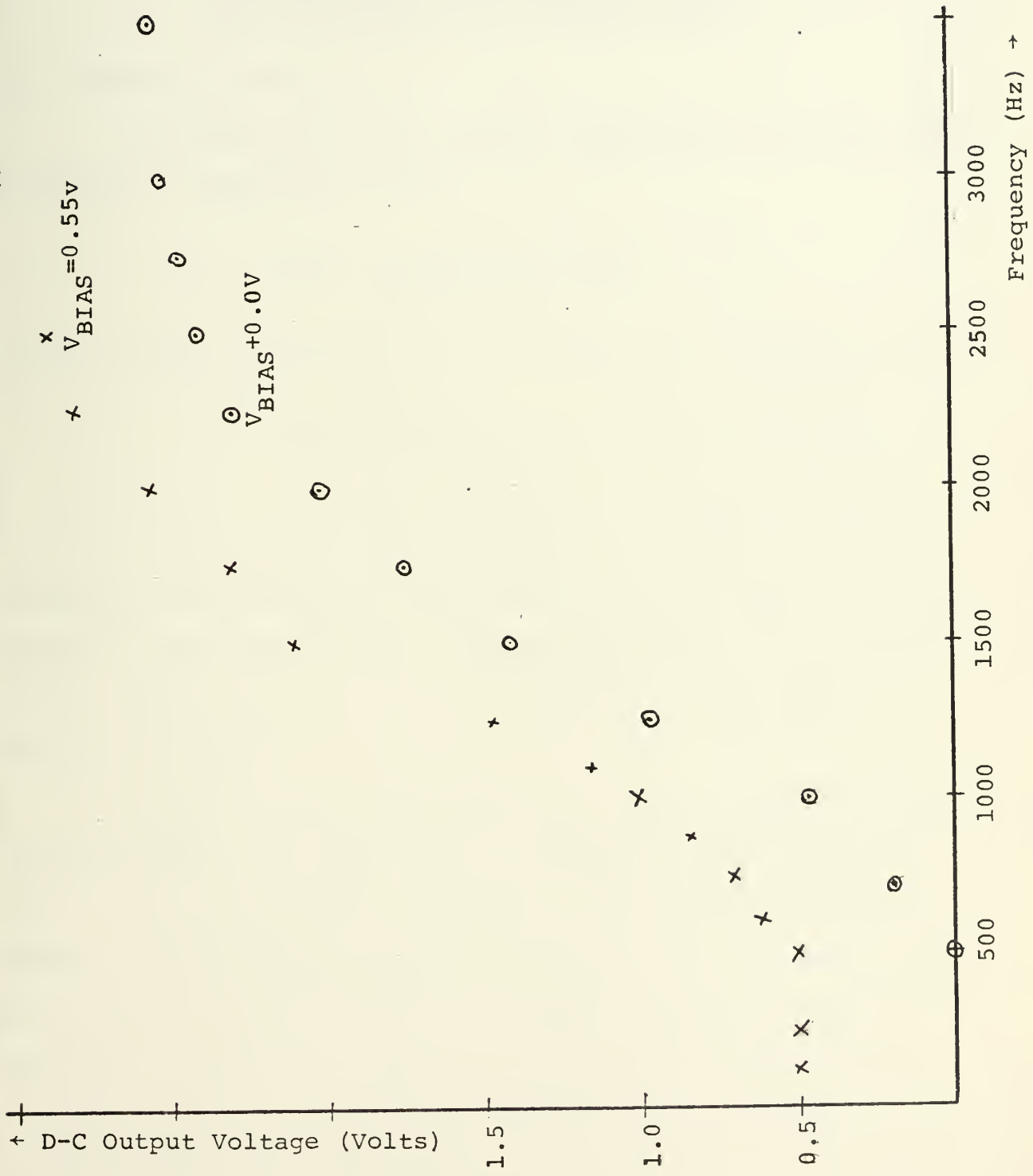


Figure 58. Filter Discriminator Characteristic. Bias Voltage is the parameter.



## V. ANALYTIC AND EXPERIMENTAL DESIGN OF HYBRID NONLINEAR ACTIVE FILTERS

### A. LOW-PASS FILTER

1. Beginning with the transfer function of a second-order system for a low-pass filter,

$$F(s) = \frac{1}{\omega_n^2 + 2\zeta\omega_n s + s^2} ,$$

and normalizing by setting  $\omega_n = 1$  and  $2\zeta = \alpha$ , results in

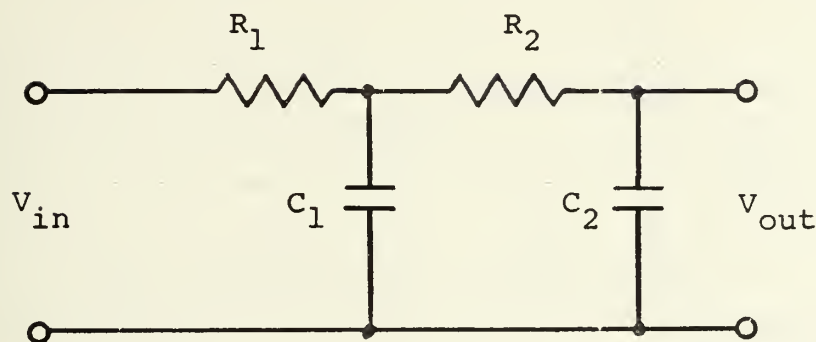
$$F(s) = \frac{1}{1 + \alpha s + s^2} .$$

It can be seen from the possible pole locations of the quadratic denominator in the transfer function that the filter could be realized by an R-C ladder or a series L-R-C arrangement. Typical passive filter configurations are shown in Figures 59 and 60.

2. Active filter realizations for the low-pass frequency characteristic take many forms. Figure 61 shows a second-order active Rauch filter [Foster]. This was the linear filter chosen for the synthesis of an active nonlinear filter. The Butterworth second-order low-pass characteristic was selected. Normalized values of  $C_1 = 2.12132$  farads and  $C_2 = 0.47140$  farads were extracted from Table II in Foster. Choosing a roll-off frequency of  $f_c = 1\text{kHz}$  resulted in resistance values of  $47.0\text{ k}\Omega$ . The circled numbers in Figure 61 refer to the connection points for the nonlinear resistance.



Figure 59. Low-Pass Filter, RC Ladder.



$$F_1(S) \triangleq \frac{V_o(S)}{V_{in}(S)} = \frac{1}{S^2 R_1 C_1 R_2 C_2 + S [R_1 (C_2 + C_1) + R_2 C_2] + 1}$$

Line of possible poles

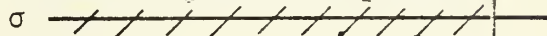
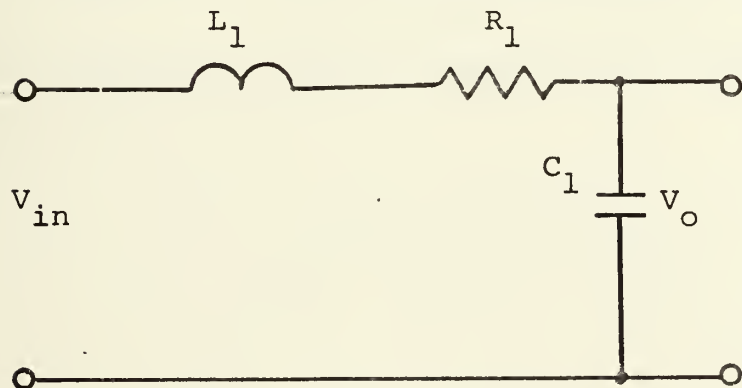
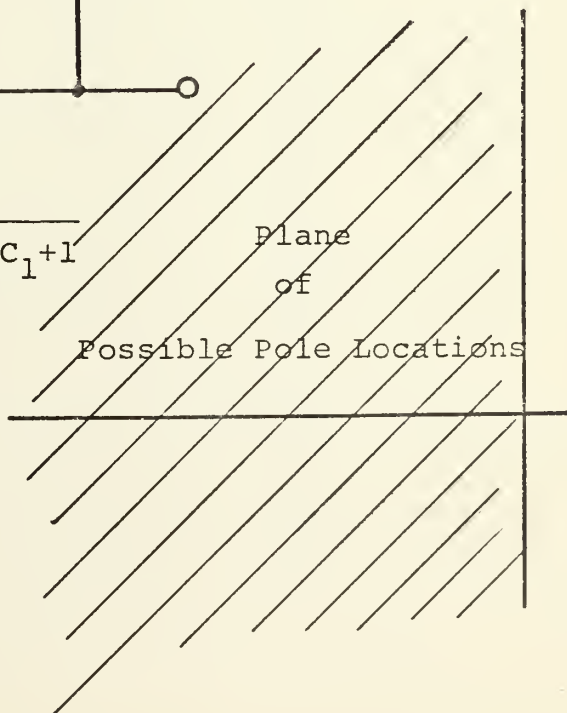


Figure 60. Low-Pass Filter, L-R-C Series Circuit.



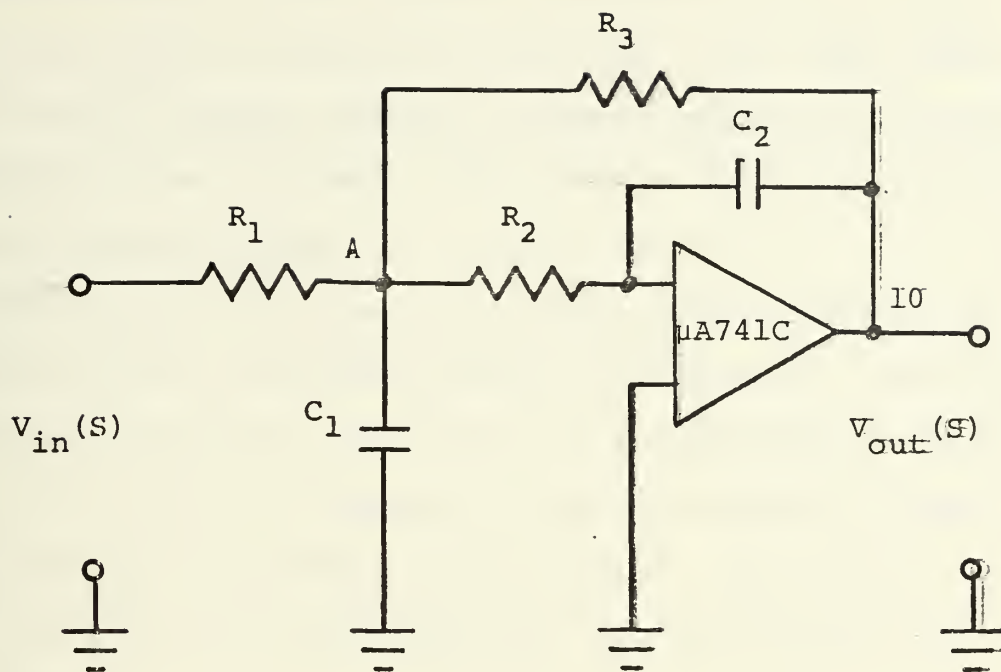
$$F_2(S) \triangleq \frac{V_o(S)}{V_{in}(S)} = \frac{1}{S^2 L_1 C_1 + S R_1 C_1 + 1}$$

Plane  
of  
Possible Pole Locations



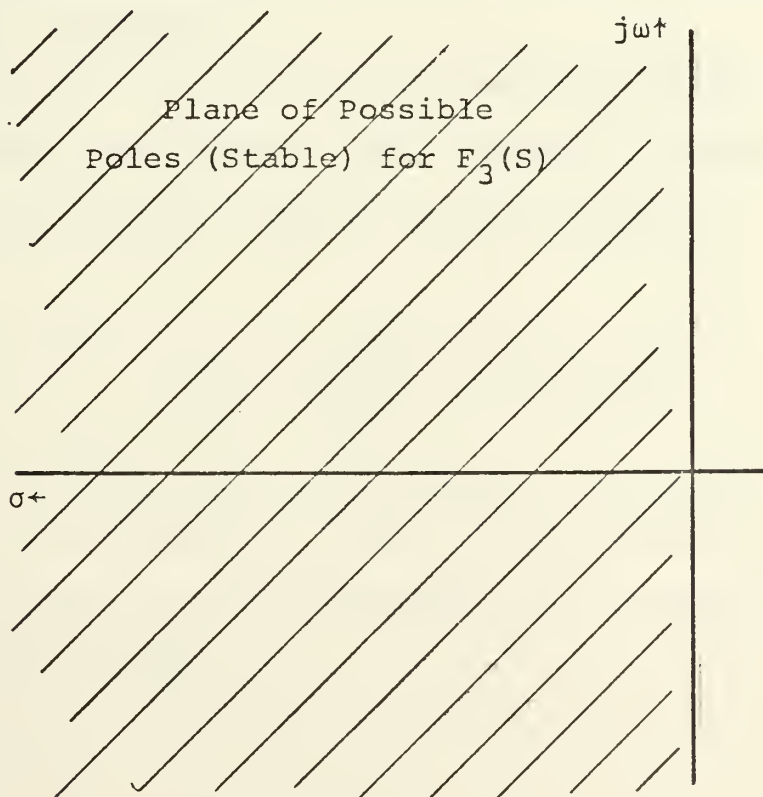






$$F_3(S) = - \frac{R_3}{R_1 R_2 R_3 C_1 C_2 S^2 + [(R_2 R_3 + R_1 R_3 + R_1 R_2) C_2] S + R_1}$$

Figure 61. Second Order Rauch Low-Pass Active Filter.





Measurements of the frequency response of the linear filter are shown in Figures 62a and 62b. The -15db level was chosen so that larger values of voltage would not be across the FET-nonlinear resistor, which will be  $R_3$  in the synthesis of the nonlinear filter.

The transient response of the linear active filter is portrayed by the photographs shown in Figure 63.. The test signal was a 20-hertz square wave, the amplitude of the signal was  $\pm 1.0v$  and the horizontal setting of the oscilloscope was set at four milliseconds per centimeter. The vertical sensitivity of the oscilloscope was set at 0.5 volts per centimeter.

A small rise time, approximately 300-400  $\mu s$ , is noted with less than 10% overshoot. A small amount of low-frequency distortion is also noted but appears to be less than the input low-frequency distortion.

3. With  $R_3$  set equal to  $\alpha$  and normalized values of the other components substituted in the transfer function, the parameter plane transfer function  $F_3 (S)$  becomes

$$F_3 (S) = \frac{-\alpha}{\alpha S^2 + (0.94280\alpha + 0.47140)S + 1.0}$$

Note that this normalization will permit the parameter plane curves to be read directly in hertz. The normalized values of components are:  $C_1 = 2.12132$  farads,  $C_2 = 0.47140$  farads,  $R_1 = R_2 = 1$  ohm, and  $R_3 = \alpha$ .



Measurements of the frequency response of the linear filter are shown in Figures 62a and 62b. The -15db level was chosen so that larger values of voltage would not be across the FET-nonlinear resistor, which will be  $R_3$  in the synthesis of the nonlinear filter.

The transient response of the linear active filter is portrayed by the photographs shown in Figure 63. The test signal was a 20-hertz square wave, the amplitude of the signal was  $\pm 1.0v$  and the horizontal setting of the oscilloscope was set at four milliseconds per centimeter. The vertical sensitivity of the oscilloscope was set at 0.5 volts per centimeter.

A small rise time, approximately 300-400  $\mu s$ , is noted with less than 10% overshoot. A small amount of low-frequency distortion is also noted but appears to be less than the input low-frequency distortion.

3. With  $R_3$  set equal to  $\alpha$  and normalized values of the other components substituted in the transfer function, the parameter plane transfer function  $F_3 (S)$  becomes

$$F_3 (S) = \frac{-\alpha}{\alpha S^2 + (0.94280\alpha + 0.47140)S + 1.0}$$

Note that this normalization will permit the parameter plane curves to be read directly in hertz. The normalized values of components are:  $C_1 = 2.12132$  farads,  $C_2 = 0.47140$  farads,  $R_1 = R_2 = 1$  ohm, and  $R_3 = \alpha$ .



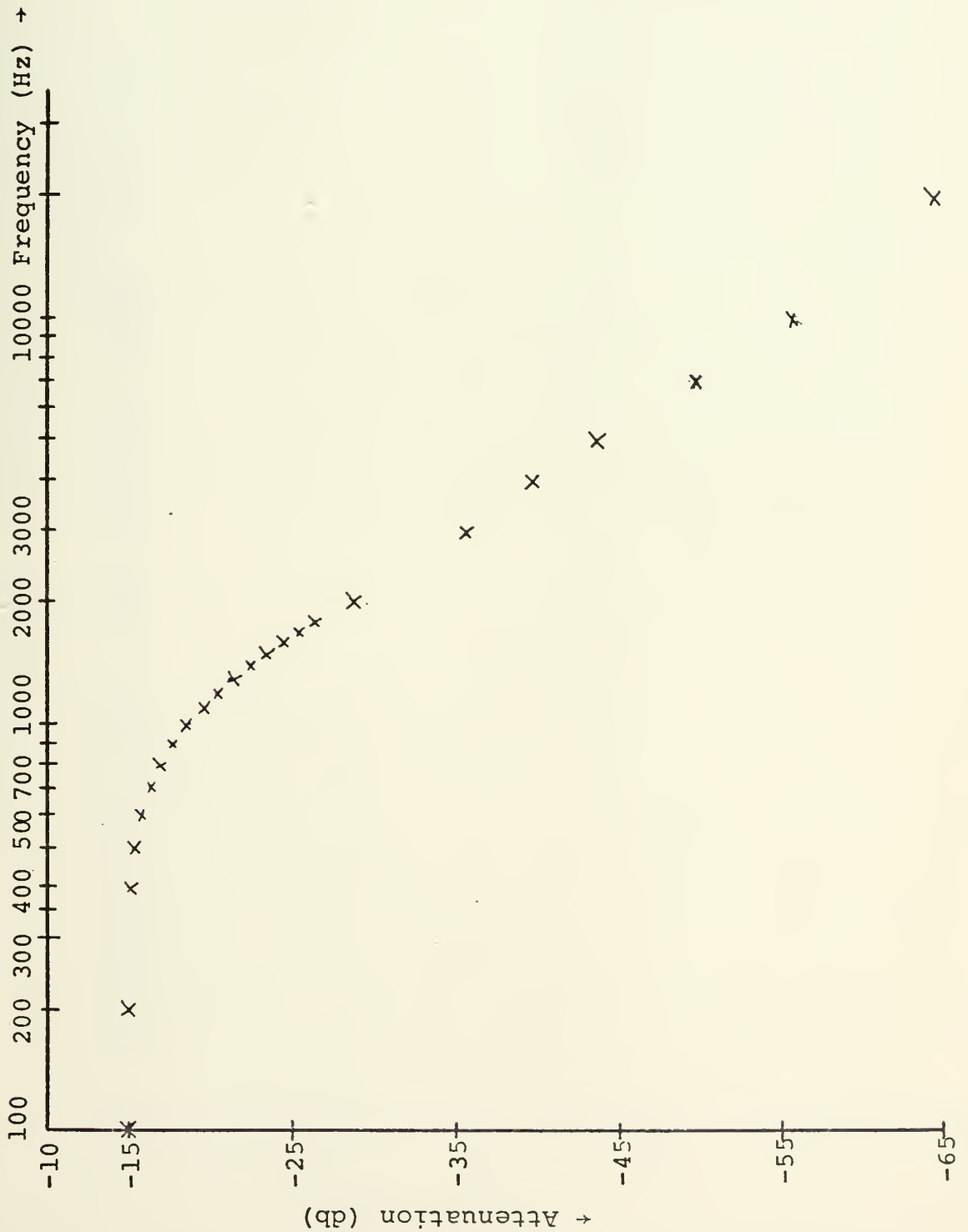


Figure 62a. Low-Pass Active Filter Frequency Response Characteristic  $V_{in} = 435$  mv rms.





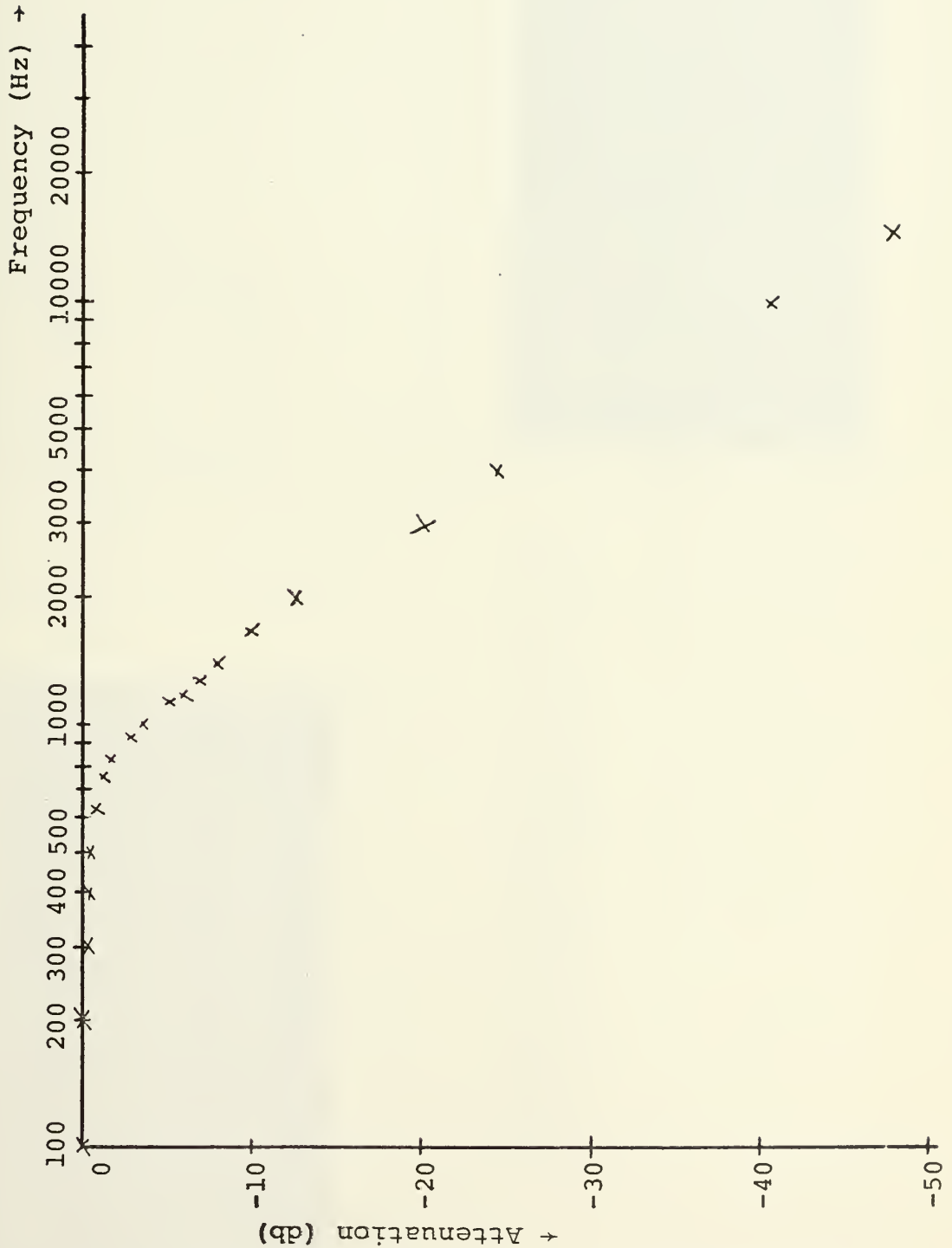
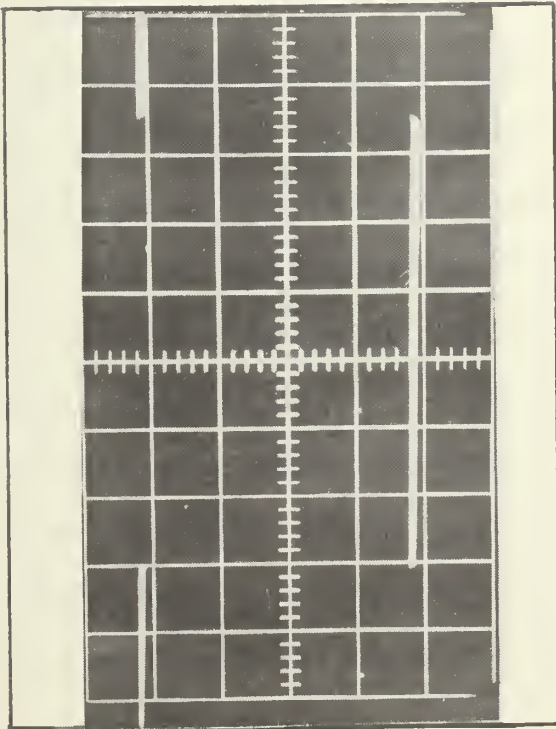


Figure 62b. Low-Pass Active Filter Frequency Response Characteristic.  $V_{in} = 2.78v$  rms.



(Left)

Input to Filter  
Vert. = 0.5v/cm  
Horiz. = 4ms/cm



(Below)

Output to Filter  
Vert. = 0.5v/cm  
Horiz. = 4ms/cm

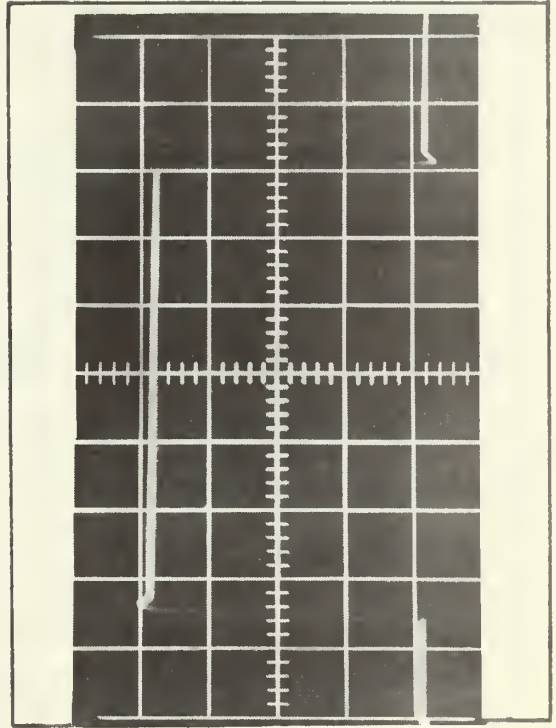


Figure 63. Photographs of the Transient Response of the Low-Pass Linear Active Filter. (Voltage Magnitude vs. Time).



Values of  $\alpha$  to be displayed on the parameter plane Bode plots were chosen from Table VIII (the FET nonlinear frequency-dependent  $\alpha$ -characteristic).

The physical configuration of the frequency-dependent nonlinear resistor is shown in Figure 64. (Note that Figure 64 does not show the feedback resistors used in the FET). The test circuit and pertinent formulae for calibrating the frequency dependent nonlinear resistor are shown in Figure 65. The voltage-divider  $R_1 - R_2$  was used to keep the voltage across the FET at -15.2db (345 mv) at 200 HZ.  $\alpha$  values for the parameter plane analysis are shown as  $\alpha^*$  in Table VIII. The effects of the series capacitor,  $C_1$ , and the feedback network  $R_3/R_4$  are ignored. Figure 66 shows the frequency-dependent attenuation factor,  $A$ , as a function of frequency. The FET used was the feedback-configured n-channel JFET, 2N3819.

Parameter plane curves are shown in Figure 67 with the  $\alpha$ -characteristic superimposed on the family of Bode curves. The experimental measurements of the nonlinear active filter are shown in Figure 68 plotted with x's, and the parameter plane values plotted with dots. Note that the parameter plane values were translated from 0db to -15.2 db at 200 H<sub>Z</sub> by adding -13.792 db to all parameter plane analytic results. The parameter plane analysis program is a linear analysis tool and a rescaling of the driving voltage will not effect the plots except to translate them up or down. The tabular data are summarized in Table IX. Figure 69 contains four photographs



TABLE VIII. Low-Pass Nonlinear Filter  $\alpha$ -Characteristic Tabular Data

f (Hz)	A (db)	A/20	Req(n)	$\alpha$	$\alpha^*$ (Values for PARTFl)
100	15.2	0.76	40319.7	0.8578	1.0
200	15.1	0.755	41855.1	0.8905	
600	15.1	0.755	41855.1	0.8905	0.85
700	15.2	0.76	40319.7	0.8578	
800	15.2	0.76	40319.7	0.8578	
900	15.2	0.76	40319.7	0.8578	
1000	15.4	0.77	37519.1	0.7983	0.79
1100	16.3	0.815	28143.3	0.599	0.59
1200	18.2	0.91	17364.1	0.3694	0.36
1300	21.3	1.065	9457.04	0.2012	0.20
1400	26.5	1.325	3595.8	0.07650	0.07
1500	32.5	1.625	1894.8	0.0403	0.04
1600	36.2	1.81	1194.6	0.0254	0.02
1700	39.2	1.96	829.9	0.0177	
1800	40.8	2.04	685.	0.0146	
1900	42.0	2.10	593.8	0.0126	0.01
2000	43.0	2.15	527.3	0.0112	
3000	46.2	2.31	361.6	0.00769	
4000	46.5	2.325	349.1	0.00742	
5000	46.5	2.325	↓		
6000	46.5	2.325			
7000	46.5	↓			
10000	46.5	↓			





Figure 64. Physical Configuration of Frequency-Dependent Nonlinear Resistor.

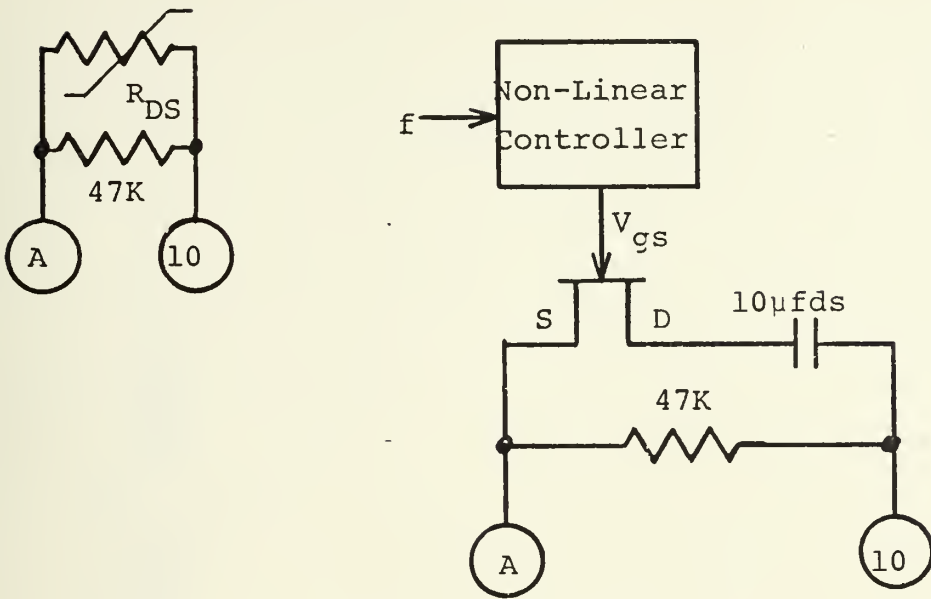
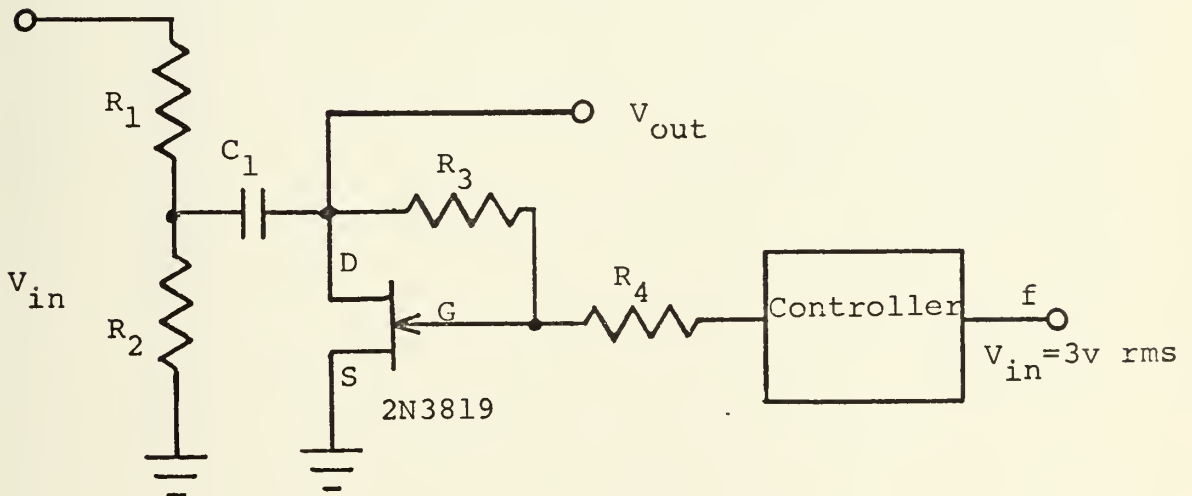


Figure 65.  $\alpha$ -Characteristic Test Circuit with Pertinent Formulae



$$R_3 = R_4 = 4.7M; C_1 = 10\mu\text{fds}.$$

$$R_{eq} = R_2 \text{ in parallel with } R_{DS} \text{ (Ignore effects of } C_1, R_3, R_4).$$

$$\alpha_N = \alpha / 47.0K$$

$$\frac{V_{out}}{V_{in}} = \frac{R_{eq}}{R_{eq} + R_1}$$

$$20 \log \left( \frac{V_{out}}{V_{in}} \right) = A = \text{Attenuation Factor}$$



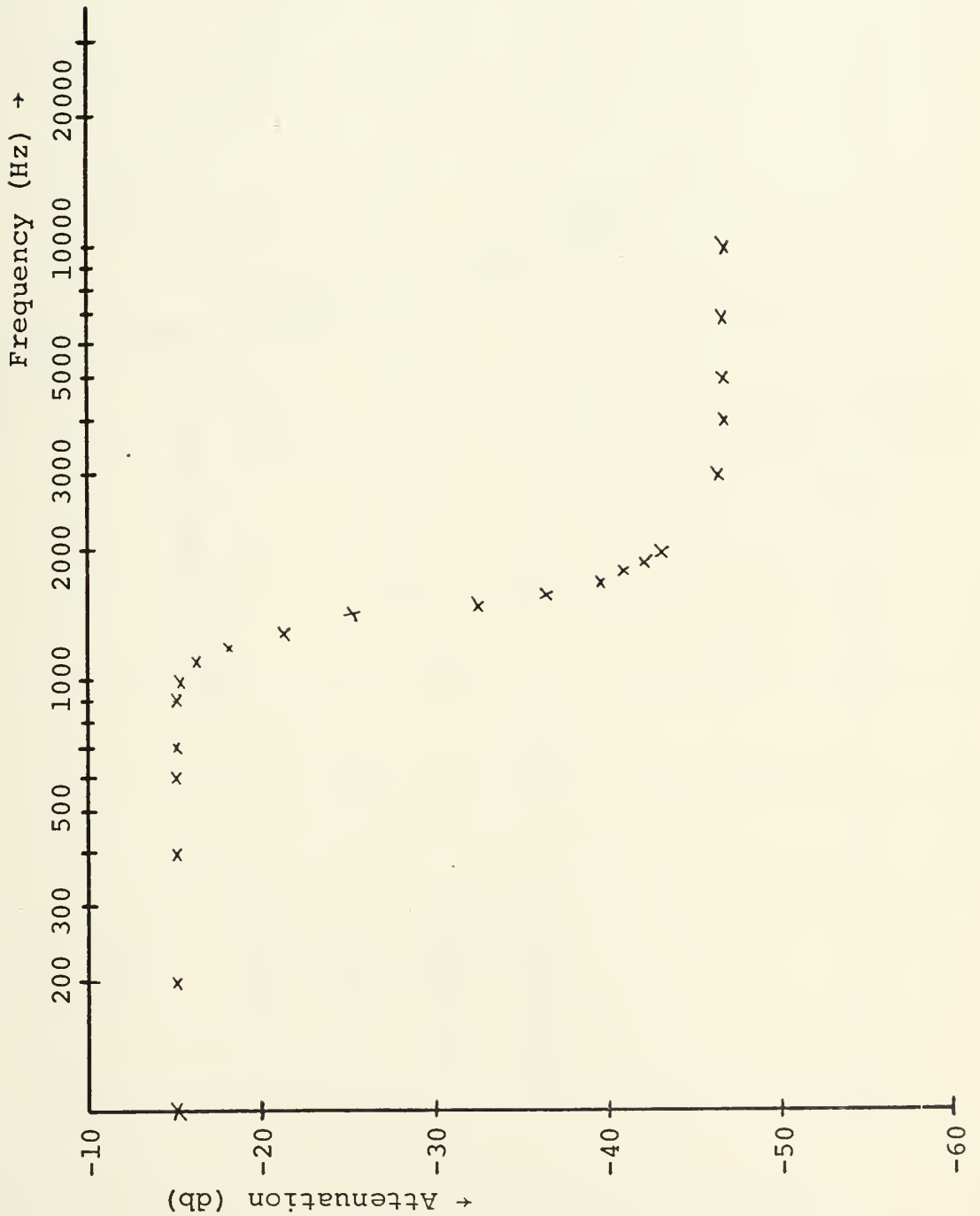


Figure 66. Frequency Dependent Attenuation Factor Characteristic. FET Type 2N3819. Low-Pass Filter  $\alpha$ .



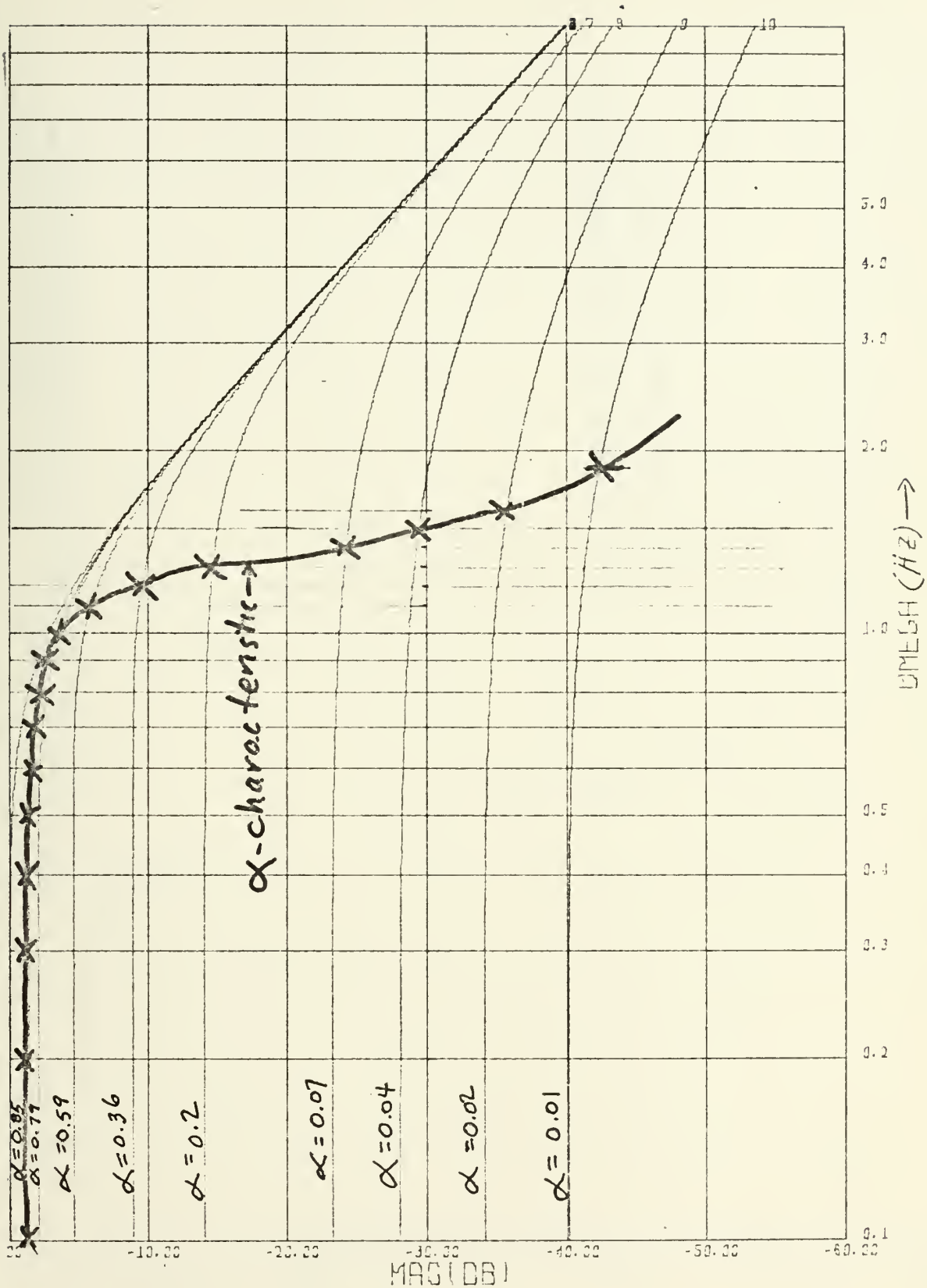


Figure 67. Parameter Curves, Low-Pass Filter with Superimposed  $\alpha$ -Characteristic.



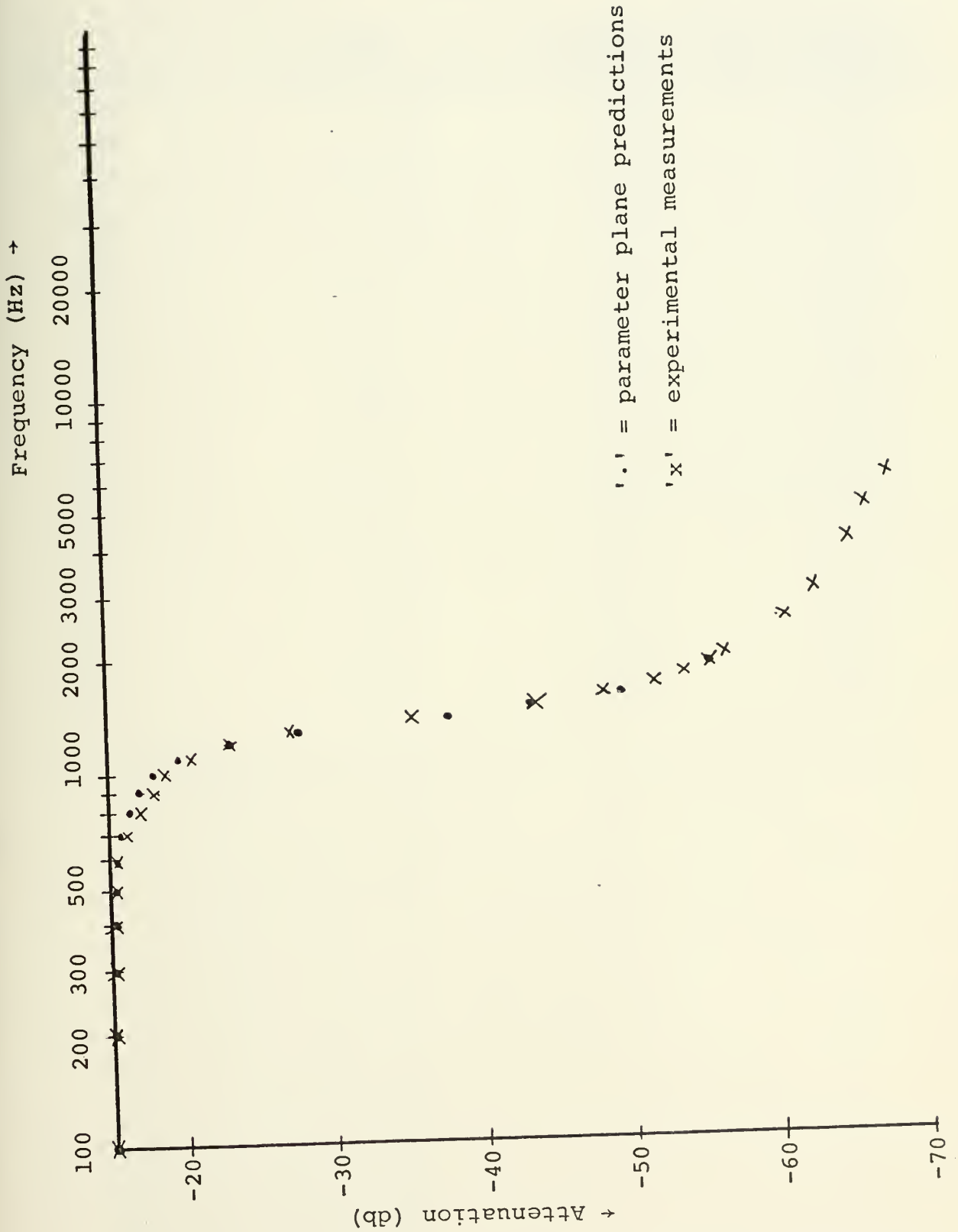


Figure 68. Nonlinear Active Low-Pass Filter Frequency Response Characteristics (Experimental and Parameter-Plane Predictions).

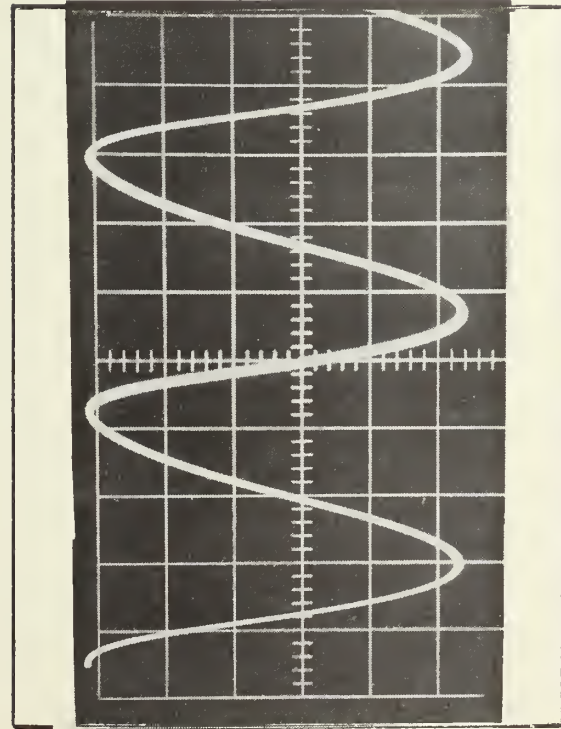




TABLE IX. Low-Pass Nonlinear Filter Frequency Response Data

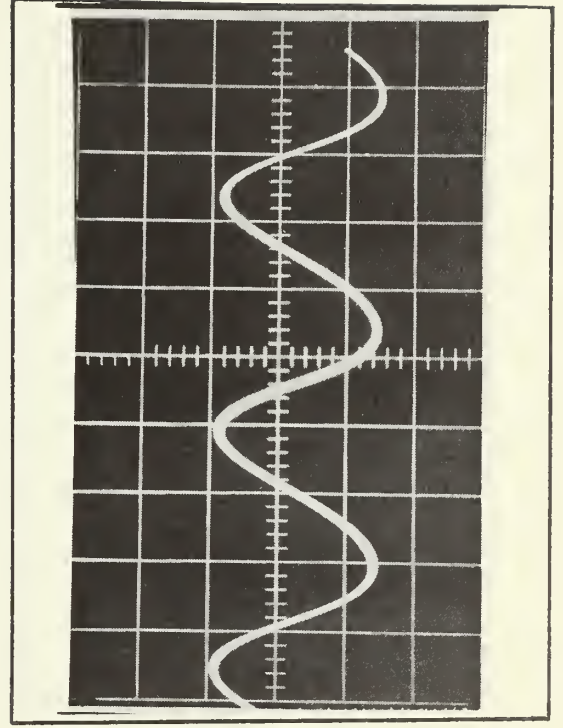
Freq. (Hz)	(DB) Parameter Plane	Translated (DB) Parameter Plane	(DB) Ex- perimental
100	-1.408	-15.20	-15.20
200	-1.403	-15.20	-15.20
300	-1.406	-15.20	-15.20
400	-1.436	-15.22	-15.40
500	-1.523	-15.31	-15.50
600	-1.60	-15.39	-15.80
700	-2.10	-15.9	-16.20
800	-2.35	-16.14	-16.80
900	-3.00	-16.79	-17.30
1000	-3.90	-17.69	-18.20
1100	-6.10	-19.90	-19.20
1200	-9.50	-23.29	-22.20
1300	-15.00	-28.79	-26.90
1400	-24.30	-38.09	-35.20
1500	-29.50	-43.29	-44.0
1600	-35.80	-49.59	-48.2
1900	-42.00	-55.79	-55.2





a. (Left)

Frequency = 1300 Hz  
 Vert. = 0.05v/cm  
 Horiz. = 0.2ms/cm

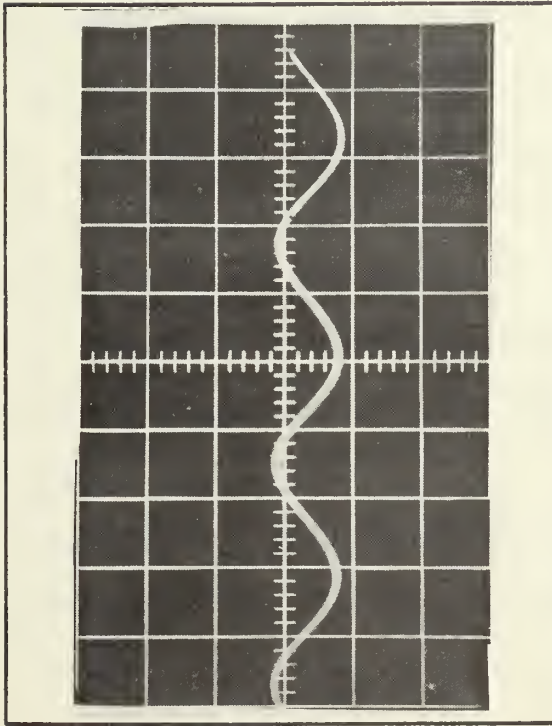


b. (Below)

Frequency = 1400 Hz  
 Vert. = 0.05v/cm  
 Horiz. = 0.2ms/cm

Figure 69. Harmonic Distortion Photographs for Nonlinear Low-Pass Filter. Output Voltage vs. Time.





c. (Left)

Frequency = 1500 Hz

Vert. = 0.05v/cm

Horiz. = 0.2ms/cm

d. (Below)

Frequency = 1800 Hz

Vert. = 0.05v/cm

Horiz. = 0.2ms/cm

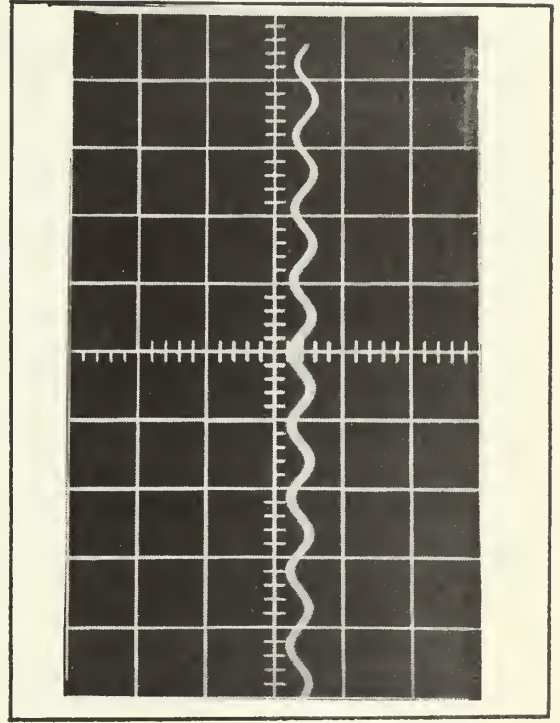


Figure 69. Harmonic Distortion Photographs  
for Nonlinear Low-Pass Filter (Output  
Voltage vs. Time).



of the output of the nonlinear filter for specified sinusoidal frequency inputs. Noticeable harmonic distortion is evident in photographs 3 and 4.

The test for superposition was conducted in two ways: the first used just two frequencies, 800 HZ and 1000HZ; the second, a modification of the first, used two frequencies at a time and consisted of a series of bi-frequency measurements. In the first case all detectable harmonic and subharmonics were recorded. In the second, all frequencies above a selected threshold value, 35db below selected signal input level, were recorded.

The first test was intended to reveal a region of the filter operation which would be near the initiation of the nonlinear region behavior of the FET (a 7% change in  $\alpha$ ). If the principles of homogeneity and superposition applied in this narrow region, then it was planned to use a wider separation between the two frequencies.

Table X summarizes the measurements taken in the first case. It can be seen that there are substantial numbers of new frequencies introduced. As expected from nonlinear behavior; the sum, difference, second harmonic of 800 H<sub>Z</sub>, second harmonic of the difference frequency (275), etc. have substantial amplitudes with respect to the amplitudes of the inputs.

Homogeneity and superposition did not obtain. The relative magnitudes of the two signals were approximately what could





TABLE X. Test One for Superposition of Two Sinusoids in Nonlinear Active Low-Pass Filter Case (Input Frequencies are 800 Hz (Odb) and 100 Hz (Odb)).

Freq. (Hz)	Input (db)	Output (db)
275	-----	-23.2
536	-----	-23.0
800	0.0	- 5.0
1000	0.0	- 7.0
1344	-----	-29.2
1605	-----	-26.5
1879	-----	-23.2
2148	-67.8	-31.5
2410	-65.2	-40.2
2680	-----	-32.3
3222	-59.5	-55.5
2945	-----	-34.5
3482	-----	-42.5
3752	-----	-40.2
4024	-----	-46.9
4286	-----	-52.5
4558	-----	-46.9
4832	-----	-50.5
5100	-----	-58.2
5360	-----	-55.2
5638	-----	-54.8
5909	-----	-60.2
6172	-----	-65.2
6441	-----	-59.2
6709	-----	-62.5
6979	-----	-68.0



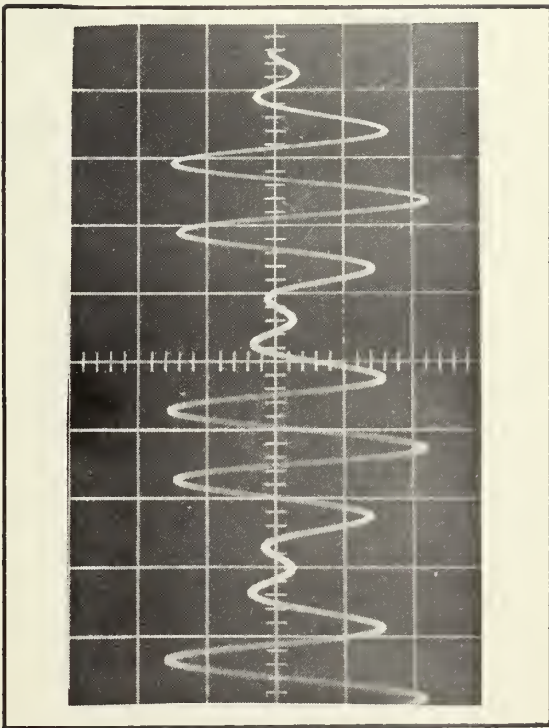
be predicted from the response curve, i.e. the 800 Hz output is 2db higher than the 1000 Hz output. Photographs of the input and output waveform for test one are shown in Figure 70.

Test two was intended to examine sections of the frequency response of the filter in a consecutive manner by investigating the operation of the filter in each small region and comparing results of adjacent regions. To improve the correlation of comparison of adjacent regions, one frequency will belong to both subregions.

Data are tabulated in Table XI. In the first three subsections the operation is nearly linear. There are no significant harmonics or subharmonics generated. The output of the filter nearly satisfies superposition and homogeneity in that the data are very close to values predicted from the single sinusoidal frequency response curve. In addition, adjacent sub-regions do not show an appreciable shift in operation for the common frequency of the contiguous sub-regions. In this region the FET is observed to be operating in the high-resistance state, the post-pinch-off region (see Table VIII).

The subregions 4, 5, 6, and 7 all show shifts of operation from one sub-region to the next. Difference in the readings for a common frequency dependent upon sub-region of operation are observed. The increase in harmonic content for subregions 4 and 5 is observed. In subregion 4 and 5 there are





(Left)

Input to Filter

Horiz. = 1ms/cm

Vert. = 0.5v/cm

(Below)

Output of Filter

Horiz. = 1ms/cm

Vert. = 0.5v/cm

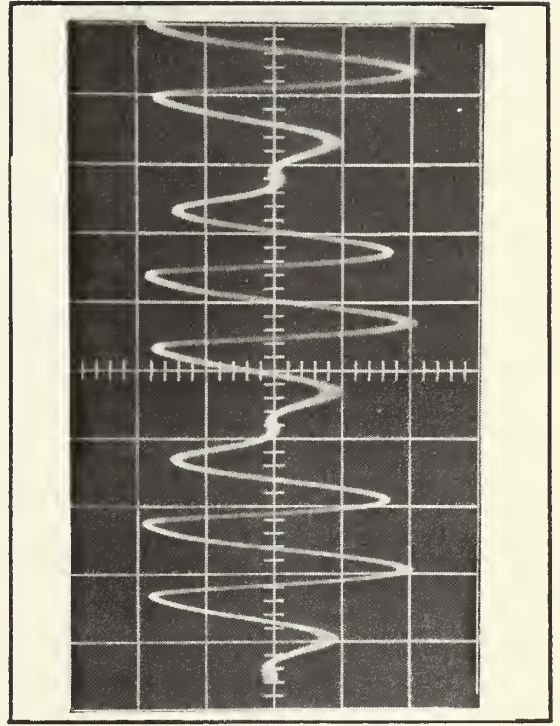


Figure 70. Test of Superposition (Test One). Photographs of Input and Output Waveforms of Filter ( $F_1=808\text{Hz}$ ,  $F_2=1015\text{Hz}$ ) (Voltage Magnitude vs. Time).



TABLE XI. Test Two for Superposition of Two Sinusoids  
in Nonlinear Active Low-Pass Filter Case.

Subregion 1 Freq (Hz)	Input to Nonlinear Filter (db)	Output of Filter > -40db
100	-15.2	-15.5
400	-15.3	-16.0
Subregion 2		
Subregion 2 Freq (hz)		
400	-15.5	-15.8
615	-15.5	-16.6
Subregion 3		
Subregion 3 Freq (Hz)		
615	-15.3	-16.8
806	-15.3	-18.0
Subregion 4		
Subregion 4 Freq (Hz)		
808	-15.3	-20.0
1015	-15.3	-21.3
604	-----	-39.0
206	-----	-46.8
420	-----	-47.0
1220	-----	-44.0
1615	-----	-44.0
1820	-----	-41.2
2022	-----	-47.3
⋮		
Subregion 5		
Subregion 5 Freq (Hz)		
1021	-15.2	-25.2
1102	-15.2	-25.5
94	-----	-37.6
935	-----	-46.3
1186	-----	-48.0
2030	-----	-47.6
2112	-----	-40.6
2198	-----	-48.0





TABLE XI. (Cont.)

Subregion 6 Freq (Hz)	Input to Nonlinear Filter (db)	Output of Filter > -40db
1108	-15.2	-43.2
1400	-15.3	-43.8
Subregion 7		
Subregion 7 Freq (Hz)		
1405	-15.2	-58.2
2000	-15.2	-59.5
Subregion 8		
Subregion 8 Freq (Hz)		
2000	-15.3	-63.0
4029	-15.3	-67.2



substantial changes in  $R_{DS}$  at significant signal levels. This is the region where the FET is switching from the high-resistance state of the post-pinch-off region to the low resistance state of the pre-pinch-off region.

The transient response photographs for the nonlinear filter are included in Figure 71. The 20Hz square wave caused the filter discriminator nonlinear-device controller to produce -2.5v of bias for  $V_{GS}$  which put the FET in the low-resistance state, accounting for the diminished signal output. Increased low-frequency distortion is observed. There is curvature on the tops of the square waves which indicates nonlinear behavior, i.e. the Fourier series sum in the input is distorted resulting in a non-square output.

Figure 72 shows the block diagram of the test circuit used in superposition tests one and two.

## B. THE HIGH-PASS FILTER

1. Considering a second-order system with transfer function

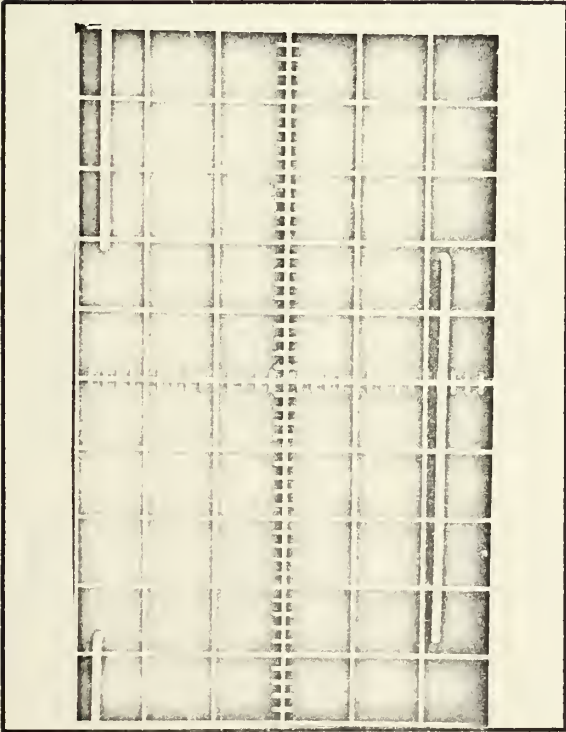
$$H(s) = \frac{s^2}{1 + \alpha s + s^2},$$

the filter can be realized for passive circuits by an R-C ladder or a series R-L-C circuit (see Figures 73 and 74).

2. The Butterworth active high pass filter can be realized by the circuit shown in Figure 75. For the Butterworth approximation

$$H(s) = \frac{s^2}{s^2 + 1.414s + 1},$$





(Left)

Input to Filter  
20 Hz Square Wave  
Vert. = 0.2v/cm  
Horiz. = 4ms/cm

(Below)

Output of Filter  
Vert. = 0.05v/cm  
Horiz. = 4ms/cm

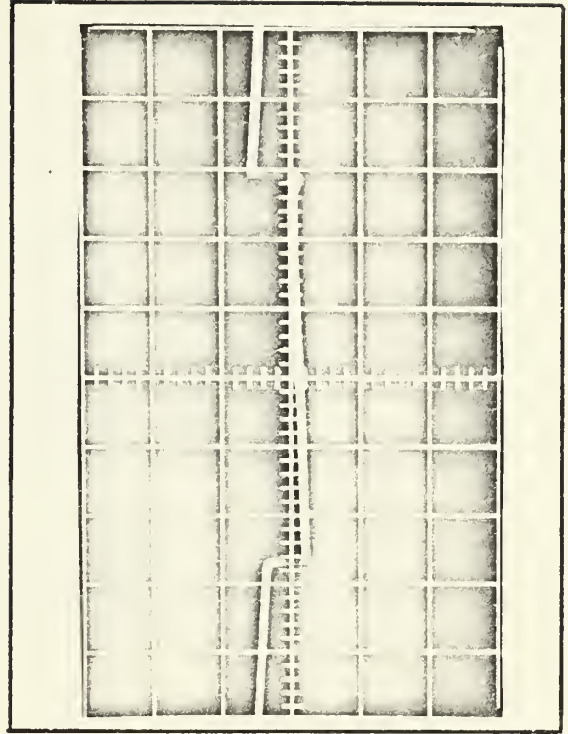
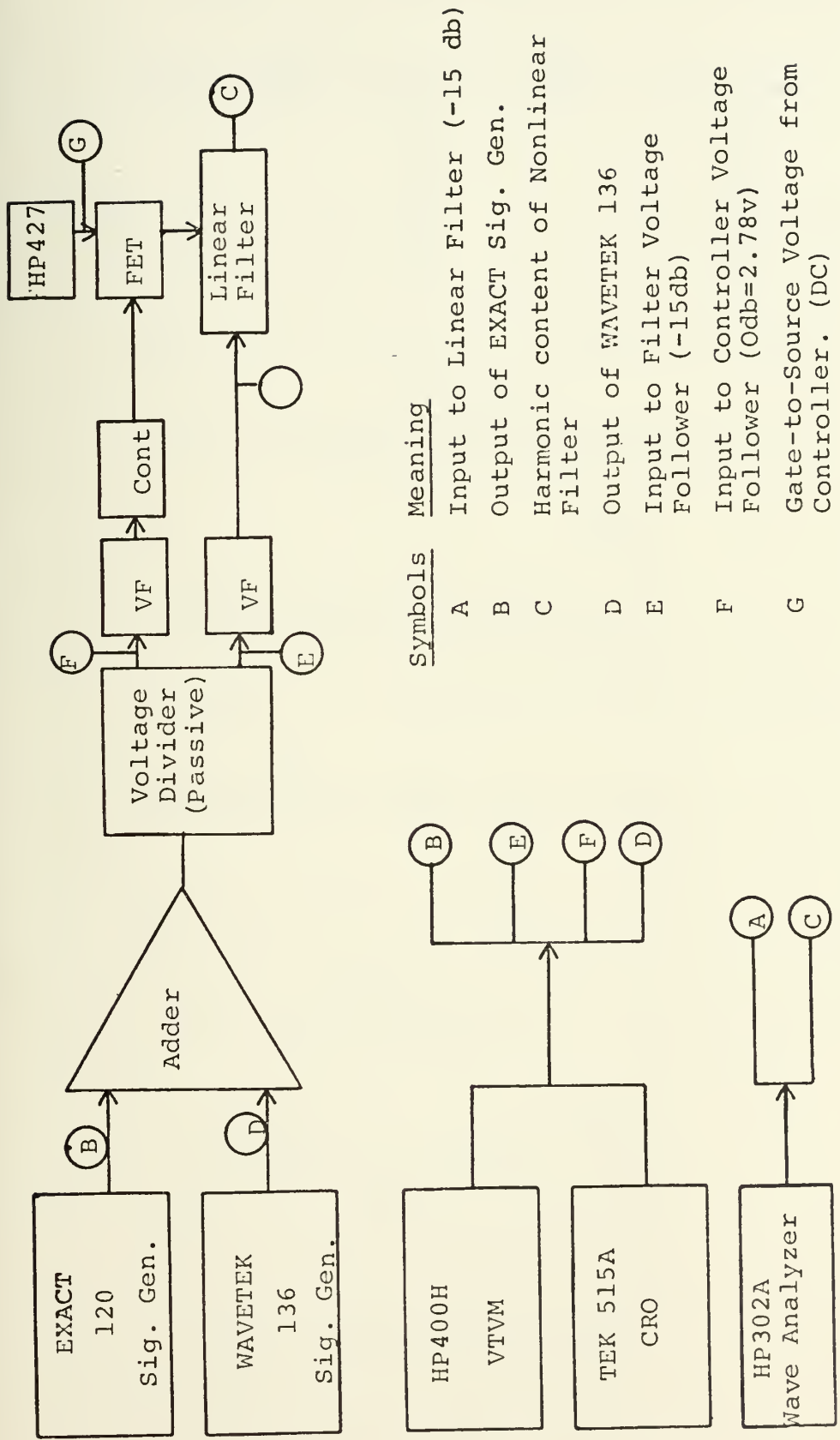


Figure 71. Transient Response Photographs  
of the Nonlinear Active Filter.  
(Voltage Magnitude vs. Time).





<u>Symbols</u>	<u>Meaning</u>
A	Input to Linear Filter (-15 db)
B	Output of EXACT Sig. Gen.
C	Harmonic content of Nonlinear Filter
D	Output of WAVETEK 136
E	Input to Filter Voltage Follower (-15db)
F	Input to Controller Voltage Follower (Odb=2.78v)
G	Gate-to-Source Voltage from Controller. (DC)

Figure 72. Test Circuit for Harmonic Measurements.





Figure 73. High-Pass Filter, R-C Ladder.

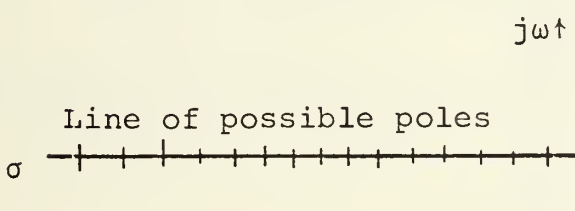
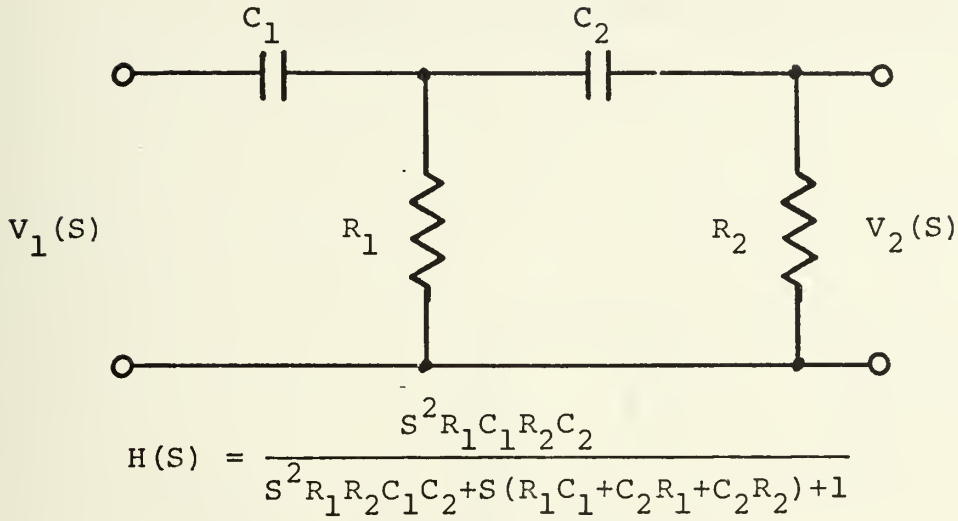


Figure 74. High-Pass Filter, R-L-C Circuit

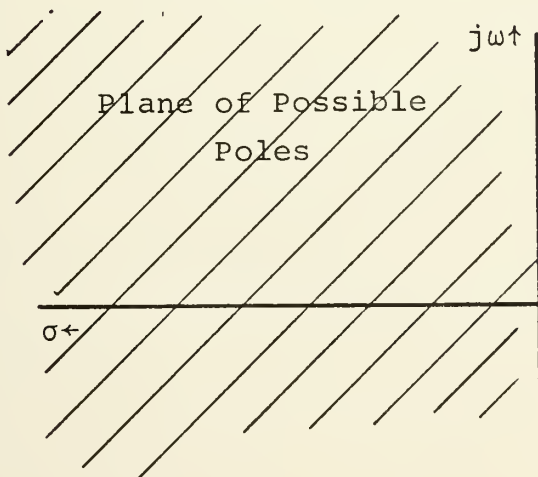
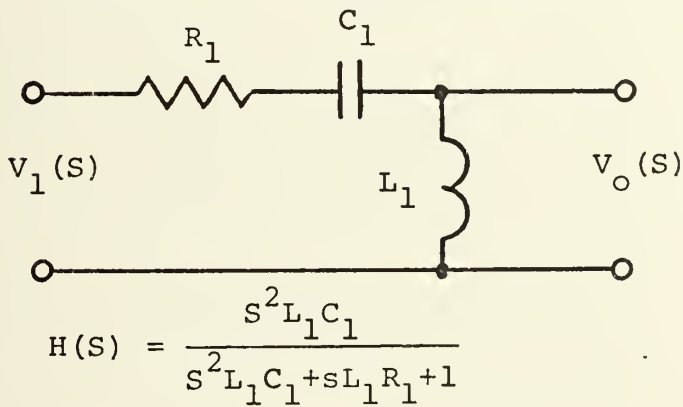
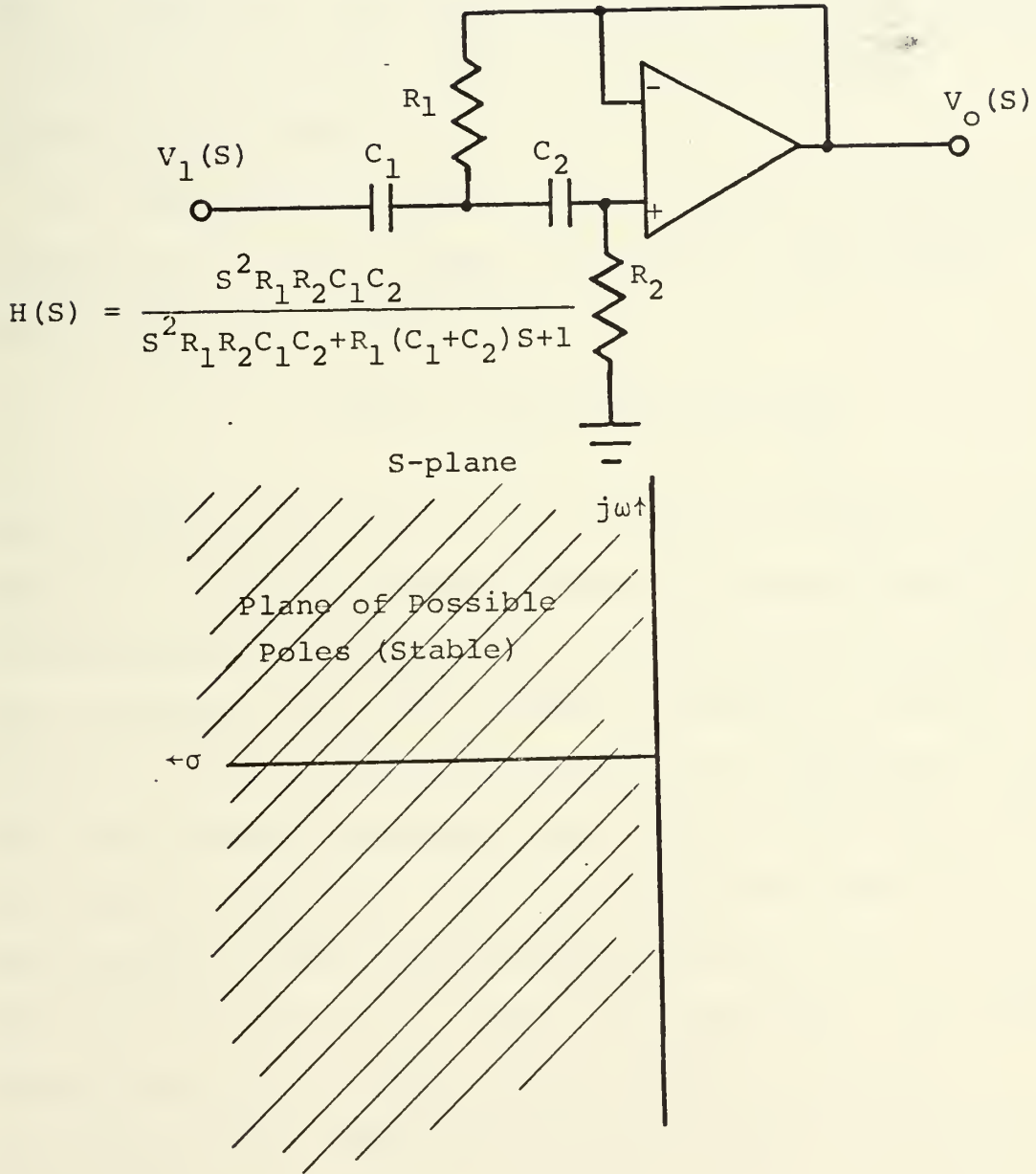




Figure 75. High Pass Active Filter.





where  $C_1 = C_2 = 1$  farad,  $R_1 = \frac{1}{\sqrt{2}}$  ohms; and  $R_2 = \sqrt{2}$  ohms. The filter was chosen to have a 3db roll-off frequency of 1KHZ. Choosing  $C_1 = C_2 = 0.022$  ufds led to values of  $R_1 = 5$  k $\Omega$ , and  $R_2 = 10$  k. A uA741C internally-compensated operational amplifier was chosen for the unity-gain amplifier. The Bode plot for the linear high-pass Butterworth active filter is shown in Figure 76. The high-frequency roll-off starting at  $f = 10$ KHZ is due to the internal compensation of the operational amplifier.

3. The parameter plane transfer function was derived by selecting  $R_2$  as the nonlinear resistance. The transfer function for this configuration is:

$$H(s) = \frac{s^2}{\alpha s^2 + 1.5\sqrt{2} s + \sqrt{2}}$$

The parameter plane Bode plots are shown in Figure 77. The range of  $\alpha$  values was chosen from the frequency-dependent  $\alpha$ -characteristic in Figure 78. The test circuit for measuring the  $\alpha$ -characteristic with pertinent formulae are shown in Figure 79. The  $\alpha$ -characteristic data are tabulated in Table XII. The frequency response plots for the high-pass filter are shown in Figure 80. The parameter plane predicted values are plotted in dots; the experimental values for the nonlinear case are plotted in X's. Table XIII summarizes the frequency response data for the two cases. Harmonic distortion measurements were made and the data are given in tabular form in Table XIV.



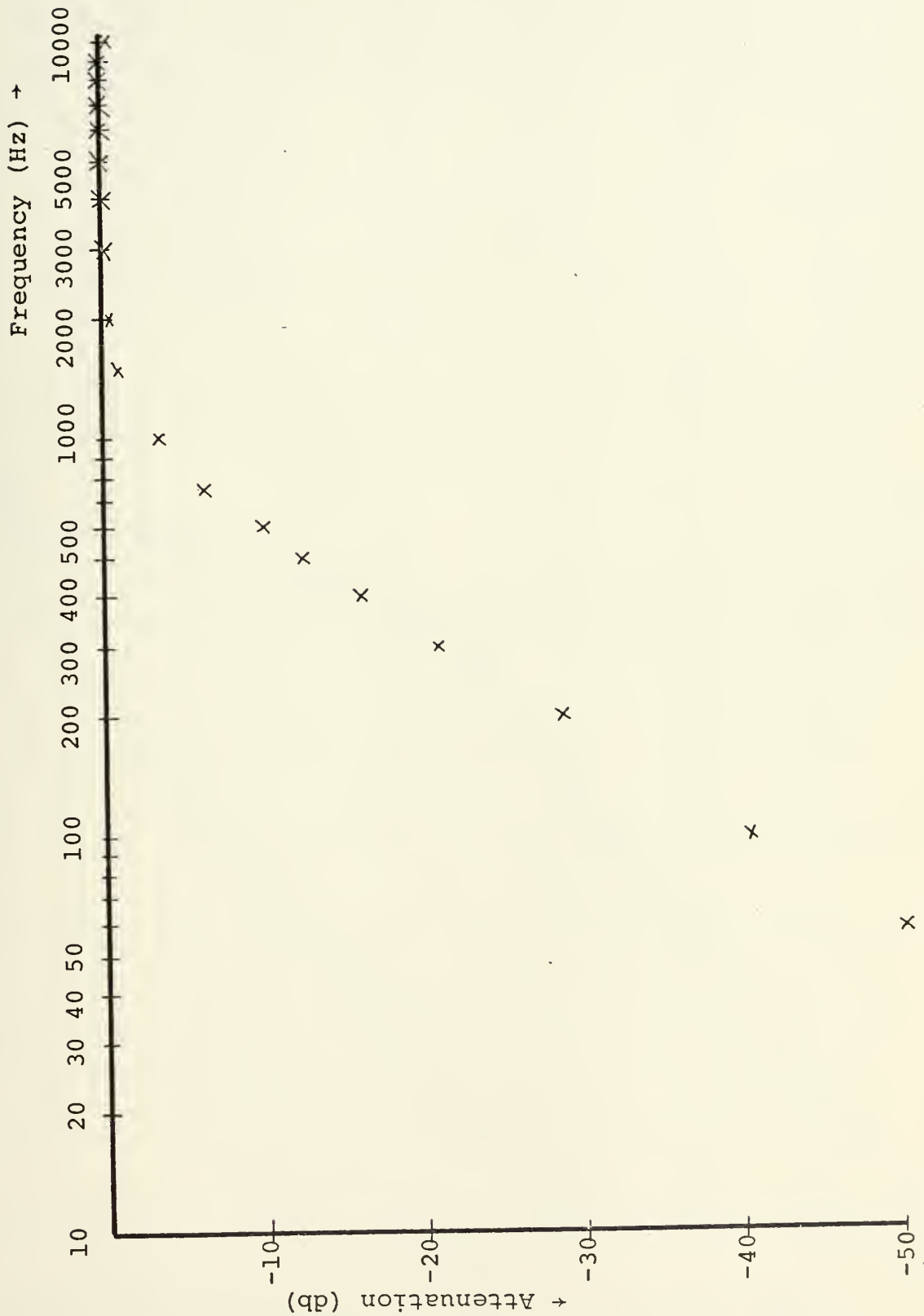


Figure 76. Linear Active High-Pass Filter Frequency Response (Example 1).





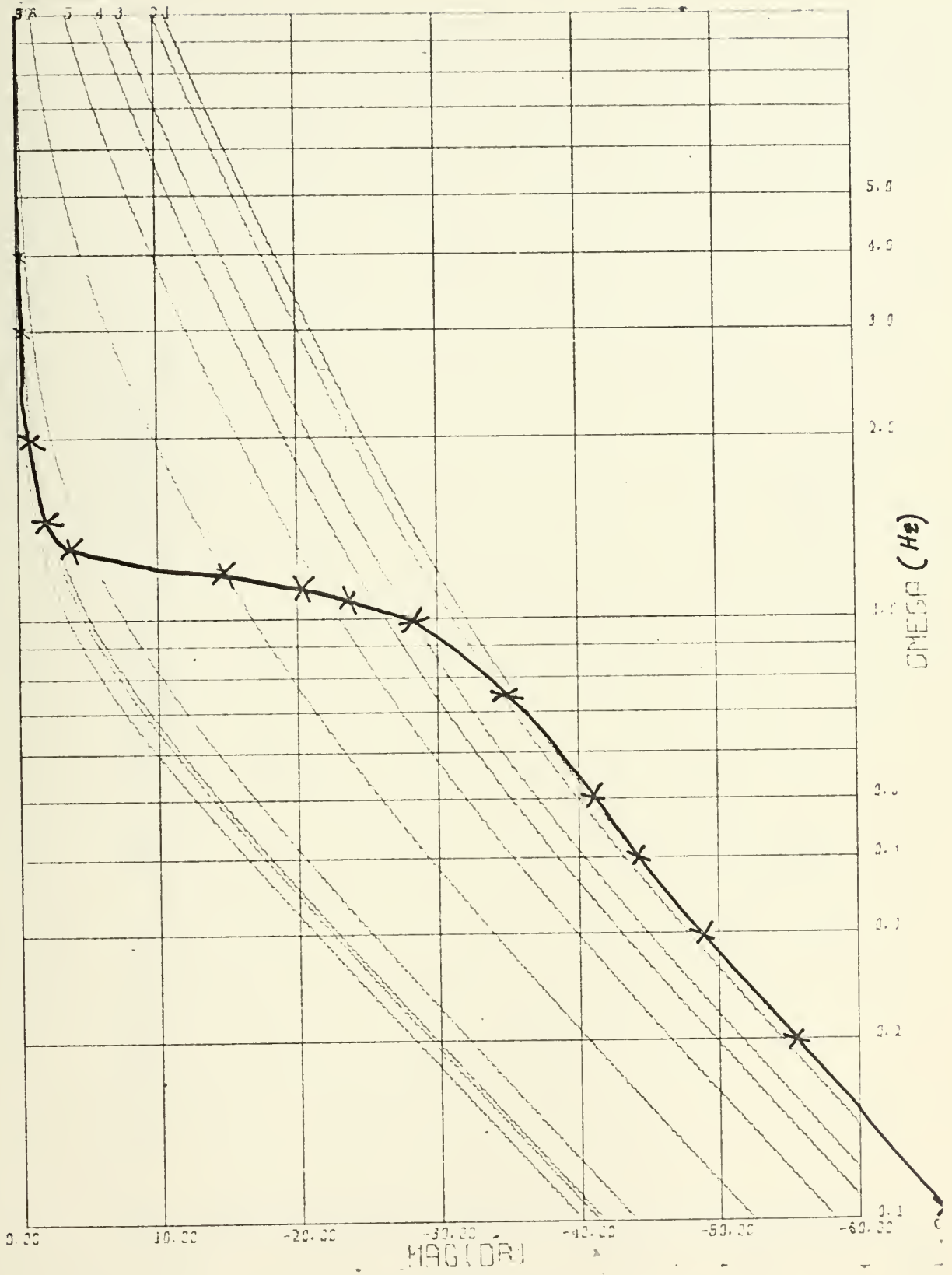


Figure 77. High-Pass Active Filter Parameter Plane Curves (Example 1).



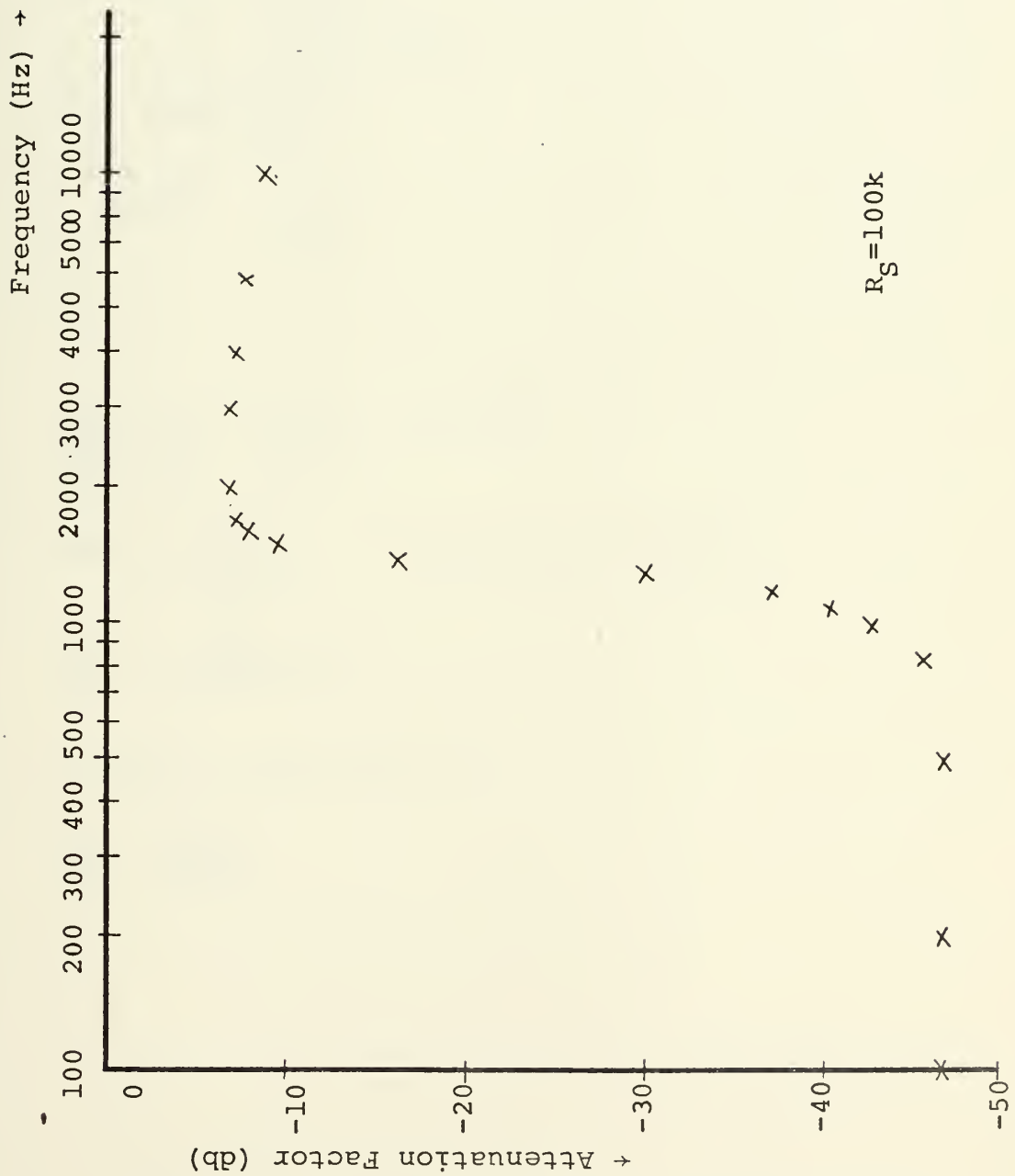
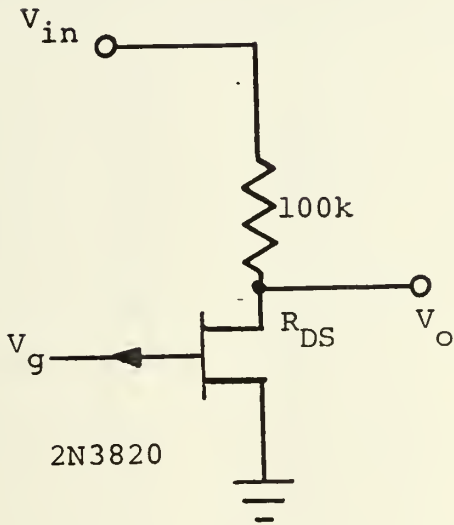


Figure 78. Frequency-Dependent  $\alpha$ -Characteristic FET Type 2N3820. High-Pass Filter (Example 1).



Figure 79.  $\alpha$ -Characteristic Test Circuit (Example 1).



$$\frac{R_{DS}}{R_{DS} + 100k} = \frac{V_o(S)}{V_{in}(S)} = 10^{-A/20}$$

$$20 \log \frac{V_o(S)}{V_{in}(S)} = A \triangleq \text{Attenuation Factor}$$

$$R_{DS} = \frac{10^5}{10^{-A/20} - 1}$$

$$\alpha = R_{DS} \text{ in parallel } 10k$$

$$\alpha_N = \frac{\alpha \sqrt{2}}{10k}$$



TABLE XII. High-Pass Nonlinear Filter  $\alpha$ -Characteristic  
Tabular Data

Freq (Hz)	A(db) (-A120)	R <sub>DS</sub> (ohms)	$\alpha$	$\alpha_N$	Para Plane Curve #
100	-46.5 (2.325)	475.4	453.8	0.06417	
200	-46.5 (2.325)	475.4	453.8	0.06417	
500	-46.5 (2.325)	475.4	453.8	0.06417	1
750	-45.5 (2.275)	533.7	506.67	0.0716	2
1000	-42.5 (2.125)	755.56	702.48	0.09935	3
1100	-40.5 (2.025)	953.06	870.13	0.12305	4
1200	-37.0 (1.85)	1432.78	1253.2	0.177229	5
1300	-30.0 (1.5)	3265.54	2461.7	0.34813	6
1400	-16.2 (0.81)	18326.624	6469.7	0.9149	7
1500	- 9.2 (0.46)	53077.6	8414.6	1.1900	8
1600	- 8.0 (0.40)	66142.5	8686.6	1.22847	
1800	- 7.5 (0.375)	72919.6	8794.0	1.2436	9
2000	- 7.5 (0.375)	72919.6	8794.0	1.2436	
3000	- 8.0 (0.400)	66142.5	8686.6		
4000	- 9.0 (0.45)	54993.9	8461.4	1.197	
				1.414	10





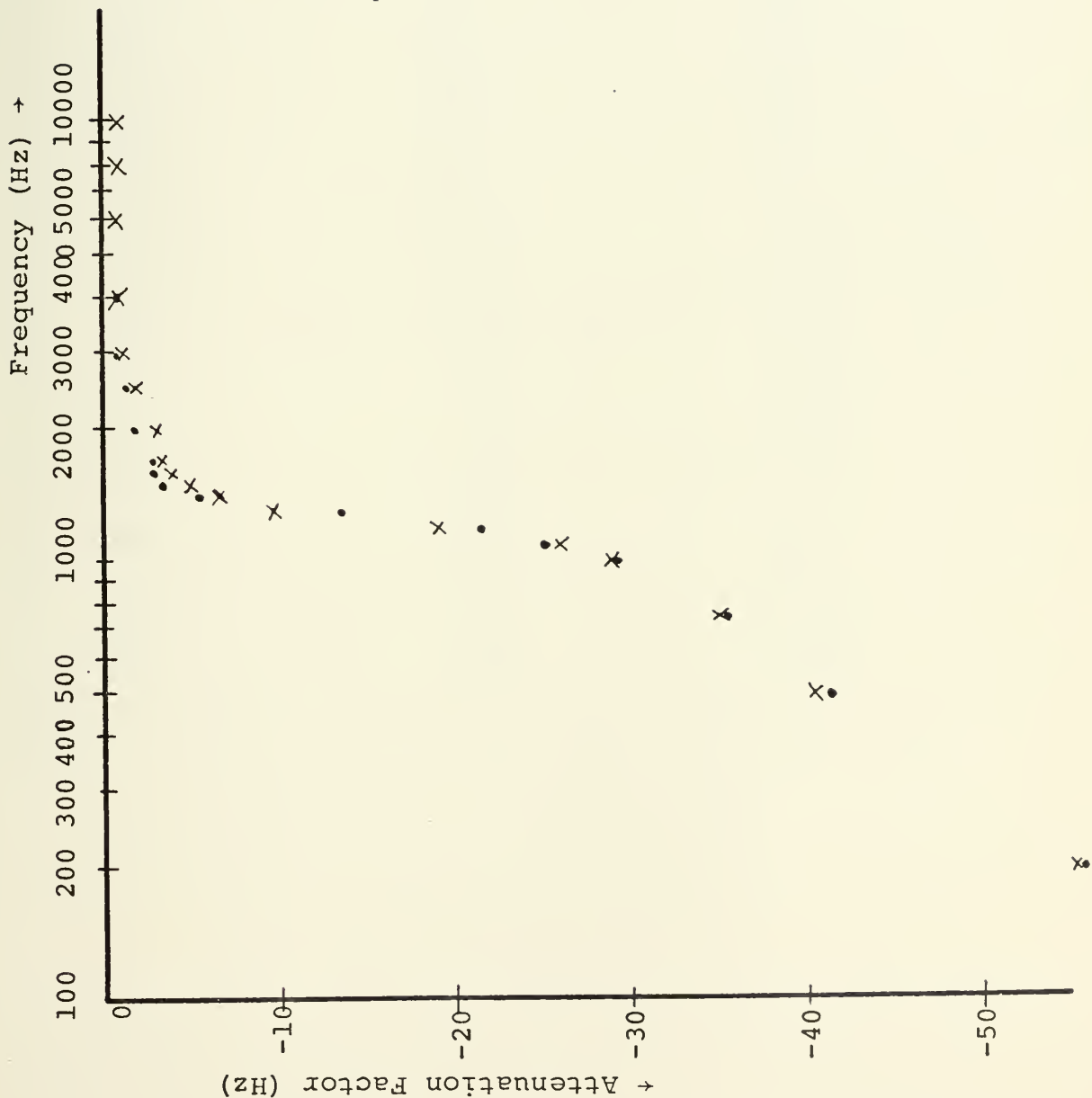


Figure 80. High-Pass Nonlinear Active Filter Frequency Response Characteristic (Experimental and Parameter-Plane Predictions). Example 1.



TABLE XIII. High-Pass Nonlinear Filter Frequency Response Data.

Frequency (Hz)	Parameter Plane (db)	Freq. Response Experimental (db)
100	-67.8	-64.5
200	-56.0	-55.5
500	-41.5	-40.5
750	-36.4	-35.0
1000	-28.8	-28.5
1100	-26.0	-25.0
1200	-21.6	-18.5
1300	-14.5	- 9.5
1400	- 5.40	- 6.50
1500	- 3.02	- 5.00
1600	- 2.50	- 4.00
1800	- 2.02	- 2.50
2000	- 1.70	- 2.50
2500	- 1.30	- 1.50
3000	- 0.80	- 1.0
4000	- 0.80	- 1.0
6000	- 0.80	- 0.8
8000	- 0.80	- 0.80
10000	- 0.80	- 0.80



TABLE XIV. Harmonic Distortion of High-Pass  
Filters (Linear and Nonlinear)  
 $V_{in}=2.0v$  pk-pk 500 Hz.

F	WAVETEK 136 Signal Generation	Linear Filter Output (db)	Nonlinear Filter Output (db)
500	Odb	-16.5	-10
1000	<-55	-52	-13.5
1500	- 9.5	-12.5	-20.5
2000	<-55	-52	-32.5
2500	-14.0	-16.0	-23.5
3000	<-55	-52.5	-33.5
3500	-17.0	-19.5	-24.5
4000	<-55	-52.5	-34.5
4500	-19.0	-20.0	-25.0
5000	<-55	-52.5	-34.5
5500	-20.8	-21.5	-25.6
6000	<-55	-52.5	-34.5
6500	-22.5	-23.0	-26.5
7000	<-55	-54.5	-35.0
7500	-24.5	-24.5	-27.5
8000	<-55	-54.0	-35.5
8500	-24.5	-25.5	-28.0
9000	<-55	-54.5	-36.0
9500	-25.5	-26.5	-28.5
10000	<-55	-54.5	-37.0
10500	-26.5	-27.5	-29.5



4. A second example of a high-pass nonlinear filter was conducted to investigate the effect of the feedback-connected FET 2N3819 nonlinear resistance and the introduction of a voltage follower in the input circuit of the filter.

The same type of linear high-pass filter with the same values of components was used as was used in the first example of the high pass filter. A voltage follower was added in cascade as shown in Figure 81. The frequency response obtained with this configuration is plotted in Figure 82 and can be compared to Figure 76.

The FET  $\alpha$ -characteristic is depicted in Figure 84. Tabular data for the  $\alpha$ -characteristic are summarized in Table XV.

Figure 85 depicts the experimentally-derived frequency response plotted in X's; the parameter plane frequency specification is plotted in ' · ' 's for comparison. Again close agreement is noted. Tabular Data for frequency response measurements and specification are summarized in Table XVI.





Figure 81. High-Pass Linear Filter (Example 2).

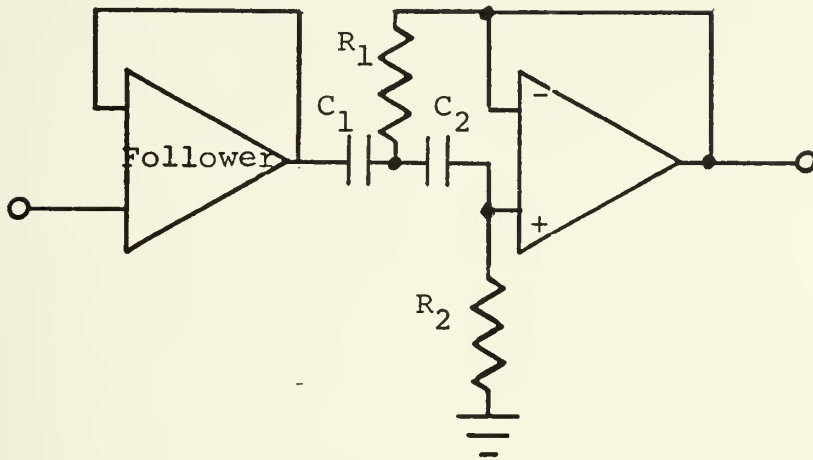
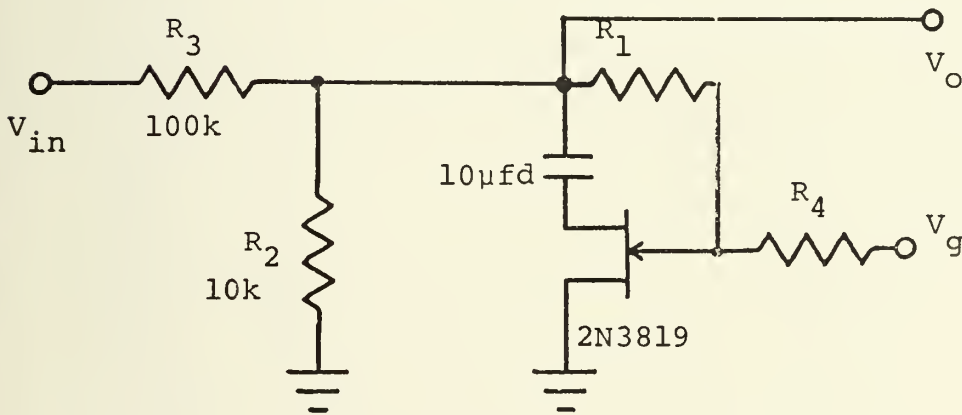


Figure 83. Frequency Dependent  $\alpha$ -Characteristic Test Circuit with Appropriate Formulae (Example 2).



$$V_{in} = -16\text{db @ 1KHz}$$

$$R_{eq} = R_{DS} \parallel R_2; \text{ (Ignore effects of } R_3, R_4 \text{ and Capacitor)}$$

$$\frac{V_o}{V_{in}} = \frac{R_{eq}}{R_1 + R_{eq}}$$

$$20 \log \frac{V_o}{V_{in}} = A \triangleq \text{Attenuation Factor}$$

$$A_n = A + 16 \text{ db}$$

$$R_{eq} = \frac{10^5}{10^{-A_n/20} - 1}$$



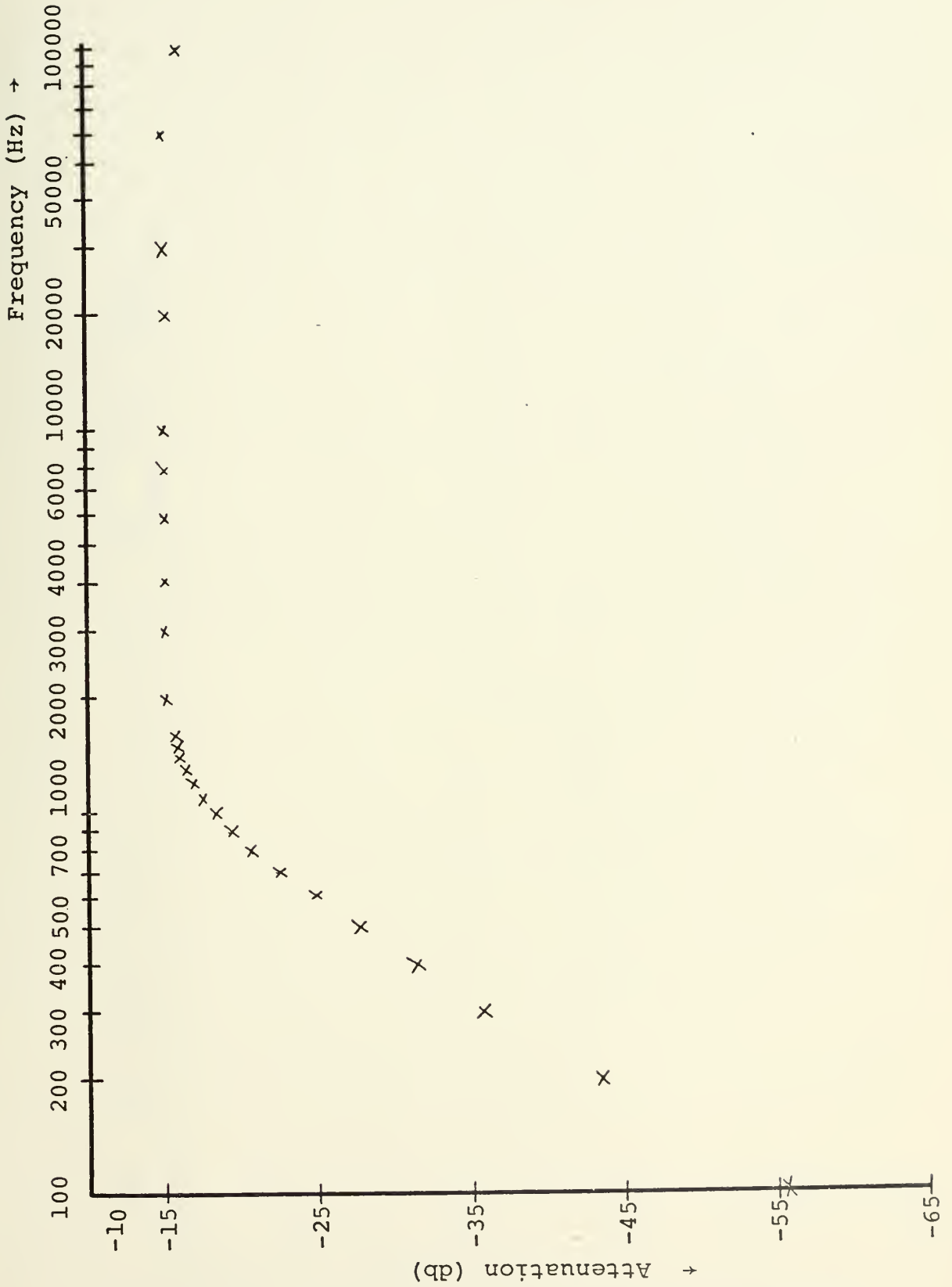


Figure 82. Linear Active High-Pass Filter Frequency Response Characteristic (Example 2).  $V_{in} = -15\text{db}$  (0db = 2.78v).



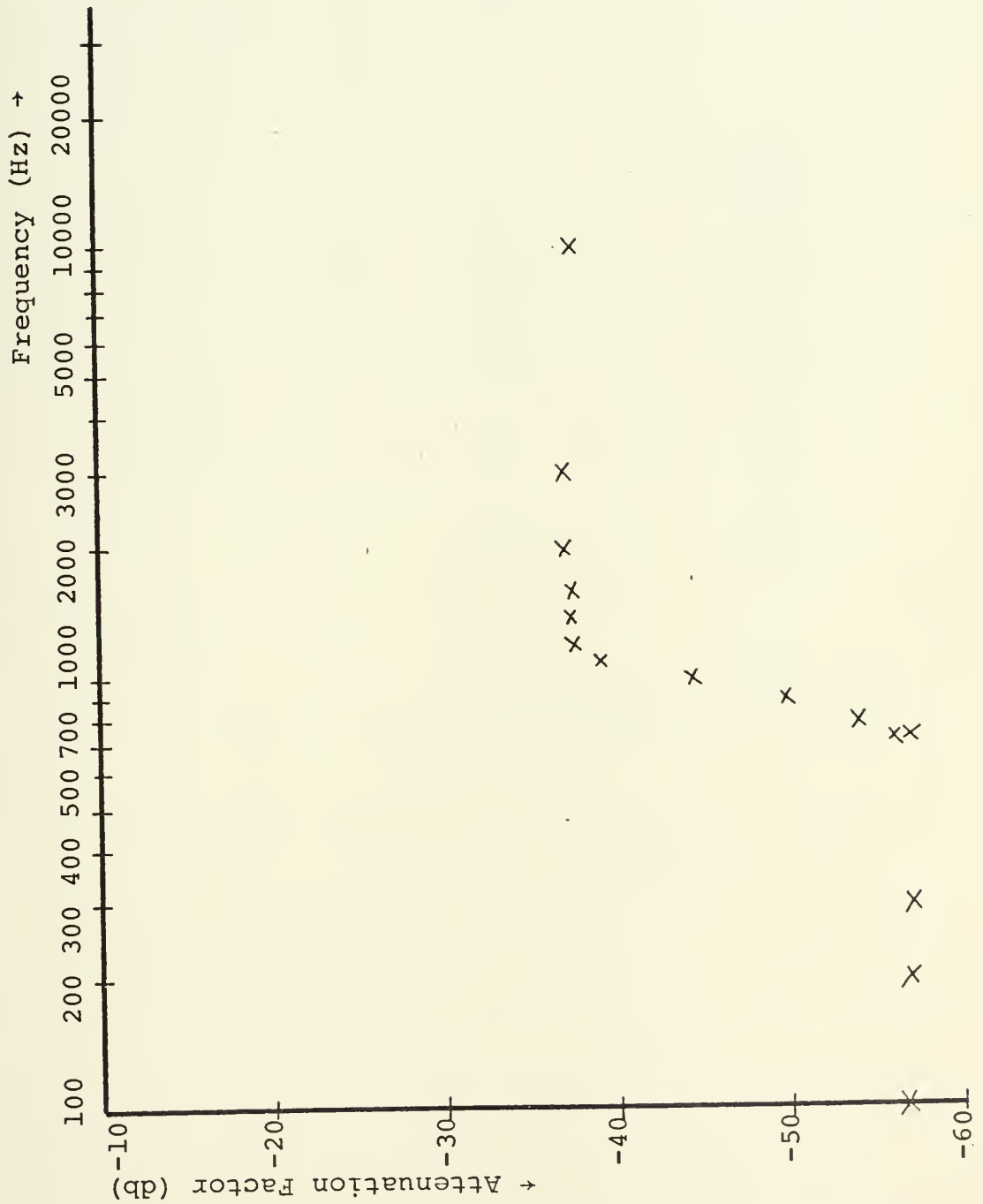


Figure 84.  $\alpha$ -Characteristic Frequency Response, FET Type 2N3819. High-Pass Filter (Example 2).



TABLE XV. Tabular Data For  $\alpha$ -Characteristic

Freq. (Hz)	Attenuation Factor $A_N$ (db)	Req( $\lambda$ )	$\alpha_N$	Para Plane Curve#	
10	-56.3+16.0 = 40.3	975.47	0.138	2	
40	-56.8+16.0 = 40.8	920.4	0.130	1	
200	-56.8+16.0 = 40.8	↓			
300	-56.8+16.0 = 40.8				
400	-56.8+16.0 = 40.8				
720	-56 +16.0 = 40	1010.1	0.142	3	
800	-53.8+16.0 = 37.8	1305	0.185	4	
900	-49.8+16.0 = 33.8	2084.3	0.295	5	
1000	-44.2+16.0 = 28.2	4047.9	0.572	6	
1100	-39.0+16.0 = 23.0	7618.2	1.077	7	
1200	-37.5+16.0 = 21.5	9186.9	1.299	8	
1300	-37.5+16.0 = 21.5	↓	↓		
1400	-37.5+16.0 = 21.5				
1600	-37.5+16.0 = 21.5				
2000	-37.5+16 = 21	9784.6	1.38	9	
3000	-37 +16 = 21				
10000	-37.5+16.0 = 21.5		1.414	10	





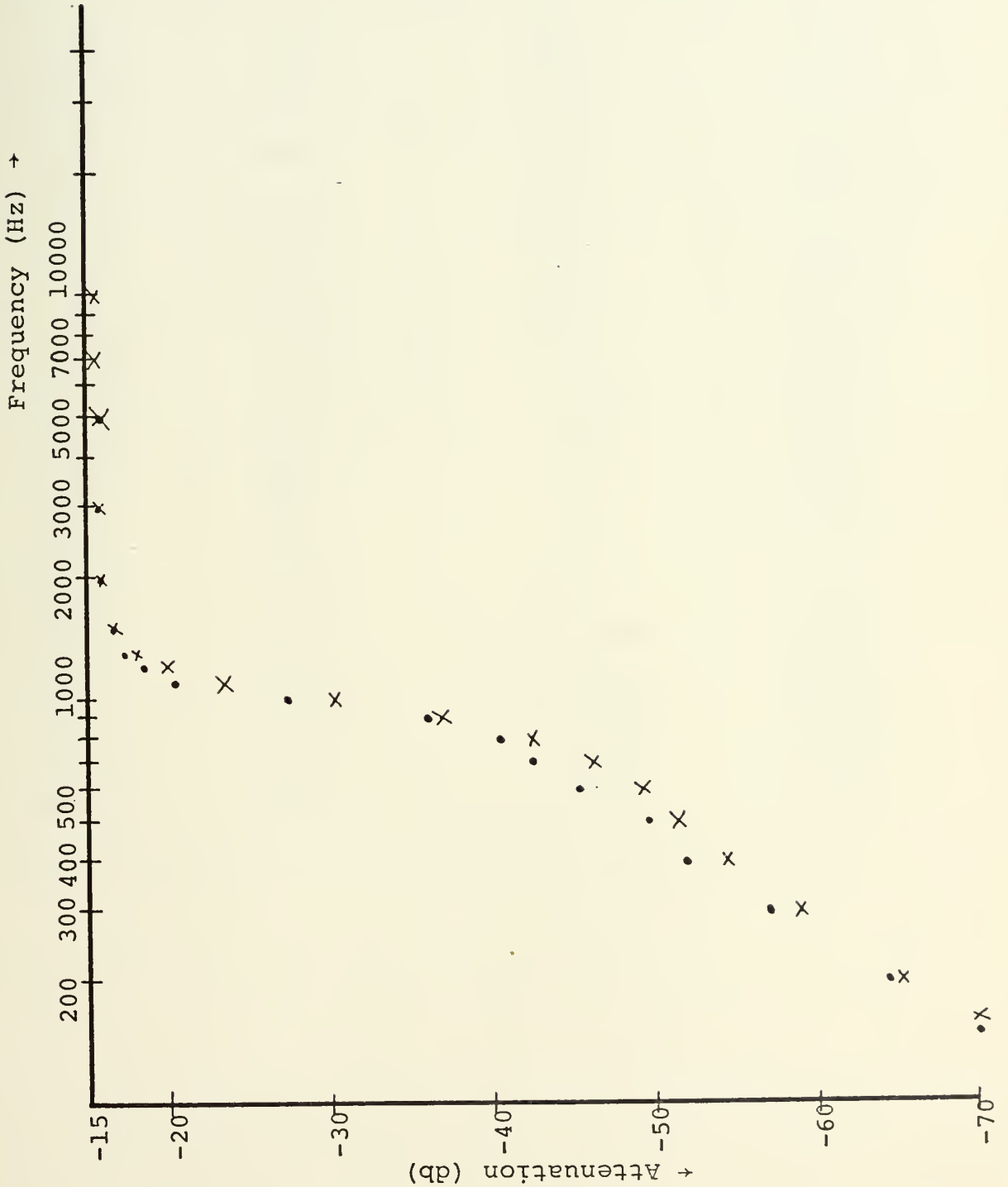


Figure 85. High-Pass Nonlinear Active Filter Frequency Response Characteristic (Experimental and Parameter Plane Predictions). Example 2.



TABLE XVI. High-Pass Nonlinear Filter Frequency Response Data (Example 2).

Frequency (Hz)	Experimental Measurement (db)	Parameter Plane Specification db	
		$V_{in}=0\text{db}$	$V_{in}=-15.5\text{ db}$
100	-78.0	-60.8	-76.3
200	-65.2	-49.1	-64.6
300	-59.0	-41.5	-57.0
400	-54.5	-37.4	-52.4
500	-51.5	-33.8	-49.3
600	-49.0	-31.0	-46.5
700	-46.2	-27.0	-42.5
800	-42.3	-25.2	-40.7
900	-36.8	-19.5	-36.0
1000	-30.2	-11.97	-27.5
1100	-23.7	- 5.0	-20.5
1200	-20.0	- 3.0	-18.5
1300	-18.1	- 2.4	-17.9
1400	-17.2	- 2.2	-17.7
1500	-16.2	- 1.7	-17.2
2000	-16.2	- 0.578	-16.07
3000	-16.0	- 0.22	-15.72
5000	-15.8	- 0.06	-15.56
7000	-15.5	- 0.03	-15.53
10000	-15.5	- 0.01	-15.51



## VI. CONCLUSION

The research in this thesis has demonstrated the validity of the parameter plane frequency response techniques for synthesis of nonlinear networks of specified frequency response for sinusoidal driving voltages of fixed amplitude. Although discrete and integrated-circuit devices were used in a hybrid manner, it is felt that incorporation of these techniques into monolithic/hybrid integrated circuit components could be easily implemented. The amount of circuit complexity was high; substantial reduction should result as more design experience is gained.

The most serious limitation to this synthesis technique is the inability of the nonlinear networks to filter a complex signal consisting of several frequency components in a prescribed manner. The nonlinear filter frequency response is identical to the parameter plane specification for a slowly-varying (in frequency) sinusoid. The inability to filter a complex waveshape is attributed to the FET nonlinear resistance and its controller. Some means of preconditioning the complex signal must be found to permit the FET resistance to behave as a slowly-varying quantity. The describing function-type graphical technique would obtain causing good correlation of prescribed frequency response and measurements. At present the instantaneous FET resistance is established by such factors



as the amplitude of the incoming signal, the frequency spread of the components of the signal input, the relative amplitudes of the components of the complex signal, the filtering action of the controller, and the magnitude and frequency of harmonic distortion components.

In an attempt to enhance the filtering capability of these nonlinear networks different configurations of frequency-dependent nonlinear device controllers should be investigated. The use of feedback from the output of the nonlinear filter to the input of the controller is suggested as a means of obtaining cumulative filtering of the signal. An AGC or amplitude-stabilization technique would be necessary in the controller for small signal inputs from the filter, allowing the controller to function independently of the magnitude of the controller input signal.

Other types of nonlinearities should be investigated. The use of a voltage-dependent nonlinear capacitance would permit variable  $-Q$  or variable bandwidth bandpass or bandreject filters. The use of current-dependent nonlinear inductance would permit more versatility in the nonlinear filters realized.

As the number of nonlinearities is increased by experimentation the use of transformation devices: mutator, gyrator, scolor, and reflector would permit the realization of any type of specified nonlinearity.





## BIBLIOGRAPHY \*

1. Aaronson, Gerald, "Active Filters: part 10, Synthetic Inductors From Gytrators," Electronics, Vol. 42, pp. 118-125, July 7, 1969.
2. Applications Manual for Operational Amplifiers, Philbrick-Nexus, 1968.
3. Bilotti, A., "Operation of a MOS Transistor as a Variable Resistor," Proceedings IEEE, pp 1093-1094, August 1966.
4. Bilotti, A., "Applications of a Monolithic Analog Multiplier," IEEE Journal of Solid State Circuits, Vol. SC-3, #4, pp 373-380, December 1968.
5. Botos, B., "Breadboard Techniques for Low Frequency Integrated Circuit Feedback Amplifiers," Motorola Application Note AN-271.
6. Botos, B. and McRoberts, L., "Using the FET Designers Data Sheet for Worst Case Amplifier Circuit Design," Motorola Application Note AN-455.
7. Burr-Brown Research Corporation, "Handbook and Catalog of Operational Amplifiers," 1969.
8. Camenzind, H. R., Circuit Design for Integrated Electronics, Addison-Wesley Publishing Company, Reading, Massachusetts, 1968.
9. Camenzind, H. R. and Gribene, A. B., "An Outline of Design Techniques for Linear Integrated Circuits," IEEE Journal of Solid State Circuits, Vol. SC-4, #3, pp 110-122, June 1969.
10. Christensen, R., and Wollesen, D., "Matching FET's by Design is Faster and Cheaper Then by Pick and Choose," Electronics, Vol. 42, #25, pp 114-116, December 8, 1969.
11. Chua, Leon O., "Synthesis of New Nonlinear Network Elements," Proceedings IEEE, Vol. 56, #8, pp 1325-1341, August 1968.
12. Chua, Leon O., Introduction to Nonlinear Network Theory, McGraw-Hill Book Company, New York, 1969.

---

\* Bibliography numbers do not correspond to Reference numbers introduced in text.



13. Crawford, R. H., MOSFET In Circuit Design, McGraw-Hill Book Company, New York, 1967.
14. Davis, J. P., Frequency Response Analysis and Design of Single-Valued Nonlinear Systems Using the Parameter Plane, M. S. Thesis, U. S. Naval Postgraduate School, 1969.
15. Dawson, R., Akrons, R., and Ditrick, N., "Understanding and Using the Dual Gate MOS FET," The Electronic Engineer, Vol. 26, #9, pp 36-39, September 1967.
16. Delpeck, J. F., "Audio Discriminator Measures Large Frequency Changes," Electronics, Vol. 39, #9, p 76, May 2, 1966.
17. Dutta Roy, S. C., and Nagarajan, V., "On Inductor Simulation Using a Unity-Gain Amplifier," IEEE Journal of Solid State Circuits, Vol. SC-5, #3, pp 95-98, June 1970.
18. Eimbinder, J., editor, Designing With Linear Integrated Circuits, John Wiley and Sons, Inc., New York, 1969.
19. Fairchild Semiconductor Integrated Circuit Data Catalog, 1970.
20. Foster, E. J., "Active Low-Pass Filter Design," IEEE Transaction on Audio, AV-13, #5, pp 104-111, September-October 1965.
21. Fullagar, D., "A New High Performance Monolithic Operational Amplifier," Fairchild Application Note.
22. Geffe, P. R., "Toward High Stability In Active Filters," IEEE Spectrum, Vol 7, pp 63-66, May 1970.
23. Giles, James, editor, Fairchild Semiconductor Linear Integrated Circuits Applications Handbook, 1967.
24. Ghausi, M. S., Principles and Design of Linear Active Circuits, McGraw-Hill Book Company, New York, 1965.
25. Glavis, G. O., Frequency Response in the Parameter Plane, M. S. Thesis, U. S. Naval Postgraduate School, 1968.
26. Gosling, W., Field Effect Transistor Applications, John Wiley and Sons, Inc., 1965.
27. Gosling, W., "Voltage-Controlled Attenuators Using Field Effect Transistors," IEEE Transactions on Audio, AV-13, #5, pp 112-120, September, October 1965.



28. Graham, D., and McRuer, D., Analysis of Nonlinear Control Systems, John Wiley and Sons, Inc., New York, 1961.
29. Gray, P. E., and Searle, C. L., Electron Principles, Physics, Models, and Circuits, John Wiley and Sons, Inc., New York, 1969.
30. Gray, T. S., and Walker, R. M., "Design of a Retriggerable One-Shot," IEEE Journal of Solid State Circuits, Vol. SC-5, #4, pp 141-146, August 1970.
31. Gray, T., Anderson, J., and Walker, R., "The 9601, a Second Generation Retriggerable One-Shot," Application note 173/1, Fairchild, August 1970.
32. Gribene, A. B., and Camenzind, H. R., "Frequency Selective Integrated Circuits Using Phase-Lock Techniques," IEEE Journal of Solid State Circuits, Vol. SC-4, #4, pp 216-225, August 1969.
33. Hendricks, L. V., "A Programmed Course on Field-Effect Transistors," The Electronic Engineer, Vol. 26, #9, pp 54-62, September 1967.
34. Herskowitz, G. J., editor, Computer-Aided Integrated Circuit Design, McGraw-Hill Book Company, New York, 1968.
35. Hibberd, R. G., Integrated Circuits-A Basic Course for Engineers and Technicians, McGraw-Hill Book Company, New York, 1969.
36. Hills, M., "Active Filters: Part 13, Narrowing the Choice," Electronics, Vol. 42, pp 106-111, October 27, 1969.
37. Hollister, F. H., Network Analysis and Design by Parameter Plane Techniques, Ph.D. Thesis, U.S. Naval Postgraduate School, 1965.
38. Huelsman, L. P., Theory and Design of Active RC Circuits, McGraw-Hill Book Company, New York, 1968.
39. Hurtig, Gunnar, "Active Filters: part 8, Positive Results From Negative Feedback," Electronics, Vol. 42, pp 96-102, March 31, 1969.
40. Kerwin, W. J., and Shaffer, C. V., "Active RC Bandpass Filter with Independent Tuning and Selectivity Controls," IEEE Journal of Solid State Circuitry, Vol. SC-5, #2, pp 74-75.



41. Klein, Thomas, "Technology and Performance of Integrated Complementary MOS Circuits," IEEE Journal of Solid State Circuits, Vol. SC-4, #3, pp 122-131, June 1969.
42. Linvill, J. C., and Gibbons, J. F., Transistors and Active Circuits, McGraw-Hill Book Company, New York, 1961.
43. Lynn, D. K., Myer, C. S., and Hamilton, D. J., editors, Analysis and Design of Integrated Circuits, McGraw-Hill Book Company, New York, 1967.
44. Martin, T. B., "Circuit Applications of the Field Effect Transistor," part 1, Semiconductor Products, pp 33-39, February 1962.
45. Martin, T. B., "Circuit Application of the Field Effect Transistor," part 2, Semiconductor Products, pp 30-38, March 1962.
46. Millman, J., and Halkias, C. C., Electronic Devices and Circuits, McGraw-Hill Book Company, New York, 1967.
47. Mitra, S. K., "Synthesizing Active Filters," IEEE Spectrum, Vol 6, pp 47-63, January 1969.
48. Moll, J. L., Physics of Semiconductors, McGraw-Hill Book Company, New York, 1964
49. Morgan, A. N., "The FET as an Electronically Variable Resistor," Proceedings of the IEEE, pp 892-893, June 1966.
50. Moschytz, G. S., "Active RC Filter Building Block Using Frequency Emphasizing Networks," IEEE Journal of Solid-State Circuits, Vol. SC-2, #2, pp 59-62, June 1967.
51. Moschytz, G. S. and Wyndrum, R. W., "Active Filters: part 5, Applying the Operational Amplifier," Electronics, pp 98-106, December 9, 1968.
52. Moschytz, G. S., "The Operational Amplifier in Linear Active Networks," IEEE Spectrum, Vol. 7, pp 42-50, January 1970.
53. Moschytz, G. S. and Thelen, W., "Design of Hybrid Integrated-Filter Blocks," IEEE Journal of Solid-State Circuits, Vol. SC-5, #3, pp 99-107, June 1970.
54. Moschytz, G. S., "Inductorless Filters: a Survey/Part II/Linear Active and Digital Filters," IEEE Spectrum, Vol. 7, #9, pp 63-76, September 1970.





55. Motorola Application Note, AN-2111A, Field Effect Transistors In Theory and Practice.
56. Mullaney, J. W., "Active Filters: part 11 Varying the Approach," Electronics, Vol. 42, pp 86-93, July 21, 1969.
57. Nakagawa, G. R., Parameter Plane Techniques for Active Filter Systems, M. S. Thesis, U. S. Naval Postgraduate School, 1966.
58. Neu, F. D., "Voltage Control Solid State Nonlinear Resistance," Electronics, Vol. 38, pp 36-37, February 21, 1964.
59. Nichols, R. A., Parameter Plane Design of Electrical Filters Containing Nonlinear Elements, EE Thesis, U. S. Naval Postgraduate School, 1969.
60. Norwood, M. H. and Shatz, E., "Voltage Variable Capacitor Tuning: a Review," Proceedings of the IEEE, Vol. 56, #5, pp 788-798, May 1968.
61. Orchard, H. J., and Sheahan, D. F., "Inductorless Band-pass Filters," IEEE Journal of Solid State Circuits, Vol. SC-5, #3, pp 108-118, June 1970.
62. RCA Transistor, Thyristor and Diode Manual, SC-14, 1969.
63. Salerno, Joseph, "Active Filters: part 7, Analog Blocks Ensure Stable Design," Electronics, Vol. 42, pp 100-105, February 17, 1969.
64. Sallen, R. P. and Key, E. L., "A Practical Method of Designing RC Active Filters," IRE Transactions on Circuit Theory, Vol. CT-2, #1, pp 74-86, March 1955.
65. Shepard, R. P., "Active Filters: part 12, Short Cuts to Network Design," Electronics, Vol. 42, pp 82-91, August 18, 1969.
66. Sherwin, J. S., "FET's as Voltage-Controlled Resistors," Solid State Design/CDE, pp 12-14, August 1965.
67. Siljak, D. D., Nonlinear Systems-The Parameter Analysis and Design, John Wiley and Sons, Inc., New York, 1969.
68. Stern, T. E., Theory of Nonlinear Networks and Systems-An Introduction, Addison-Wesley Publishing Company, Inc., Reading, Miss., 1965.
69. Texas Instruments, "Preferred Semiconductors and Components from Texas Instruments," September 1, 1969.



70. Thaler, G. J., and Brown, R. G., Analysis and Design of Feedback Control Systems, McGraw-Hill Book Company, New York, 1960.
71. Thaler, G. J., and Pastel, M. P., Analysis and Design of Nonlinear Feedback Control Systems, McGraw-Hill Book Company, New York, 1962.
72. Thaler, G. J. and Thompson, A. G., Parameter Plane Methods for the Study of the Frequency Response of Linear Time-Invariant Systems, paper presented at the 1967 Applied Mechanics Conference, Adelaide, Australia, June 1967.
73. Thaler, G. J., Siljak, D. D., and Dorf, R. C., Algebraic Methods for Dynamic Systems, NASA, CR-617, November 1966.
74. Tow, J., "A Step-By-Step Active-Filter Design," IEEE Spectrum, Vol. 6, pp 64-68, December 1969.
75. Truxal, J. G., Control System Synthesis, McGraw-Hill Book Company, New York, 1955.
76. Warner, R. M., editor, Integrated Circuits-Design Principles and Fabrication, McGraw-Hill Book Company, New York, 1965.
77. Weinberg, Louis, Network Analysis and Synthesis, McGraw-Hill Book Company, New York, 1962.
78. Welling, Brent, "Active Filters: part 6, The OP AMP Saves Time and Money," Electronics, Vol. 42, pp 82-90, February 3, 1969.
79. Welling, B., "Analysis and Design of Active Filters Using Operational Amplifiers," Motorola Application Note AN-438.



## INITIAL DISTRIBUTION LIST

	No. Copies
1. Defense Documentation Center Cameron Station Alexandria, Virginia 22314	2
2. Library, Code 0212 Naval Postgraduate School Monterey, California 93940	2
3. Prof. G. J. Thaler Department of Electrical Engineering Naval Postgraduate School Monterey, California 93940	1
4. LT. W. A. Tate, USN NavElecSysCom Hq. Washington, D. C. 20360	1
5. Assoc. Professor D. E. Kirk Department of Electrical Engineering Naval Postgraduate School Monterey, California 93940	1

INTERNALLY DISTRIBUTED  
REPORT



## DOCUMENT CONTROL DATA - R &amp; D

*(Security classification of title, body of abstract and indexing annotation must be entered when the overall report is classified)*

ORIGINATING ACTIVITY (Corporate author) aval Postgraduate School onterey, California 93940	2a. REPORT SECURITY CLASSIFICATION <b>Unclassified</b>
	2b. GROUP

REPORT TITLE Active Nonlinear Filter Design Utilizing Parameter Plane Analysis Techniques
---

DESCRIPTIVE NOTES (Type of report and, inclusive dates) Master's Thesis and Electrical Engineer, December 1970
---

AUTHOR(S) (First name, middle initial, last name) William August Tate
--

REPORT DATE December 1970	7a. TOTAL NO. OF PAGES 160	7b. NO. OF REFS 79
------------------------------	-------------------------------	-----------------------

CONTRACT OR GRANT NO.	9a. ORIGINATOR'S REPORT NUMBER(S)
PROJECT NO.	9b. OTHER REPORT NO(S) (Any other numbers that may be assigned this report)

DISTRIBUTION STATEMENT This document has been approved for public release and sale; its distribution is unlimited.
--

SUPPLEMENTARY NOTES	12. SPONSORING MILITARY ACTIVITY Naval Postgraduate School Monterey, California 93940
---------------------	---

ABSTRACT A technique for designing nonlinear active networks having a specified frequency response is presented. The technique, which can be applied to monolithic/hybrid integrated-circuit devices, utilizes the parameter plane method to obtain a graphical solution for the frequency response specification in terms of a frequency-dependent resistance. A limitation to this design technique is that the nonlinear parameter must be a slowly-varying quantity - the quasi-frozen assumption. This limitation manifests itself in the inability of the nonlinear networks to filter a complex signal according to the frequency response specification. Within the constraints of this limitation, excellent correlation is attained between the specification and measurements of the frequency response of physical networks. Nonlinear devices, with emphasis on voltage-controlled nonlinear RET resistances and nonlinear devices frequency controllers, are realized physically and investigated. Three active linear filters, modified with the nonlinear parameter are constructed, and comparisons made to the required frequency specification.
---





KEY WORDS	LINK A		LINK B		LINK C	
	ROLE	WT	ROLE	WT	ROLE	WT
Parameter Plane Nonlinear Active Filter Design Voltage Control Nonlinear Resistance						



18 AUG 71

14 APR 73  
27 DEC 78

18909

20728

26034

Thesis

T165 Tate

c.1

**126562**

Active non-linear  
filter design utilizing  
parameter plane analysis  
techniques.

18 AUG 71  
19 APR 73  
27 DEC 78

18909

20728

26034

Thesis

T165 Tate

c.1

**126562**

Active non-linear  
filter design utilizing  
parameter plane analysis  
techniques.

thesT165

Active non-linear filter design utilizin



3 2768 001 01387 3

DUDLEY KNOX LIBRARY